K-DOMINANT REGION IN 2-D FUNCTIONALLY GRADED MATERIALS UNDER MIXED MODE LOADING

by

Gökce Altay

B.S., in M.E., Bogazici University, 2004

Submitted to the Institute for Graduate Studies in
Science and Engineering in partial fulfillment of
the requirements for the degree of
Master of Science
in
Mechanical Engineering

Boğaziçi University

2007

K-DOMINANT REGION IN 2-D FUNCTIONALLY GRADED MATERIALS UNDER MIXED MODE LOADING

APPROVED BY:

Prof. Günay Anlaş (Thesis Supervisor)	.....
Prof. Uğur Güven	.....
Assoc. Prof. Fazıl Önder Sönmez	.....

DATE OF APPROVAL: 09.01.2007

ACKNOWLEDGEMENTS

This thesis would not have been possible without the help, encouragement, and resources of a number of people. Firstly, I want to express my deep appreciation to my thesis advisor, Prof. Dr. Günay Anlaş, for his constant guidance, enthusiasm, dedication and interest during this study.

I would like to acknowledge support from FGM laboratory graduate students, Alpay Oral, Çiğdem Sürücüoğlu and Hakan Çopur for all the encouragement and essential help to learn the software and analyze the results.

I would like to extend my thanks to Mechanical Engineering Department of Yeditepe University staff, especially Prof. Dr. Nilüfer Eğrican for the support during my study.

No words would be enough to thank my family for their love and support, not only throughout my college career, but also throughout the years leading up to it, and for their always encouraging me to pursue my interests.

Lastly, I would like to express my deepest appreciation and gratitudes to Hasan Cem Çıtak, without his support, effort, love and understanding, it would not have been possible for me to complete this thesis.

ABSTRACT

K-DOMINANT REGION IN 2-D FUNCTIONALLY GRADED MATERIALS UNDER MIXED MODE LOADING

The extent of K-dominant region around the crack tip of a functionally graded plate under mixed mode loading is investigated. A center cracked plate is used for the study. The stress intensity factors and T-stresses are calculated using mode extraction and J-integral method. Stress fields near the crack tip are calculated by using finite elements and the results are compared to two different asymptotic stress field results available in literature. Deviations of the asymptotic solutions from finite element solutions are shown in terms of contour plots around the crack tip to show the extent of K-dominant region. Effects of the material nonhomogeneity, crack size and crack angle on the extent of K-dominant region are examined. Stress contours and error contours are plotted.

ÖZET

KARMA TİP YÜK ALTINDA FONKSİYONEL DERECELENDİRİLMİŞ MALZEMELERİN İKİ BOYUTLU K-BASKIN BÖLGE ANALİZİ

Malzeme özellikleri fonksiyonel olarak değişken dikdörtgen plakalarda çatlak etrafındaki K-baskın bölgenin büyüklüğ karma tip yük altında incelenmiştir. Çalışmada merkez çatlaklı plaklar kullanılmıştır. Tip 1 ve Tip 2 gerilim yoğunluk faktörleri ile T-gerilimi hesaplanmıştır. Çatlak ucu civarındaki sonlu elemanlar programı ile hesaplanan gerilme alanı ile literatür yer alan iki farklı asimtotik gerilme alanı karşılaştırılmıştır. Asimtotik gerilme alanlarının, sonlu elemanlar ile hesaplanan gerilme alanlarından sapması çatlak ucu civarındaki eş sapma eğrileri ile gösterilmiştir. K-baskın bölgenin büyüklüğü belirlenmişi oldu. Homojen olmayan malzeme özellik- lerinin, çatlak uzunluğunun ve çatlak açısının K-baskın bölge üzerindeki etkisi araştırılmıştır. Sonuçlar daha detaylı analizler için grafiğe dökülmüştür.

TABLE OF CONTENTS

LIST OF FIGURES

LIST OF TABLES

LIST OF SYMBOLS/ABBREVIATIONS

a	Crack length
E	Elastic Modulus
E_1	Elastic Modulus at the left edge of the plate
E_2	Elastic Modulus at the right edge of the plate
E_o	Elastic Modulus at the origin
E_{tip}	Elastic Modulus at the crack tip
G	Energy released rate
H	Height of the plate
J	J-integral
K_I	Stress intensity for Mode I
k_I	Nondimensional stress intensity for Mode I
K_{II}	Stress intensity for Mode II
k_{II}	Nondimensional stress intensity for Mode II
T	T-stress
U	Strain Energy
u, v	Displacement along x and y directions
x, y	Cartesian coordinates at the crack tip
W	Width of the plate
μ	Shear Modulus
υ	Poisson's ratio
β	Material nonhomogeneity parameter
σ_o	Uniform traction applied to upper and lower edge of the plate
σ_{xx}	Normal stress along x-direction
σ_{yy}	Normal stress along y-direction
σ_{xy}	Shear stress on x-plane along y-direction
α	Crack angle
ASY	Asymptotic equations around the crack tip

ASYNEW	Asymptotic equations derived by Konda and Erdogan
FE	Finite element solution
FEM	Finite element method
FGM	Functionally graded material
SIF	Stress Intensity Factor
ASY	Asymptotic equations around the crack tip
ASYNEW	Asymptotic equations derived by Konda and Erdogan

1. INTRODUCTION

1.1. General

To meet demands of new high technologies new materials with better performances are needed. One direction of work has been the creation of nonhomogeneous materials by joining different materials, to take advantage of their respective favorable properties. In high temperature applications discretely nonhomogeneous materials such as metals coated by ceramics or ceramic metal bonded materials have shortcomings of poor interfacial bonding, high residual and thermal stresses and low toughness.

A composite material of a different kind, namely functionally graded material (FGM) was proposed in 1984 by Japanese material scientists to prepare thermal barrier coatings using a heat resistant material on high temperature side, and a tough material inside with a gradual composition variation in between, from ceramic to metal. FGMs are continuously non-homogeneous materials because the volume fractions of their composite constituents vary continuously in space [1].

Generally, these are ceramic/metal graded mixtures that exploit the beneficial properties of both metals (toughness, thermal conductivity, ductility, etc.) and ceramics (hardness, heat and corrosion resistance, etc.), while enhancing bond strength and reducing residual stresses when compared to metal/ceramic interfaces.For instance, partially stabilized zirconia (PSZ) shows a high resistance to heat and corrosion, and CrNi alloy has high mechanical strength and toughness, which is shown in Figure 1.1 [2]. FGMs were initially conceived as thermal protections systems for aerospace applications, but are also being considered in applications such as energy conversion, military, microelectronics, biomedical and machining [3].

However, manufacturing of FGMs are expensive and difficult. Functionally graded coating can be produced by plasma spraying techniques using gas-injection tubes. Another method can be considered by melt processing. Gradient formation is achieved

by transporting a refractory material in the molten state of the metal. A special production method is electrochemical gradation used to introduce porosity gradients in materials such as bronze and copper [4]. Powder metallurgy, combustion synthesis, self propagating high temperature synthesis, reactive infiltration, diffusion treatments and sedimentation are also used in fabrication of FGMs for structural applications.

Progress in implementing FGM designs has been slower than initially expected, not only because of the difficulty in manufacturing such materials, but also because of a lack understanding of their mechanical response [5]. Although FGMs do not contain sharp interfaces to start a crack or discontinuities that cause high residual and thermal stress, which are the main reasons of cracking and failure, one important issue in the design, optimization and engineering applications of FGMs is concerned with their fracture and fatigue properties, which are essential to their integrity, reliability and durability [6].

However, the equations of fracture mechanics used for homogeneous materials can not be used directly for FGMs since some of the fracture mechanics parameters are affected by material gradients.

In linear elastic fracture mechanics, the fracture parameters describing the crack tip fields include stress intensity factors (SIFs). In FGMs the material gradation does not affect the order of singularity and the angular functions of the crack-tip fields but does affect the stress intensity factors. The mixed-mode SIFs in FGMs are functions of material gradients, external loading, crack length and geometry. Stress intensity factors are needed for asymptotic equations.

Asymptotic equations were derived to find the near tip stress fields in homogeneous materials and they are valid in a region defined as K-dominant region. Thus, in FGMs because of the change of stress intensity factors there is a change in K-dominant region. The aim of this study is to identify the extent of K-dominant region when material nonhomogeneity is present.

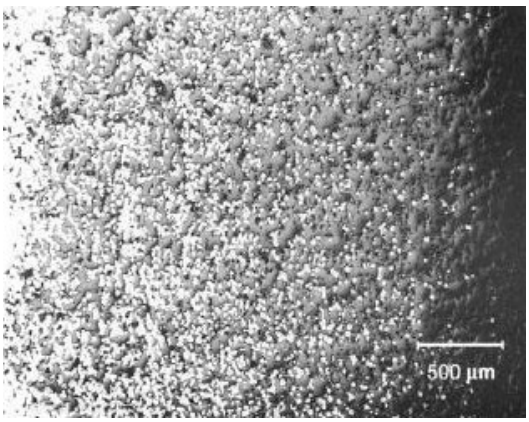

Figure 1.1. Micrograph illustrating graded transition region between CrNi alloy and PSZ [2]

1.2. Literature Review

Analytical work on nonhomogeneous materials begins as early as 1960 when soil was modeled as a non-homogeneous material by Gibson [7]. In his study due to the complexity, a linear functional form of the material property variation was assumed.

Works on fracture mechanics of FGMs come later. Assuming an exponential spatial variation of the elastic modulus Delale and Erdogan [8] studied crack problem with Mode I deformation with a modulus parallel to crack line. They showed that the crack tip inverse square-root singularity should not be affected by material non-homogeneities as long as Young's modulus and Poisson's ratio are sufficiently smooth functions of spatial position. Erdogan [9] further showed that square-root singularity of a crack tip should also apply to materials with continuous but only piecewise differentiable properties.

Eischen [10] studied mixed-mode conditions in non-homogeneous materials using finite element method (FEM) and he showed that stress singularities at the crack tip in an FGM are exactly of the same order as those of a homogeneous material. This result was reconfirmed by Jin and Noda [11] for materials with piecewise differentiable

property variations as shown below:

$$\sigma_{ij}(r,\theta) = \frac{K_I}{\sqrt{2\pi r}} F_{ij}^{I}(\theta) + \frac{K_{II}}{\sqrt{2\pi r}} F_{ij}^{II}(\theta) \tag{1.1}$$

where functions $F_{ij}^{I}(\theta)$ and $F_{ij}^{II}(\theta)$ are the same as those in the expression for a homogeneous material, with the coordinate system attached to the crack tip, and K_I and K_{II} are the mode I and mode II stress intensity factors respectively.

In a homogeneous material J-integral is path independent. However, material nonhomogeneity of FGMs affects J-integral and it is not path independent. Eischen [10] generated a quasi-path-independent integral for nonhomogeneous materials. He showed relation of the integral with G, K_I, K_{II}.

Konda and Erdogan [12] studied mixed mode problem in an infinite plane where the crack is arbitrarily oriented with respect to the direction of property gradient. They approximated the shear modulus an exponential function, $\mu(x,y) = \mu_0 e^{\beta x + \gamma y}$ and the poisson's ratio ν of the medium was assumed to be constant. Mode I and mode II SIFs were calculated analytically. They derived asymptotic stresses near the crack tip as;

$$\sigma_{ij}(r,\theta) = e^{r(\beta cos\theta + \gamma sin\theta)}[\frac{K_I}{\sqrt{2\pi r}} F_{ij}^{I}(\theta) + \frac{K_{II}}{\sqrt{2\pi r}} F_{ij}^{II}(\theta)]. \tag{1.2}$$

Togho *et al.* [13] used finite element analysis to investigate the fracture strength of FGMs. They showed the effect of material property change on stress intensity factors and plastic zone around the crack tip.

Later, Erdogan and Wu [14] presented a Mode I study of a cracked finite width plane made of a FGM with three different loading conditions, namely fixed grip, membrane loading, and bending applied to the layer away from the crack region.

Gu and Asaro [15] considered a semi-infinite crack in a FGM strip under edge loading in an interlayer between two dissimilar materials, and they calculated mixed

mode stress intensity factors in plane. The effect of material gradients on intensity factors were determined. It was seen that the size of the K-dominant region decreases as the nonhomogenity increases.

Jin and Batra [16] gave a simple estimate on the effect of the material property gradient on the dominance of the crack tip singular field. They studied the K-dominant region where the asymptotic stress field is valid. They obtained some formulas giving the dimension of the region roughly. Their theoretical results was confirmed by the numerical study of Marrur and Tippur [17]. The results showed that fracture parameters of FGMs approach to the fracture parameters of bimaterial as the material gradient is increased. Also numerical stress were compared with those of asymptotic solution.

Gu *et al.* [18] presented a simplified method for calculating the crack-tip field of FGMs using the equivalent domain integral technique. They evaluated J-integral in a small region around the crack tip to calculate SIFs. In Anlas *et al.* [19] tried to explore the extent and the shape of the K-dominant zone in a continuously nonhomogeneous materials in Mode I. The range of dominance is sensitive to material gradient and uncracked ligament length. Stress intensity factors were calculated directly from the classical J-integrals.

Kim and Paulino [20] evaluated mixed-mode fracture parameters in FGMs using FE analysis with three different methods; path-independent J_k^*-integral method, modified crack-closure integral method, and displacement correlation technique. Results of the SIFs were compared with the ones founded theoretically by Konda and Erdogan [12].

Dolbow and Gosz [21] used a new interaction energy integral method for computation of mixed-mode stress intensity factors at tips of arbitrarily oriented cracks in FGMs. They obtained good agreement between numerical results and analytical solutions for stress intensity factors in all cases.

Recently, Shim and Paulino [22] investigated the extent of K-dominant region for

FGM fracture specimens by comparing actual stress field with Williams' asymptotic stress field under mode I loading. They concluded that the extent of K-dominance yields a curve with a peak point at a certain material gradation. Results of this study provide valuable insight into the K-dominance of FGMs.

Although in previous works SIFs for FGMs are calculated analytically and numerically, detailed study of the K-dominant region is not considered especially in the case of mixed mode loading. In this study, the extent and the shape of the K-dominant region in FGMs will be studied for different crack types, crack size and material gradients.

2. PROBLEM DESCRIPTION AND NUMERICAL PROCEDURES

2.1. Objective

The aim of the study is to investigate the extent of K-Dominant region near the crack tip in FGMs within the limits of linear-elastic fracture mechanics. K-dominant region controls the behavior of the crack as long as the plastic zone remains small compared to the specimen size. For this purpose, different models are used to investigate the effects of material gradient, external loading, geometry and crack size on K-dominant region. The extent of K-dominant region is determined by comparing crack-tip stress field calculated using finite element with the Williams asymptotic stress field.

2.2. Analysis

Assuming linear elastic material behavior, the eigenfunction expansion technique proposed by Williams [23] has been widely used to investigate the nature of the near-tip fields in a cracked body. Although these expressions were derived for homogeneous materials, Eischen [10] used an extension of this procedure to establish a general form of the stress and displacement field near a crack tip in a non-homogeneous material where the elastic moduli vary with position (x) such that the Young's modulus $E = E(x)$ and Poisson's ratio $\nu = \nu(x)$ are continuous, bounded, and differentiable. This result was further confirmed by Jin and Noda [11] for materials with piecewise differentiable property variations. Figure 2.1 shows a crack in a two dimensional FGM elastic body with applied traction and specified displacements on the boundary resulting in a state of generalized plane stress or plane strain [20].

Local Cartesian and cylindrical co-ordinates are fixed at the crack tip, body forces are neglected, and crack faces are assumed to be traction-free. The asymptotic stress

field ahead of a crack tip for mode I and mode II is given by;

$$\sigma_{xx} = [\frac{K_I}{\sqrt{2\pi r}} cos\frac{\theta}{2}(1 - sin\frac{\theta}{2}sin\frac{3\theta}{2})] - [\frac{K_{II}}{\sqrt{2\pi r}} sin\frac{\theta}{2}(2 + cos\frac{\theta}{2}cos\frac{3\theta}{2})] + T + O(r), \quad (2.1)$$

$$\sigma_{yy} = [\frac{K_I}{\sqrt{2\pi r}} cos\frac{\theta}{2}(1 + sin\frac{\theta}{2}sin\frac{3\theta}{2})] + [\frac{K_{II}}{\sqrt{2\pi r}} (sin\frac{\theta}{2}cos\frac{\theta}{2}cos\frac{3\theta}{2})] + O(r), \quad (2.2)$$

$$\sigma_{xy} = [\frac{K_I}{\sqrt{2\pi r}} cos\frac{\theta}{2}sin\frac{\theta}{2}cos\frac{3\theta}{2}] + [\frac{K_{II}}{\sqrt{2\pi r}} cos\frac{\theta}{2}(1 - sin\frac{\theta}{2}sin\frac{3\theta}{2})] + O(r) \quad (2.3)$$

where K_I and K_{II} are modes I and mode II stress intensity factors (SIFs) respectively. T is the constant nonsingular stress term. $O(r)$ are higher order terms which can be considered as negligible near the crack tip. The SIFs are functions of material gradients, external loading and geometry. The material gradients do not affect the order of singularity and the angular functions of the crack tip fields, but do effect the SIFs. It also significantly affects the extent of K-dominant region. Thus, although this asymptotic equations give the stress field near the crack tip, the range of their applications should be determined. To demonstrate the extent of K-dominant region,

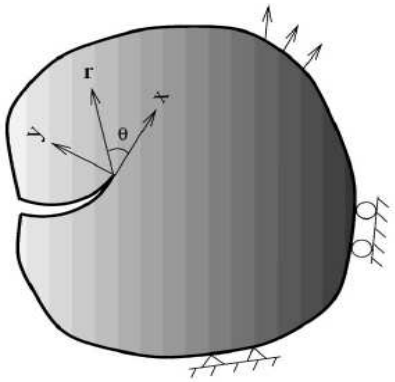

Figure 2.1. Cartesian and polar coordinate systems at the crack tip [20]

the actual elastic-tip stress fields are needed. Nodal stress values taken from finite element program are presumed to be an accurate presentation of the actual stresses.

2.3. Finite Element Model

To calculate stress intensity factors and to get the stress field around the crack MSC Marc Mentat 2001 Finite Element Program is used. In all finite element models, two dimensional 4-node quadrilateral plane stress elements are used. These are isoparametric quadrilateral 2-D continuum elements with straight edges and bilinear interpolation. The node numbering is counterclockwise as shown in Figure 2.2. These elements use a four-point Gaussian integration scheme. In average, 10000 elements are used.

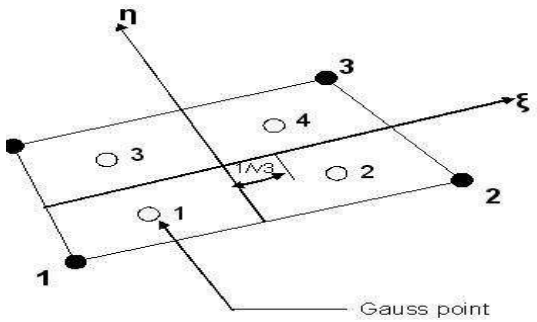

Figure 2.2. Four node quadrilateral element

The crack-tip region is modeled using a refined circular mesh to obtain crack-tip stress and displacement fields and fracture parameters. In the outer region, rectangular mesh is used. A transition region from the circular mesh to rectangular mesh is needed in which elements do not have a definite shape. Triangular elements involving degenerate nodes are also allowed with the same element formulation. Figure 2.3 shows the mesh detail around the crack tip.

The edge and center cracked plate geometries are shown in Figure 2.4 (a, b). In the case of edge cracked plate, the height of the plate is twice its width, and the crack is on the x-axis with a length a. In the center cracked case, a square plate is used and the crack has a length $2a$. These geometries are chosen to compare the results with the results available in literature. In both models, cracks are inclined with an angle α,

and the crack is under mixed-mode loading.

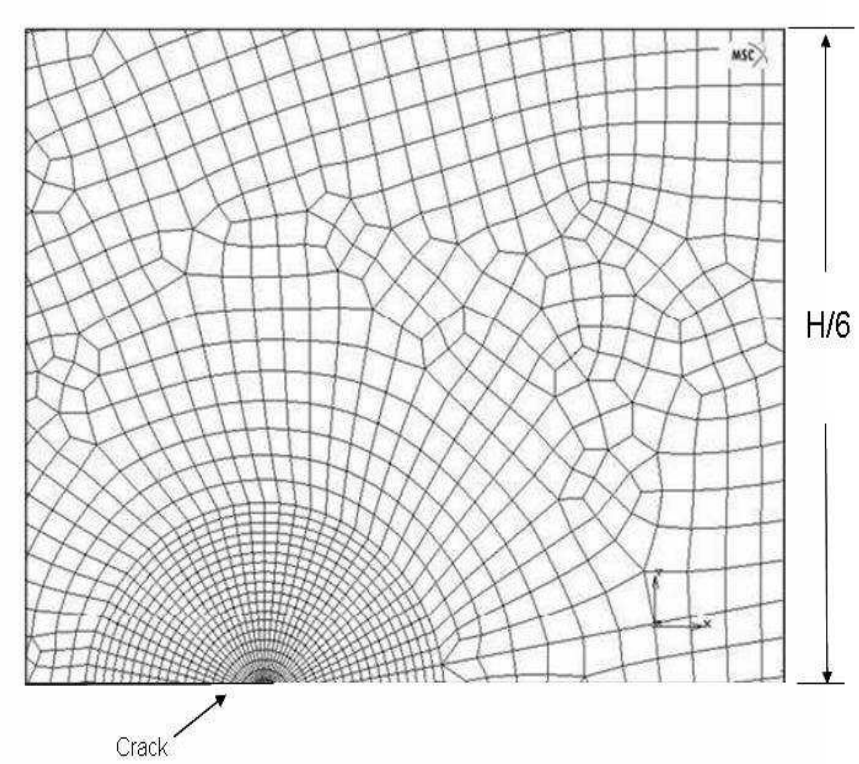

Figure 2.3. Mesh around the crack tip

2.3.1. Material Property Gradient in the Finite Element Model

In this study, it is assumed that Poisson's ratio ν is constant ($\nu = 0.3$) and the modulus of elasticity E is changing exponentially along the x-axis as shown below;

$$E(x) = Ee^{\beta x} \tag{2.4}$$

where β is the material nonhomogeneity parameter and it denotes an intrinsic length scale. E represents the elastic modulus at the origin of the coordinate system. For the edge cracked plate, E is taken as E_1, which is the elastic modulus of left edge of the plate. However, for the center cracked plate E_0 represents the modulus at the center of the crack, $x = 0$. The exponential change of the material property is discretized in

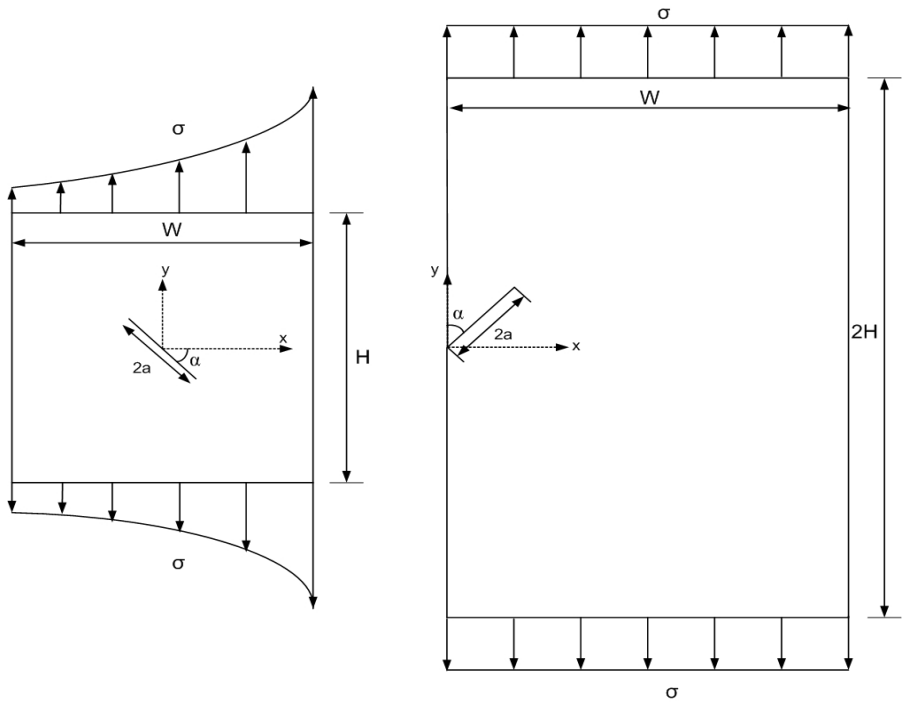

Figure 2.4. Geometry of edge and center cracked plates

finite element program. To every node of the element a discrete value of E is aspired.

2.3.2. Accuracy of Finite Element Solution

As mentioned in the previous part, approximately 10000 elements for each model are used. The number of elements is selected to provide sufficiently good numerical results with reasonable CPU time. The calculated mode I stress intensity factors are compared to the analytical and numerical ones available in literature for the model with different number of element. The difference is calculated as the error percentage.

The models with 400 and 1600 elements do not give accurate results. The errors are 2.7 and 0.6 percent respectively. If a refined mesh of 10000 elements is used the error reduces to 0.37 percent. If the geometry is discretized with a much refined mesh of 40000 elements, only 0.04 error occurs. Obviously solution for 40000 elements takes 6.39 times more CPU time than that of 10000 elements. Thus, it is suitable to select

approximately 10000 elements mesh in this study. Although it is not mentioned in this simple example, using circular mesh around the crack tip reduces the error percentage. The figure given below shows the CPU time and the error percentage of different mesh types briefly.

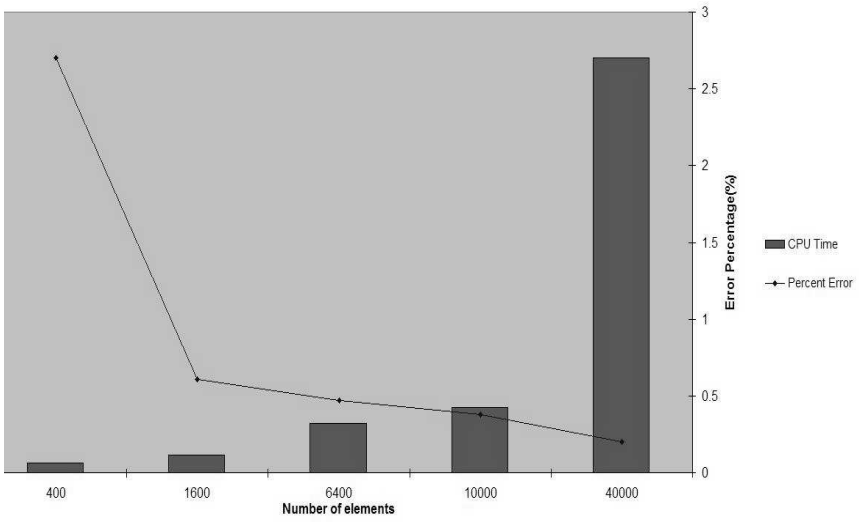

Figure 2.5. The CPU time and error percentage for different element numbers

2.4. Determination of Stress Intensity Factors

To analyze the influence of material gradient variation on SIFs, to check the accuracy of our finite element model, and to use the asymptotic equations SIFs are needed. A large number of techniques to calculate SIFs have been presented in the literature. Techniques fall into one of two categories; direct approaches, which correlate SIF's with FEM results directly, and energy approaches, which first compute energy release rate. In general, energy approaches are more accurate and are used preferentially. In this study, one of the energy approach; a J-integral method is used to calculate SIFs.

2.4.1. J-integral

The J-integral is a well known nonlinear fracture parameter. Using a crack coordinate system where the x_1 axis is tangential and the x_2 axis is perpendicular to the crack in a two dimensional body, the J-integral is defined as

$$J = \int_{\Gamma} (W n_1 - \sigma_{ij} n_i \frac{\partial u_j}{\partial x_1}) ds \tag{2.5}$$

where Γ is any path beginning at the bottom crack face and ending on the top crack face, W is the strain energy density, σ is the stress tensor, $\mathbf{n}$ is the unit outward normal to the contour, $\mathbf{u}$ is the displacement vector.

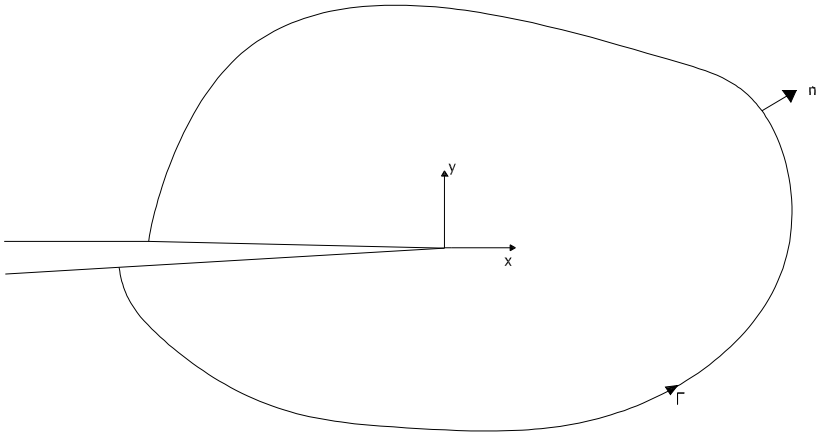

Figure 2.6. Definition of J-integral

2.4.1.1. Homogeneous material. For homogeneous materials, the contour integral can be shown to be path independent providing no body forces inside the integration area, there are no thermal strains and no tractions on the crack surface. In addition to that, the J-integral can be interpreted as equivalent to energy release rate, $J = G$. The energy release rate is the change in energy per unit crack extension per unit thickness [10]. It is denoted as

$$G = \frac{dU}{dA} \tag{2.6}$$

where U is the strain energy and A is the crack surface area. Stress intensity factors are related to the energy relase rate for mixed mode loading as

$$G = \frac{K_I^2}{E'} + \frac{K_{II}^2}{E'} \tag{2.7}$$

where for plane strain

$$E' = \frac{E}{1 - v^2} \tag{2.8}$$

and for plane stress

$$E' = E. \tag{2.9}$$

Thus, first G should be calculated using J-integral to find stress intensity factors. In finite element program, Marc Mentat, J-integral can be evaluated. The J-integral evaluation in Marc Mentat is based upon the area integration as described in Equation 2.5.

The nodes along the crack front, the shift vector, and the nodes of the rigid region are required to evaluate the J-integral in Marc Mentat. The program makes an automatic search for the nodes of the rigid region where a number of regions of increasing size are found. The first region consists of the nodes of all elements connected to the crack tip node. The second region includes of all nodes in the first region and the nodes of all elements connected to any node in the first region and so on for a given number of regions. This way, contours of increasing size are determined. Since the mesh is circular around the crack tip the elements within a region are certain radius apart from the crack tip. In this study, eight different regions are used in finite element program to evaluate J-integral.

For mixed-mode loading, separate calculation of the stress intensity factors is difficult. J-integral is calculated numerically and it is assumed that J-integral is a sum

of symmetric and antisymmetric parts as

$$J = J_1 + J_2 \tag{2.10}$$

where

$$J_1 = \frac{K_I^2}{E'} \tag{2.11}$$

and

$$J_2 = \frac{K_{II}^2}{E'}. \tag{2.12}$$

In Equations 2.11 - 2.12, J_1 and J_2 are needed separately to determine K_I and K_2. Mattheck and Moldenhauer [25] present a mode extraction technique to subdivide the J-integral. This technique extracts mode I from mixed mode by applying the following constraint

$$u_i = u_j \tag{2.13}$$

to all node pairs (i, j) on the free surface. Preventing relative motion in x-direction, only opening of the crack remains. Similarly, mode II is extracted from mixed mode by applying

$$v_i = v_j \tag{2.14}$$

This time, nodes only slide on the x-direction which result in mode II.

Since the J-integral is calculated on eight paths around the crack tip the constraints are applied to eight pairs of nodes on crack free surfaces to calculate J_1 and J_2 separately. In Marc Mentat, the LINKS menu is used to define constraint equations

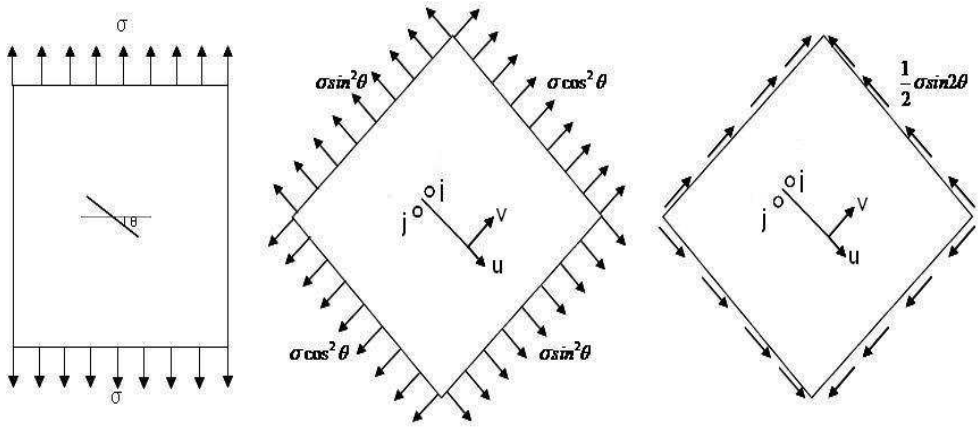

Figure 2.7. Explanation of the filter technique based on superposition and crack closure

between nodes. For determining J_I, nodal ties are set to eight pairs of nodes and the first degree of freedom (u direction) is eliminated from the system. In the same way, the second degree of freedom (v direction) is reduced for the nodes pairs to determined the J_{II}.

For an inclined center crack in a homogeneous plate subjected to far-field biaxial or uniaxial constant traction as shown in Figure 2.9, closed-form solutions for SIFs and T-stress are given by [30];

$$K_I = \sigma\sqrt{\pi a}(\lambda cos^2\alpha + sin^2\alpha), \tag{2.15}$$

$$K_{II} = \sigma\sqrt{\pi a}(1-\lambda)sin\alpha cos\alpha, \tag{2.16}$$

$$T = \sigma(1-\lambda)cos2\alpha. \tag{2.17}$$

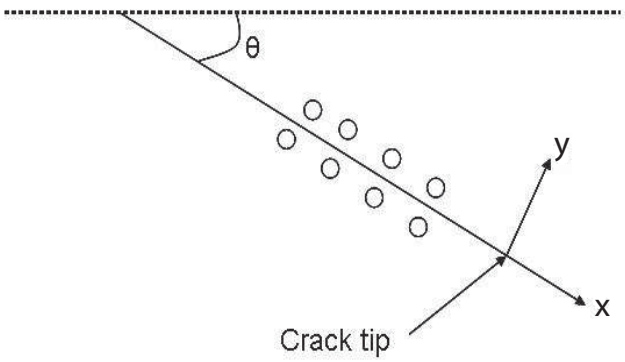

Figure 2.8. Presentation of double nodes on free crack surface

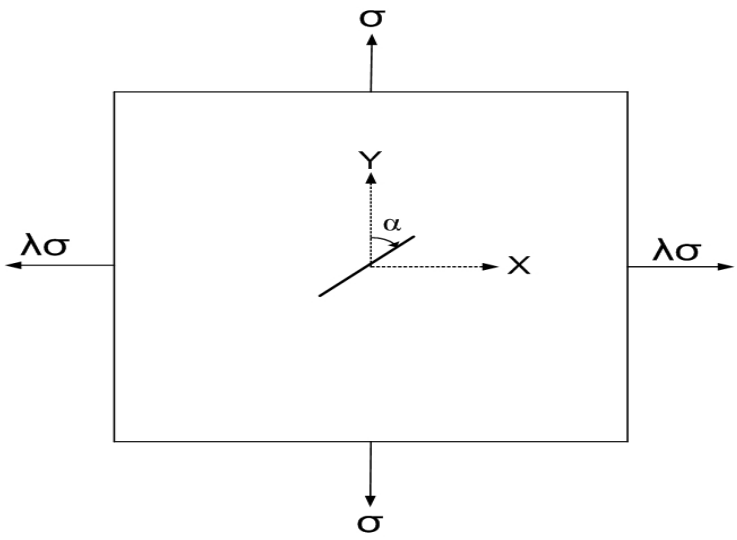

Figure 2.9. An inclined center crack in a biaxially loaded homogeneous plate

However, the closed-form solution is valid for the case of a finite plate if the crack length is small enough relative to the width of the plate. If the crack length increases the boundary effect can occur.

2.4.1.2. Nonhomogeneous material. For nonhomogeneous materials, J-integral is not path independent, $G \neq J$. Thus J values changes with contour. An example of a center crack plate under mode I case is given in Table 2.1 to compare J values for homogeneous material and FGM. The contour numbers represent contours around the crack tip.

Table 2.1. J-integral values for a center cracked homogeneous and FGM with mode I

	J-integral values	
Contour Number	Homogeneous	FGM
1	3.13	4.79
2	3.17	4.89
3	3.18	4.94
4	3.18	4.98
5	3.19	5.02
6	3.19	5.05
7	3.19	5.09
8	3.19	5.13

The J-integral value can not be used directly for FGMs in calculation of stress intensity factors. Gu *et al.* [27] show that the J-integral obtained from finite element program is sufficiently accurate when applied to nonhomogeneous materials if a very fine mesh (like $r \rightarrow 0$) is used. The drawback of this method is that it needs sufficiently fine mesh which means higher CPU time.

Anlas *et al.* introduced a simple method that uses relatively coarse mesh to calculate the stress intensity factors directly from classical J-integrals [28]. With this method, finding J-integral value as $\Gamma \rightarrow 0$ using the standard J-integral algorithm and without using very fine mesh is possible. Path dependent J-integral values are calculated along many contours around the crack tip and every path gives different J-integral values. The values are plotted versus contour numbers. Then a polynomial is fitted to data points , and a value for $\Gamma \rightarrow 0$ can be obtained. $\Gamma \rightarrow 0$ is approximated numerically as the intercept of the polynomial curve with J-axis. It is seen that the

limiting value of J is approximately equal to the energy release rate, G.

In this study, J-integrals are calculated along eight contours using Marc Mentat. First and the last contours' results are omitted to reduce the error. To obtain a limiting value for J, a linear curve is fit to data and the point where the line crosses the vertical axis is the limiting value of the J-integral. Figure 2.10 shows the six data points and the linear curve fit for the data given in Table 2.1. For mixed mode loading J_1 and J_2 integrals are extracted by applying a mode extraction technique as described in Section 2.4.1.1. Similarly, J_1 and J_2 values are determined by finding a limiting value for J_1 and J_2 integrals obtained directly from finite element program.

After J_1 and J_2 values are obtained, stress intensity factors are calculated by using Equations 2.11 - 2.12. However, because there is a material gradient instead of E', the young modulus at the crack tip, E'_{tip} is used.

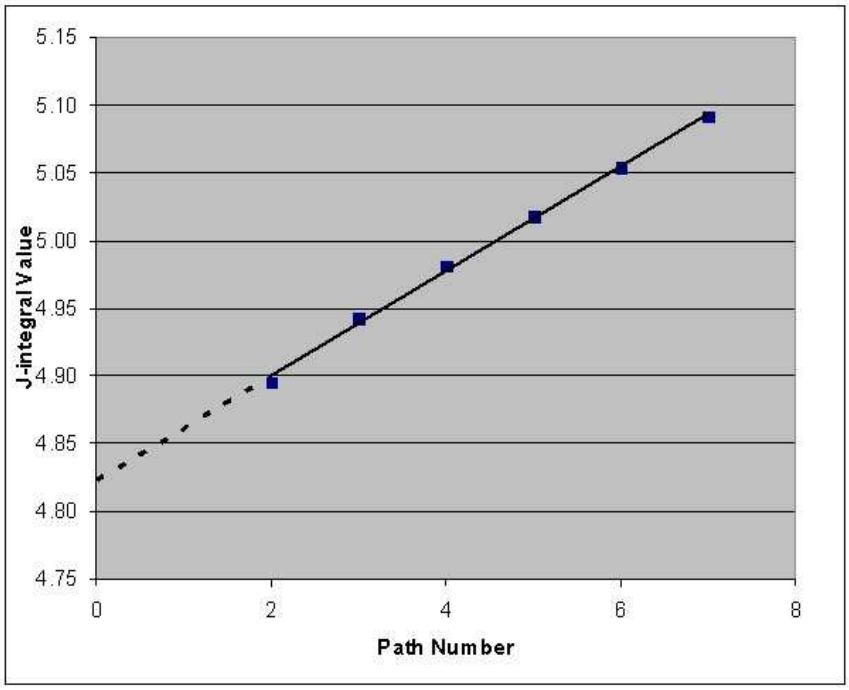

Figure 2.10. Linear curve fit for J-integral values

2.5. Calculation of K-dominant Region

Once the asymptotic stress fields are calculated by using Equations 2.1 - 2.3 and finite element stress fields are obtained, the extent of K-dominant region is defined as the deviation of symptotic stress field from finite element stress field. Lee and Rosakis [24] define the stress deviation quantity, e, as follows;

$$e = \frac{\|\sigma_{ij}^F - \sigma_{ij}^A\|}{\|\sigma_{ij}^A\|} \tag{2.18}$$

where σ_{ij}^F and σ_{ij}^A denote stress components of the finite element solution and the asymptotic field solution respectively and Einstein's summation convention is applied to the repeated subscripts. The subscripts i and j range from x to y. In the definition of error parameter, Frobenius norms which are commonly used in matrix algebra to calculate the norms of matrices are used. In Equation 2.18, the nondimensional positive scalar parameter, e, is given as the ratio of the norm of the matrix formed from the differences of the stress calculated by finite element analysis and by asymptotic equations to the norm of the matrix formed from the stresses calculated by the asymptotic equations. The error parameter is a measure of the difference between the two stress fields in brief.

2.6. Verification of Finite Element Model

An inclined crack of length $2a$ located of a center crack in a finite two-dimensional FGM plate is studied in this section for the verification of the finite element model. The geometry is shown in Figure 2.12, upper and lower edges are loaded by $\sigma_{yy} = \overline{\varepsilon} E_0 e^{\beta x}$ which is a result of a uniform strain $\varepsilon_{yy} = \overline{\varepsilon}$.

The Poisson's ratio, ν, is constant ($\nu = 0.3$) and the Young's modulus, E, is changing exponentially along x-axis and given as;

$$E(x) = E_0 e^{\beta x} \tag{2.19}$$

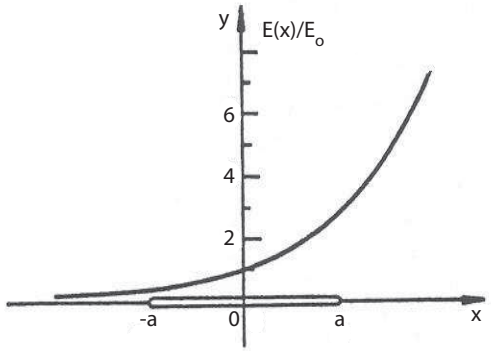

Figure 2.11. The variation of the Young's modulus $E = E_0 e^{\beta x}$ [12]

E_0 is the elastic modulus at $x = 0$ and β is a measure of the length scale of the material gradient. The variation of the elastic modulus is given in Figure 2.11. E_1 is the elastic modulus of the left edge of the plate, and E_2 is the elastic modulus of the right edge of the plate and between the two edges the modulus varies exponentially; β can be determined as follows;

$$\beta = \frac{1}{H} \ln(\frac{E_2}{E_0}) \tag{2.20}$$

or

$$\beta = \frac{1}{H} \ln(\frac{E_0}{E_1}). \tag{2.21}$$

In this study, $a/W = 0.1$; $H/W = 1.0$; $E_0 = 1.0$; $\alpha = 0^o, 18^o, 36^o, 54^o$; $\beta a = 0.25, 0.5$; $\bar{\varepsilon} = 1.0$ are used, and a plane stress assumption is made to compare the results to those of Konda and Erdogan [12] who investigated the mixed mode center crack problem in a unbounded nonhomogeneous elastic medium considering generalized plane stress. The stress intensity factors are compared with the SIFs of closed-form solutions that are available only for homogeneous center cracked plate

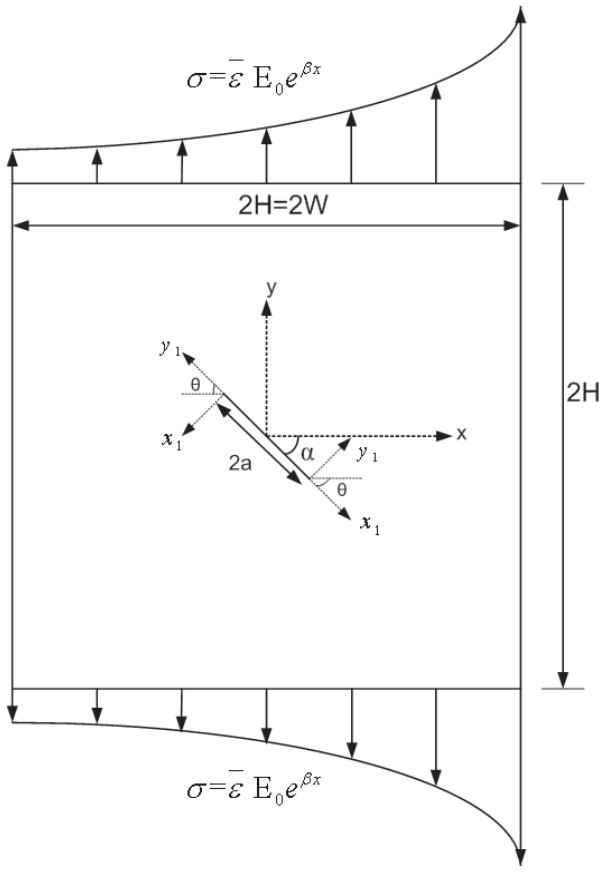

Figure 2.12. FGM plate with an inclined crack of angle α

2.6.1. Stress Intensity Factors

Stress intensity factors under mixed mode loading are calculated using the methods described in Section 2.4.1.1 and all stress intensity factors are normalized as shown below;

$$k_{I,II} = \frac{K_{I,II}}{\overline{\varepsilon} E_0 \sqrt{\pi a}} \tag{2.22}$$

Using Equations 2.11 - 2.12 with Equation 2.22, k_I and k_{II} can be rewritten as;

$$k_{I,II} = \sqrt{\frac{J_{I,II} E_{tip}}{\overline{\varepsilon}^2 E_0^2 \pi a}} \tag{2.23}$$

Before considering the nonhomogeneous case, stress intensity factors for homogeneous center cracked plate, $\beta = 0$, are calculated under uniaxial loading, $\sigma_{yy} = 1$, for two different crack lengths of $a/h = 0.05$ and $a/h = 0.1$. The results are compared to closed form solutions. The closed form solutions for SIFs can be obtained by using Equations 2.15 - 2.17. The loading is uniaxial, and λ is taken as 0.

It is seen that SIFs for $a/h = 0.05$ are very close to closed form solutions that are given for an infinite plate because in the case of $a/h = 0.05$ the boundary effect is small. However, it can be said that the results obtained for $a/h = 0.1$ are also adequate, see Table 2.2. A crack length of $a/h = 0.1$ is used to model crack in an infinite plate in subsequent calculations.

Table 2.2. Normalized stress intensity factors for $\beta a = 0$ with $\sigma_{yy} = \overline{\varepsilon} E_0 e^{\beta x}$

	$a/h = 0.05$					$a/h = 0.1$			
Method	α/π	$k_I(a)$	$k_{II}(a)$	$k_I(-a)$	k_{II}(-a)	$k_I(a)$	$k_{II}(a)$	$k_I(-a)$	$k_{II}(-a)$
Closed form solution	0	1.000	0	1.000	0	1.000	0	1.000	0
	0.1	0.905	−0.294	0.905	−0.294	0.905	−0.294	0.905	−0.294
	0.2	0.655	−0.476	0.655	−0.476	0.655	−0.548	0.655	−0.476
	0.3	0.345	−0.476	0.345	−0.476	0.345	−0.532	0.345	−0.476
Present study	0	0.998	0	0.998	0	1.004	0	1.004	0
	0.1	0.906	−0.294	0.906	−0.294	0.908	−0.294	0.908	−0.294
	0.2	0.653	−0.475	0.653	−0.475	0.656	−0.472	0.656	−0.472
	0.3	0.343	−0.474	0.343	−0.474	0.357	−0.470	0.357	−0.470

For the nonhomogeneous case, the analytical solution of this problem is obtained by Konda and Erdogan [12]. Later, Kim and Paulino [20] solved the same problem and compared the SIFs results using different numerical methods: They used modified crack-closure integral method (MCC), path-independent J_k^*-integral method, and displacement correlation technique (DCT). Analogous studies have also been made by Dolbow and Gosz [21] using an extended finite element method (X-FEM). The results of those studies are tabulated in Table 2.3 for $\beta a = 0.25$ and 0.5 for various angles α/π. Present results are compared to the analytical results of Konda and Erdogan [12] and the numerical results of Kim and Paulino [20] and Dolbow and Gosz [21]. It is seen that sufficient quantitative agreement is provided. Maximum error in the calculations is less than five percent. The values are also as good as the numerical ones presented by Kim and Paulino [20] and Dolbow and Gosz [21].

Table 2.3. Normalized stress intensity factors for $\beta a = 0.25$ and $\beta a = 0.5$ with $\sigma_{yy} = \bar{\varepsilon} E_0 e^{\beta x}$

		$\beta a = 0.25$				$\beta a = 0.5$			
Method	α/π	$k_I(a)$	$k_{II}(a)$	$k_I(-a)$	k_{II}(-a)	$k_I(a)$	$k_{II}(a)$	$k_I(-a)$	k_{II}(-a)
Konda and Erdogan [12]	0	1.196	0	0.825	0	1.424	0	0.674	0
	0.1	1.081	−0.321	0.750	−0.254	1.285	−0.344	0.617	−0.213
	0.2	0.781	−0.514	0.548	−0.422	0.925	−0.548	0.460	−0.365
	0.3	0.414	−0.504	0.290	−0.437	0.490	−0.532	0.247	−0.397
Kim and Paulino [20] (MCC)	0	1.221	0	0.827	0	1.458	0	0.664	0
	0.1	1.101	−0.325	0.752	−0.250	1.310	−0.353	0.608	−0.207
	0.2	0.789	−0.519	0.549	−0.416	0.933	−0.558	0.454	−0.355
	0.3	0.414	−0.507	0.291	−0.432	0.487	−0.536	0.244	−0.386
Kim and Paulino [20] (J_k^*-integral)	0	1.220	0	0.840	0	1.446	0	0.679	0
	0.1	1.106	−0.315	0.769	−0.239	1.306	−0.341	0.628	−0.195
	0.2	0.810	−0.494	0.582	−0.390	0.944	−0.534	0.488	−0.329
	0.3	0.404	−0.523	0.297	−0.439	0.461	−0.563	0.256	−0.392
Kim and Paulino [20] (DCC)	0	1.235	0	0.854	0	1.461	0	0.693	0
	0.1	1.140	−0.312	0.775	−0.248	1.315	−0.333	0.633	−0.209
	0.2	0.802	−0.499	0.565	−0.412	0.943	−0.529	0.469	−0.356
	0.3	0.423	−0.489	0.297	−0.425	0.498	−0.512	0.249	−0.384
Dolbow and Gosz [21]	0	1.218	0	0.838	0	1.445	0	0.681	0
	0.1	1.099	−0.329	0.761	−0.257	1.303	−0.353	0.623	−0.213
	0.2	0.788	−0.524	0.557	−0.424	0.930	−0.560	0.467	−0.364
	0.3	0.415	−0.512	0.295	−0.439	0.488	−0.540	0.251	−0.396
Present study	0	1.209	0	0.830	0	1.448	0	0.680	0
	0.1	1.087	−0.319	0.760	−0.258	1.303	−0.340	0.628	−0.217
	0.2	0.780	−0.526	0.554	−0.419	0.927	−0.559	0.479	−0.365
	0.3	0.404	−0.513	0.297	−0.437	0.474	−0.535	0.251	−0.395

2.6.2. Calculation of the crack tip stress fields

The stress fields around left and right crack tips are plotted by using both finite element method results and asymptotic equations. The finite element solution gives the two dimensional stress fields at every node. Asymptotic stress values can be calculated at the same coordinates using Equations 2.1 - 2.3.

The global coordinate system is at the center of the plate as shown in Figure 2.12. However, since the stress contours around the crack tip is examined, the coordinate system is transformed to one of the crack tip which is under investigation (left or right crack tip) and the stress values are calculated by using the new coordinates of each node. By changing the coordinate system, the crack is assumed to be flat and the change of E is adjusted to get the effect of the crack angle. By transforming the x-coordinate Equation 2.19 becomes;

$$E(x) = E_0 e^{\beta x} = E_0 e^{\beta(x_1 cos(\alpha) - y_1 sin\alpha + a cos\alpha)} \tag{2.24}$$

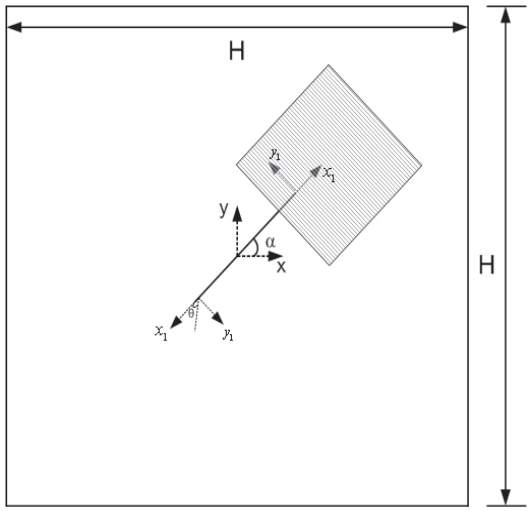

Figure 2.13. The region where stress contours are calculated for the right crack tip

In Figures 2.14 - 2.16 stress contours of σ_{xx}, σ_{xy} and σ_{yy} are plotted for $\alpha = 0^o$ with $\beta a = 0.25$ to compare finite element (FE) and the asymptotic equation (ASY) results. The plots cover x/h by y/h region which is the new coordinate system used at the crack tip and the crack tip is located at $x/h = 0$.

The stress contours obtained using finite element data has the same trend as those of asymptotic solutions. σ_{yy} values are much higher than the other stress values as expected. Since there is a geometrical symmetry, the compressive stresses and shear stresses are lower.

The stress contours are not sufficient to find the extent and shape of the K-dominant region around the crack tip in a linearly elastic two dimensional domain. The difference between finite element results and those of the asymptotic equations can be calculated at each node in the field by using an error parameter, e, given by Equation 2.18. Then, error contours are plotted. In Figure 2.17, error contours for $\alpha = 0^o$ with $\beta a = 0.25$ are given. The error parameter, e, gets smaller as the crack tip is approached; as expected the asymptotic solution gives good results near the crack tip.

The analysis of the model given in Figure 2.4 (b) is done by Yilmaz [29] for pure mode I. A uniform rectangular mesh is used in ANSYS. The stress intensity factors are calculated using the j-integral technique given by Anlas [28]. Figures 2.18 - 2.19 shows the comparison of error contours of present study and the results of Yılmaz [29] for $E_2/E_1 = 10$ ($\beta = 0.1151$) and $a/h = 0.3$. The normalized stress intensity factor, k_1 is taken as 1.2291 as given by Erdogan and Wu [14]. There are some differences in error parameter e because in the present study, a finer mesh is used, and the analysis is carried out by using a different finite element program. In Figures 2.20 - 2.21, finite element (FE) results of σ_{yy} and the σ_{yy} values obtained from asymptotic equations (ASY) are plotted on the symmetry axis between the crack tip and the right edge of the plate. The results again match well.

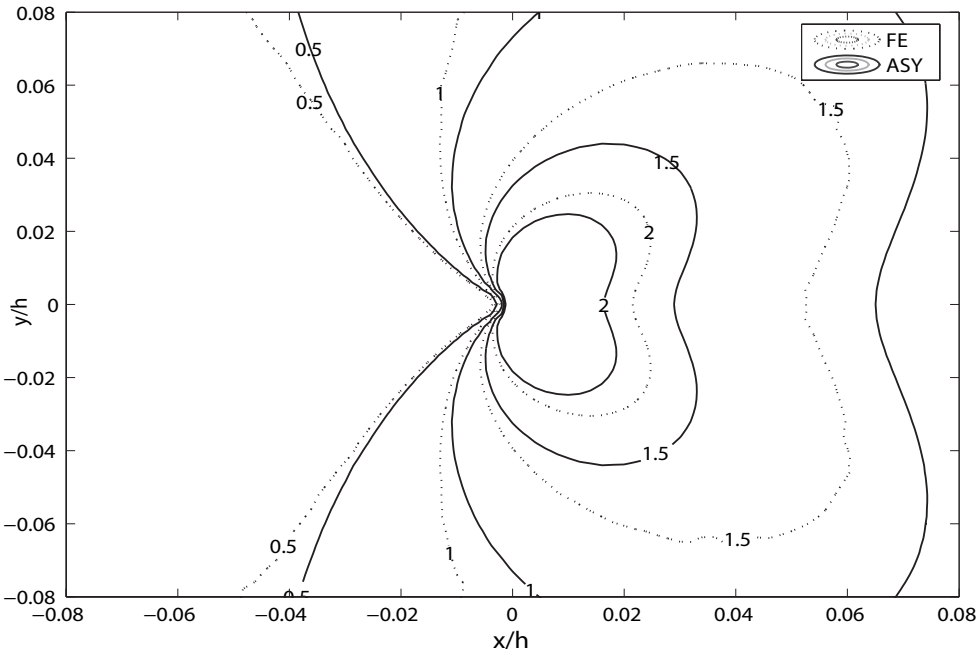

Figure 2.14. σ_{yy} contours for $\alpha = 0^o$ and $\beta a = 0.25$ around right crack tip

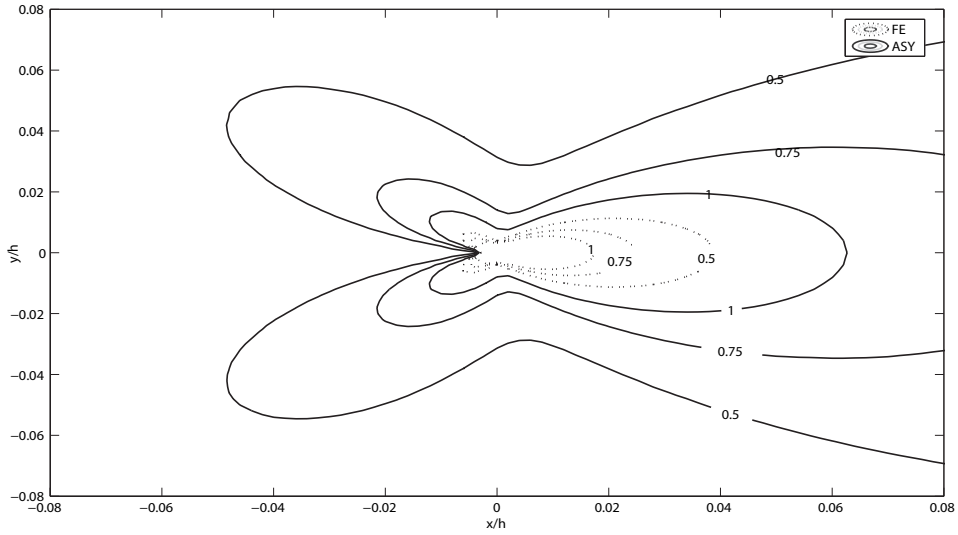

Figure 2.15. σ_{xx} contours for $\alpha = 0^o$ and $\beta a = 0.25$ around right crack tip

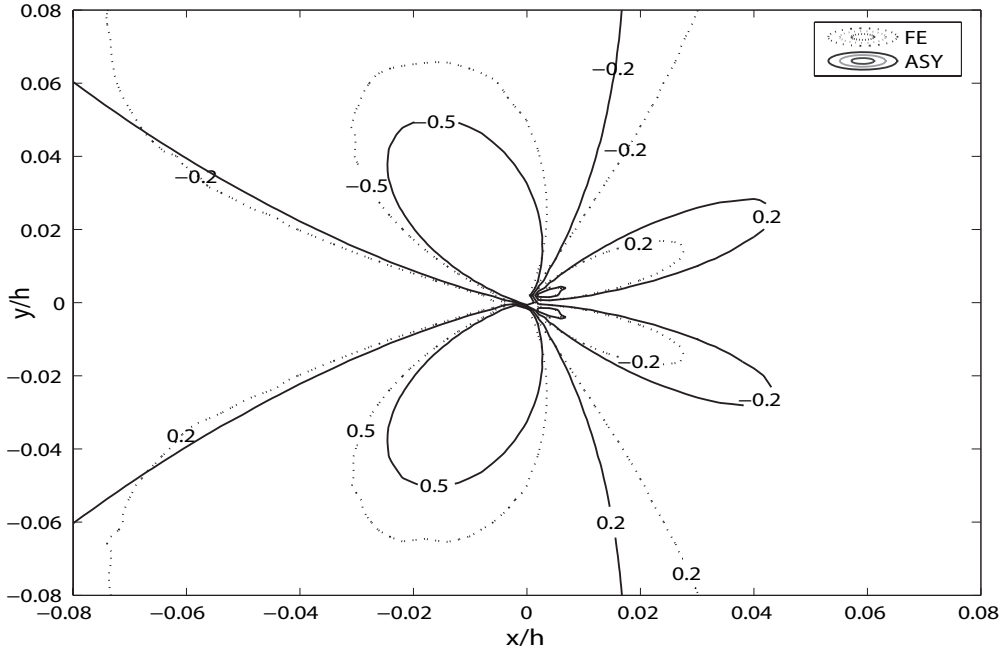

Figure 2.16. σ_{xy} contours for $\alpha = 0^o$ and $\beta a = 0.25$ around right crack tip

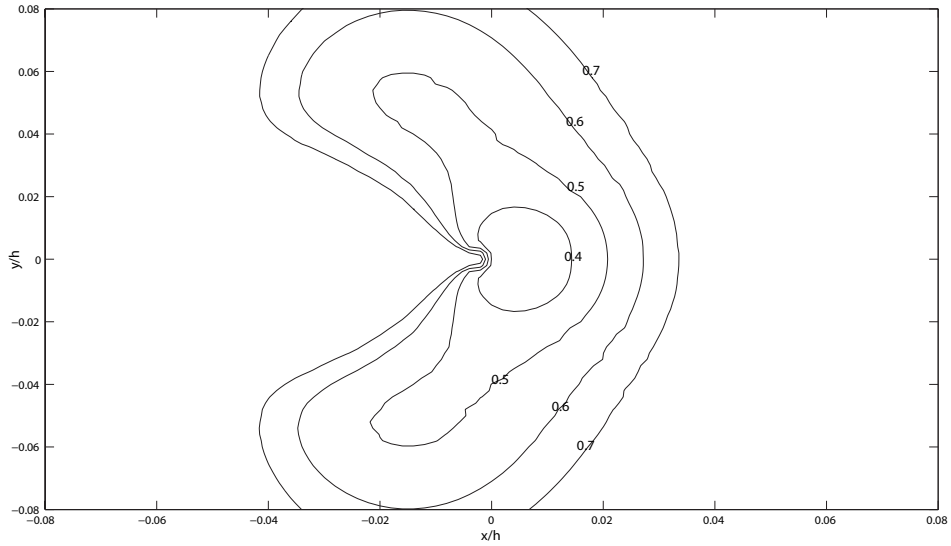

Figure 2.17. Error contours for $\alpha = 0^o$ and $\beta a = 0.25$ around right crack tip

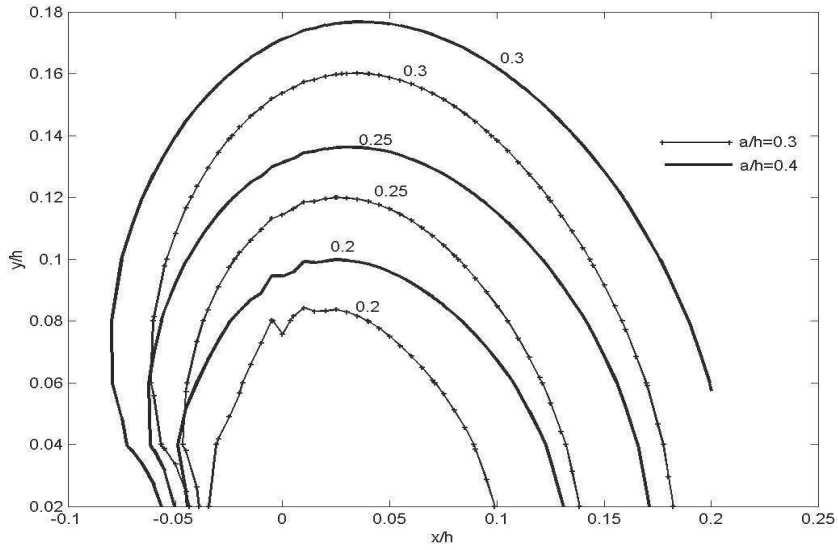

Figure 2.18. Error contours for $\alpha = 0^o$, $E_2/E_1 = 10$, $a/h = 0.3$ by Yılmaz [29]

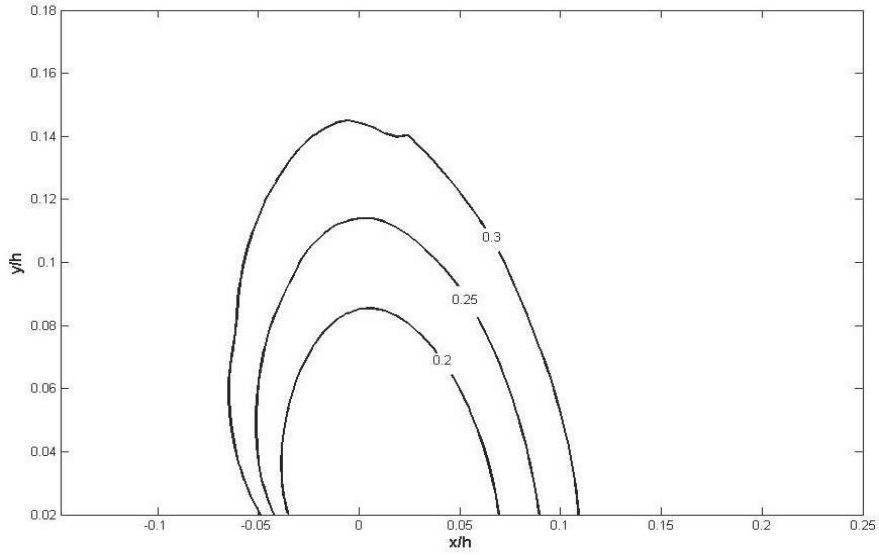

Figure 2.19. Error contours for $\alpha = 0^o$, $E_2/E_1 = 10$, $a/h = 0.3$

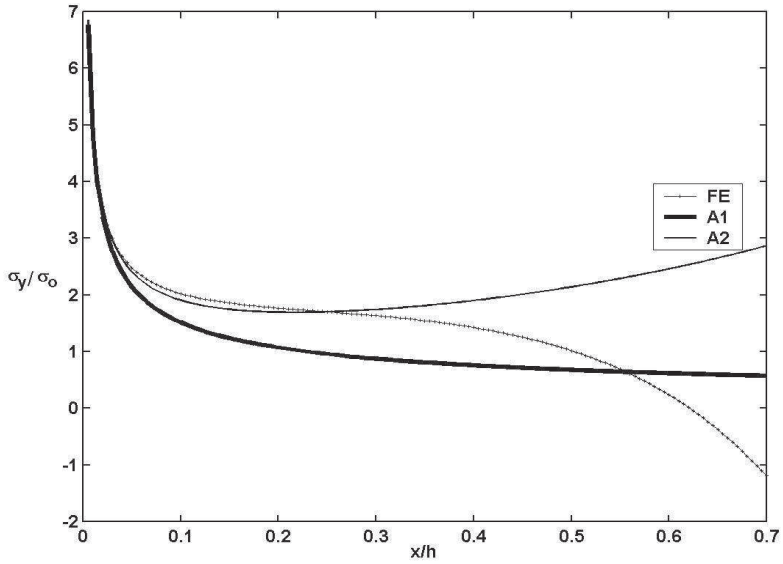

Figure 2.20. Normalized σ_{yy} for $\alpha = 0^o$, $E_2/E_1 = 10$, $a/h = 0.3$ by Yılmaz [29]

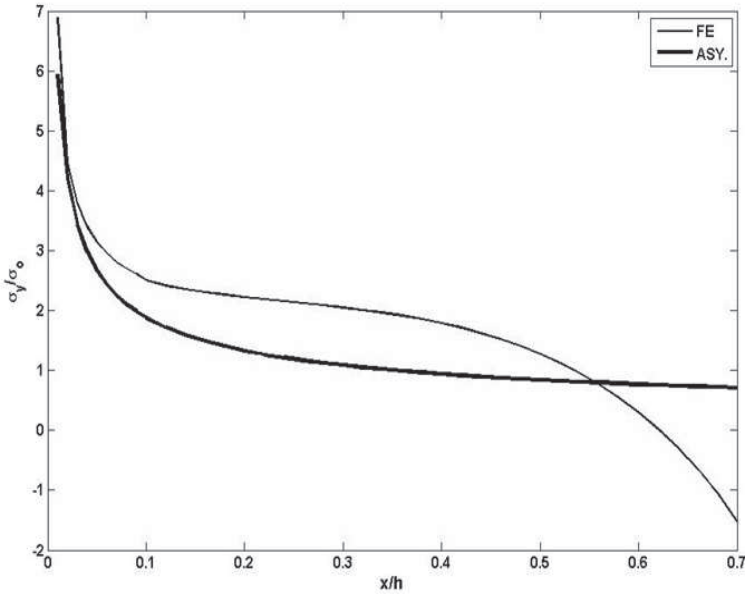

Figure 2.21. Normalized σ_{yy} for $\alpha = 0^o$, $E_2/E_1 = 10$, $a/h = 0.3$

3. MIXED MODE K-DOMINANCE FOR CENTER CRACKED FGM PLATE

3.1. General

In this chapter, a plate made of FGM with a center crack is analyzed with the numerical procedure outlined in Chapter 2. However, this time the upper and lower edges of the plate are loaded by a uniform traction, σ_0 and the crack angle is α, as shown. The new model is given in Figure 3.1.

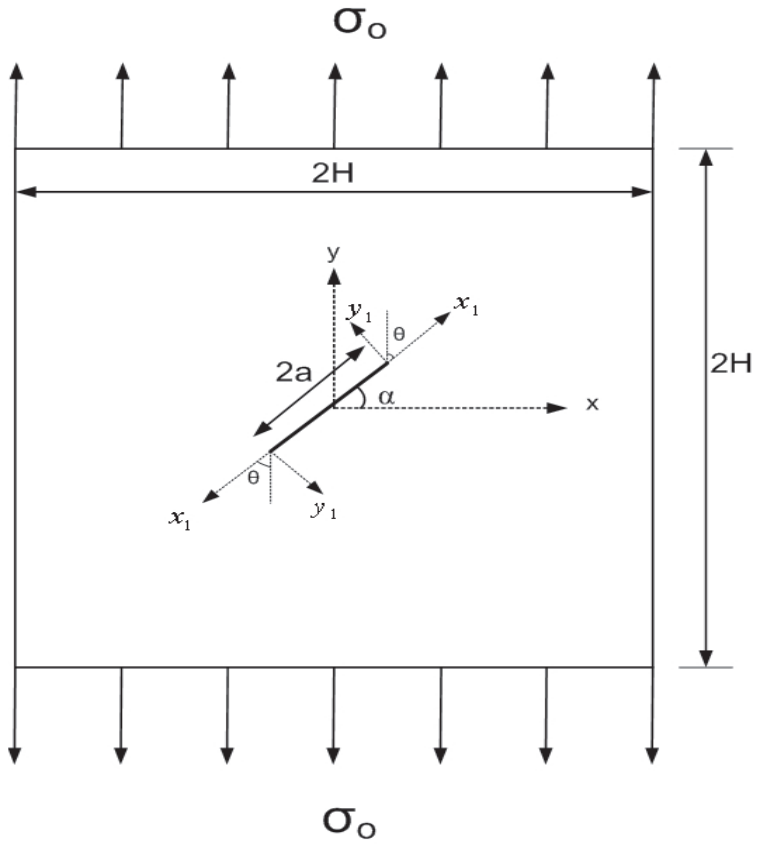

Figure 3.1. The model of center crack plate of FGM

3.2. Stress Intensity Factors

Normalized stress intensity factors are calculated for different crack lengths of $a/h = 0.2, 0.3, 0.4$ with $E_2/E_1 = 1, 2, 5, 10, 20$ and crack angle as $\alpha = 0^o, 15^o, 30^o, 45^o$ and 60^o. Results for both right and left crack tips are tabulated in Tables 3.2, 3.3 and 3.4. Since the loading is uniform the stress intensity factors are normalized by dividing K_I and K_{II} by $\sigma_o\sqrt{\pi a}$ instead of $\overline{\varepsilon}E_0\sqrt{\pi a}$ given in Equation 2.22.

In the previous section, material gradient is expressed in terms of β. Thus, β can be calculated using E_2/E_1 values. The β values are given in Table 3.1. The related equation is $E_2/E_1 = e^{\beta H}$.

Table 3.1. β values used for center cracked FGM plate

E_2/E_1	β
1	0
2	0.0347
5	0.0847
10	0.1151
20	0.1498

As it was discussed in the previous chapter, k_I values decrease as α increases and k_{II} values increase as α increases in each model. However, k_{II} values start to increase after the crack angle, α, becomes 45^o. Besides, an increase in E_2/E_1 ratio leads to an increase in mode I stress intensity factors and a decrease k_{II} for right crack tip and opposite behavior for left crack tip. It is also noted that increasing the crack length causes the increase in both k_I and k_{II} values. Figure 3.2 and Figure 3.3 are examples that show the change in stress intensity factors for the models with crack angle $a/h = 0.2$ at right crack tip.

Table 3.2. Normalized stress intensity factors for a/h = 0.2

	a/h=0.2				
E2/E1	α	$k_I(a)$	$k_{II}(a)$	$k_I(-a)$	k_{II}(-a)
1	0^o	1.051	0	1.051	0
	15^o	0.976	0.270	0.976	0.260
	30^o	0.784	0.446	0.784	0.446
	45^o	0.528	0.521	0.528	0.521
	60^o	0.263	0.460	0.263	0.460
2	0^o	1.075	0	1.036	0
	15^o	0.999	0.244	0.977	0.250
	30^o	0.802	0.447	0.774	0.443
	45^o	0.537	0.520	0.527	0.514
	60^o	0.272	0.460	0.263	0.457
5	0^o	1.114	0	1.043	0
	15^o	1.074	0.244	0.975	0.236
	30^o	0.848	0.434	0.770	0.424
	45^o	0.579	0.519	0.527	0.510
	60^o	0.311	0.460	0.267	0.458
10	0^o	1.221	0	1.060	0
	15^o	1.099	0.243	0.974	0.212
	30^o	0.896	0.418	0.790	0.398
	45^o	0.626	0.518	0.524	0.491
	60^o	0.357	0.459	0.266	0.454
20	0^o	1.236	0	1.061	0
	15^o	1.149	0.195	0.971	0.169
	30^o	0.939	0.375	0.770	0.347
	45^o	0.671	0.486	0.529	0.464
	60^o	0.416	0.457	0.262	0.453

Table 3.3. Normalized stress intensity factors for a/h = 0.3

	a/h=0.3				
E2/E1	α	$k_I(a)$	$k_{II}(a)$	$k_I(-a)$	k_{II}(-a)
1	0^o	1.119	0	1.119	0
	15^o	1.042	0.278	1.042	0.278
	30^o	0.835	0.467	0.835	0.467
	45^o	0.553	0.537	0.553	0.537
	60^o	0.276	0.463	0.276	0.463
2	0^o	1.153	0	1.091	0
	15^o	1.074	0.263	1.019	0.249
	30^o	0.863	0.467	0.825	0.461
	45^o	0.575	0.536	0.548	0.536
	60^o	0.297	0.461	0.275	0.462
5	0^o	1.227	0	1.077	0
	15^o	1.144	0.236	1.005	0.215
	30^o	0.923	0.448	0.822	0.442
	45^o	0.627	0.529	0.544	0.526
	60^o	0.309	0.460	0.270	0.449
10	0^o	1.295	0	1.074	0
	15^o	1.215	0.221	1.004	0.189
	30^o	0.973	0.405	0.820	0.399
	45^o	0.679	0.516	0.553	0.511
	60^o	0.420	0.458	0.269	0.448
20	0^o	1.360	0	1.069	0
	15^o	1.268	0.163	1.005	0.186
	30^o	1.032	0.404	0.818	0.387
	45^o	0.698	0.483	0.558	0.465
	60^o	0.504	0.449	0.267	0.442

Table 3.4. Normalized stress intensity factors for a/h = 0.4

	a/h=0.4				
E2/E1	α	$k_I(a)$	$k_{II}(a)$	$k_I(-a)$	k_{II}(-a)
1	0^o	1.210	0	1.210	0
	15^o	1.130	0.290	1.130	0.290
	30^o	0.905	0.496	0.905	0.496
	45^o	0.601	0.576	0.601	0.576
	60^o	0.302	0.490	0.302	0.490
2	0^o	1.276	0	1.174	0
	15^o	1.171	0.287	1.120	0.289
	30^o	0.956	0.503	0.882	0.491
	45^o	0.637	0.576	0.586	0.566
	60^o	0.324	0.492	0.302	0.486
5	0^o	1.414	0	1.152	0
	15^o	1.270	0.283	1.120	0.286
	30^o	1.063	0.502	0.875	0.478
	45^o	0.722	0.575	0.585	0.552
	60^o	0.390	0.491	0.307	0.478
10	0^o	1.567	0	1.146	0
	15^o	1.383	0.280	1.114	0.284
	30^o	1.181	0.499	0.873	0.467
	45^o	0.816	0.572	0.580	0.541
	60^o	0.466	0.483	0.305	0.469
20	0^o	1.760	0	1.139	0
	15^o	1.527	0.270	1.150	0.281
	30^o	1.331	0.497	0.872	0.458
	45^o	0.935	0.561	0.578	0.527
	60^o	0.563	0.470	0.304	0.457

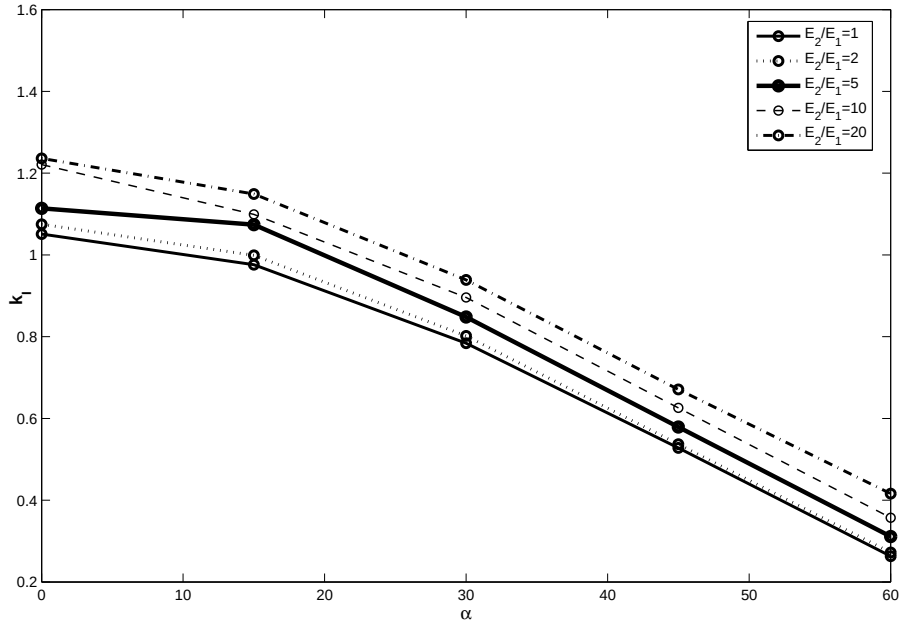

Figure 3.2. Mode I SIFs vs α for a/h=0.2 at right crack tip

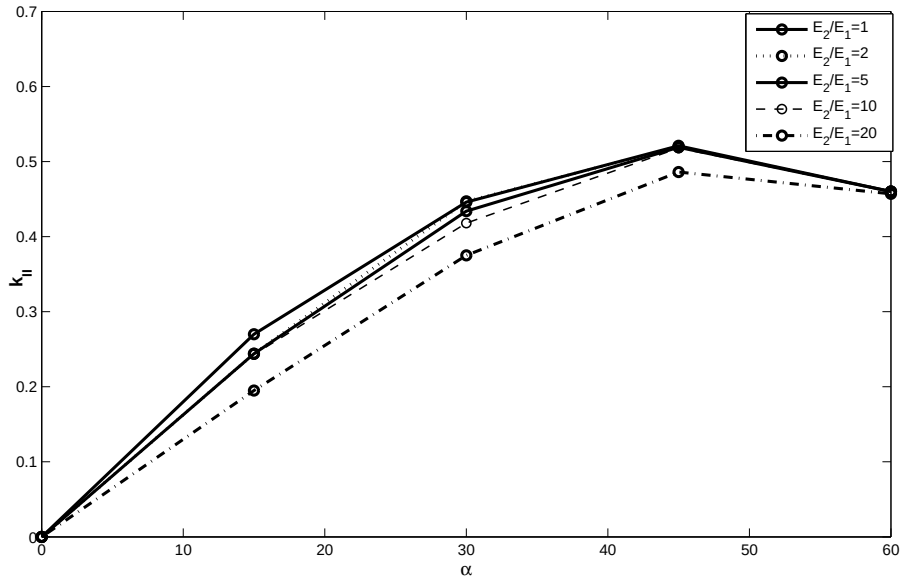

Figure 3.3. Mode II SIF vs α for a/h=0.2 at right crack tip

3.3. Calculation of K-dominant Region

After calculating the stress intensity factors, K-dominant region is studied in three steps. First, the effect of material nonhomogeneity on K-dominance is examined. Then, the extent of K-dominant region with change in crack length is analyzed. Last, the effect of mode mixity on K-dominance is studied by changing the crack angle.

The coordinate system of the model is shifted to the crack tip, and the results of the finite element solution and the results of asymptotic equations are recalculated using this new coordinate system. As a result of this coordinate transformation, the crack is flat and the elastic modulus is changing with x and y, as shown in Figure 2.13.

In all steps, the first analysis is the calculation of the stress field in y-direction; σ_{yy} values obtained from the finite element solution (FE), and σ_{yy} values obtained from asymptotic equations (ASY) are plotted along the crack tip, on $\theta = 0$ direction between the crack tip and the edge of the plate. This stress is called the opening stress.

Second, a two dimensional visualization of the K-dominant region is made possible by comparing the finite element stress field to asymptotic stress field. The analysis is done by plotting the stress distribution directly ahead of the crack. Because the plate is subjected to tensile loading in y-direction only, use of σ_{yy} is sufficient for the analysis.

Last, the error parameter which is given in Equation 2.18 is calculated in a region around the crack tip. The extent of K-dominant region is plotted via error contours. In error contours all stress components are considered. The size of K-dominant region is investigated for the model of crack lengths of $a/h = 0.2$, 0.3, 0.4 with $E_2/E_1 = 1$, 2, 5, 10, 20 and crack angles $\alpha = 0^o$, 15^o, 30^o, 45^o and 60^o.

3.3.1. Effect of Material Nonhomogeneity on Extent of K-dominant Region

The change of K-dominance with material nonhomogeneity is studied in this section. Initially, σ_{yy}/σ_o versus x/h plots are given. The coordinate system is located

at the right crack tip, $x/h = 0$, the crack lies along the negative x-axis. The finite element solution (FE) and asymptotic solution (ASY) are obtained for $E_2/E_1 > 1$. Crack lengths used are $a/h = 0.3$ and the crack angles are $\alpha = 15^o$, 30^o, 45^o and 60^o.

In Figures 3.4 - 3.7, FE curves are given for $a/h = 0.3$. It can be seen that σ_{yy} values get larger as r$\rightarrow$ 0, the highest value occuring for $E_2/E_1 = 20$. Thus, increasing the nonhomogeneity from $E_2/E_1 = 2$ to $E_2/E_1 = 20$ increases the stress level. Figures 3.8 - 3.11 show ASY curves for the same cases. These curves are in agreement with FE curves. However, the ASY values are lower than the FE values. In all graphs plotted, the curves almost overlap. Thus, a log-log graph is plotted to magnify difference between the curves. An example of log-log curve is given in Figure 3.12 for $\alpha = 15^o$ and $a/h = 0.3$ around the right tip.

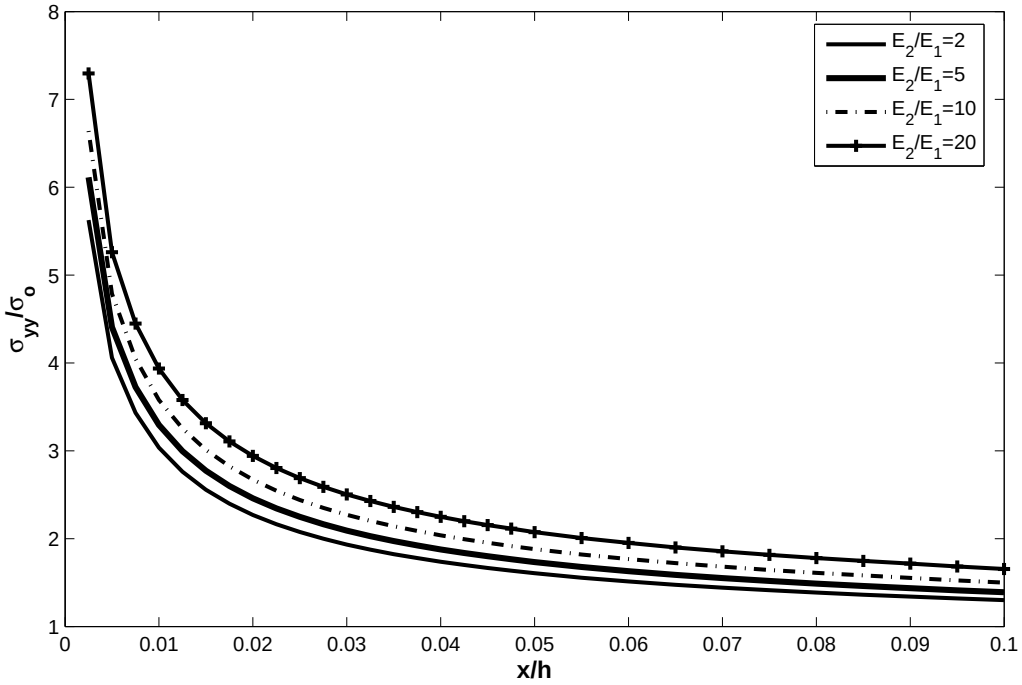

Figure 3.4. FE results for σ_{yy}/σ_o vs distance from crack tip, $a/h = 0.3$, $\alpha = 15^o$ for different E_2/E_1 ratios

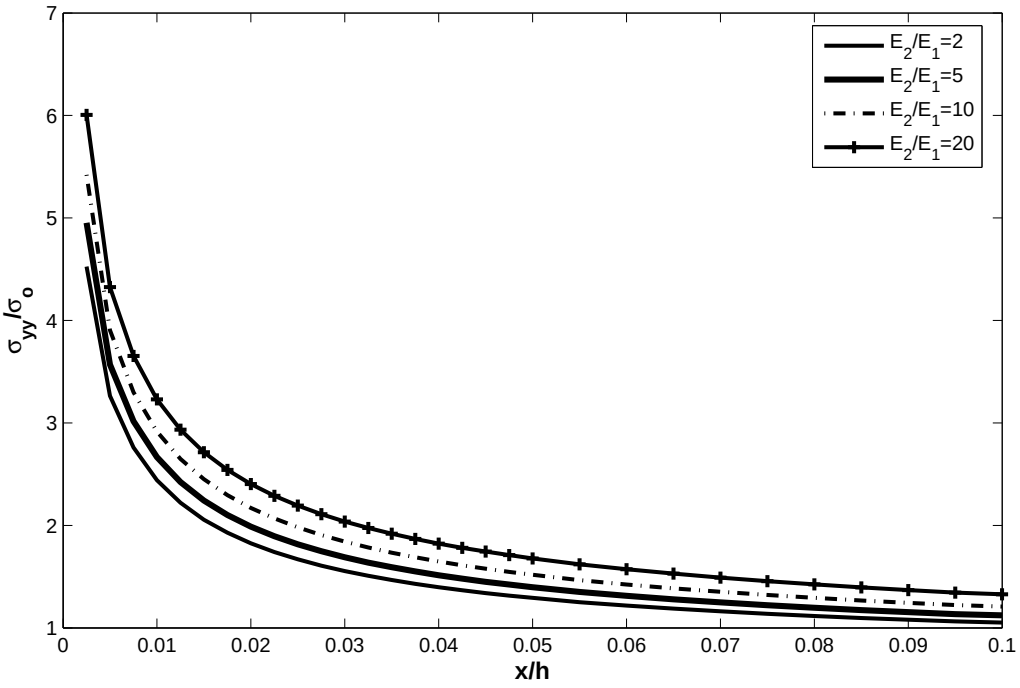

Figure 3.5. FE results for σ_{yy}/σ_o vs distance from crack tip, $a/h = 0.3$, $\alpha = 30^o$ for different E_2/E_1 ratios

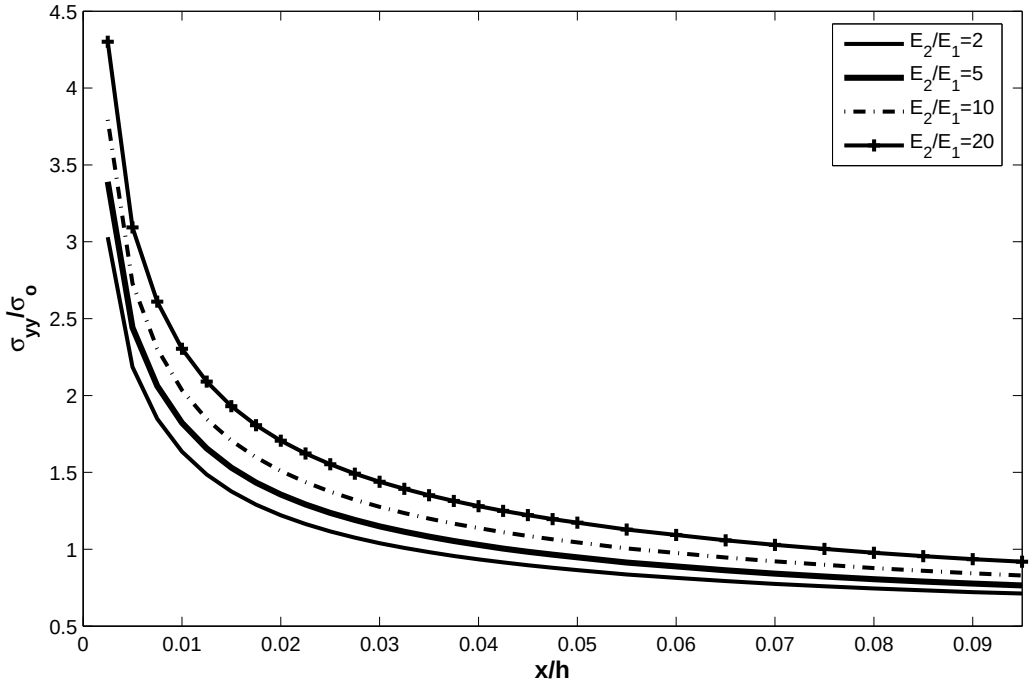

Figure 3.6. FE results for σ_{yy}/σ_o vs distance from crack tip, $a/h = 0.3$, $\alpha = 45^o$ for different E_2/E_1 ratios

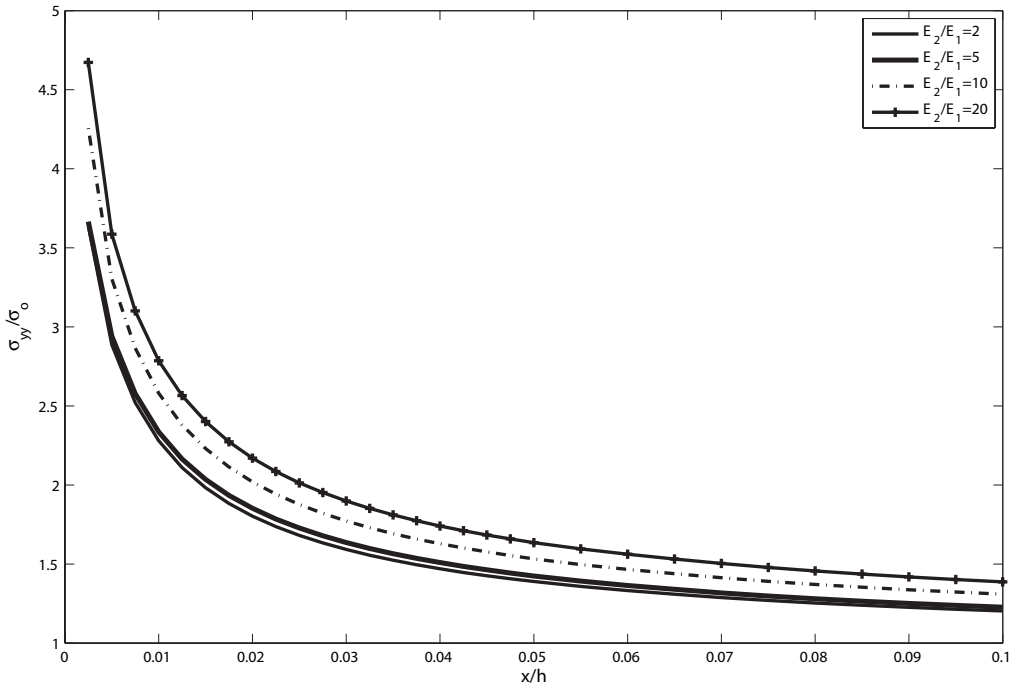

Figure 3.7. FE results for σ_{yy}/σ_o vs distance from crack tip, $a/h = 0.3$, $\alpha = 60^o$ for different E_2/E_1 ratios

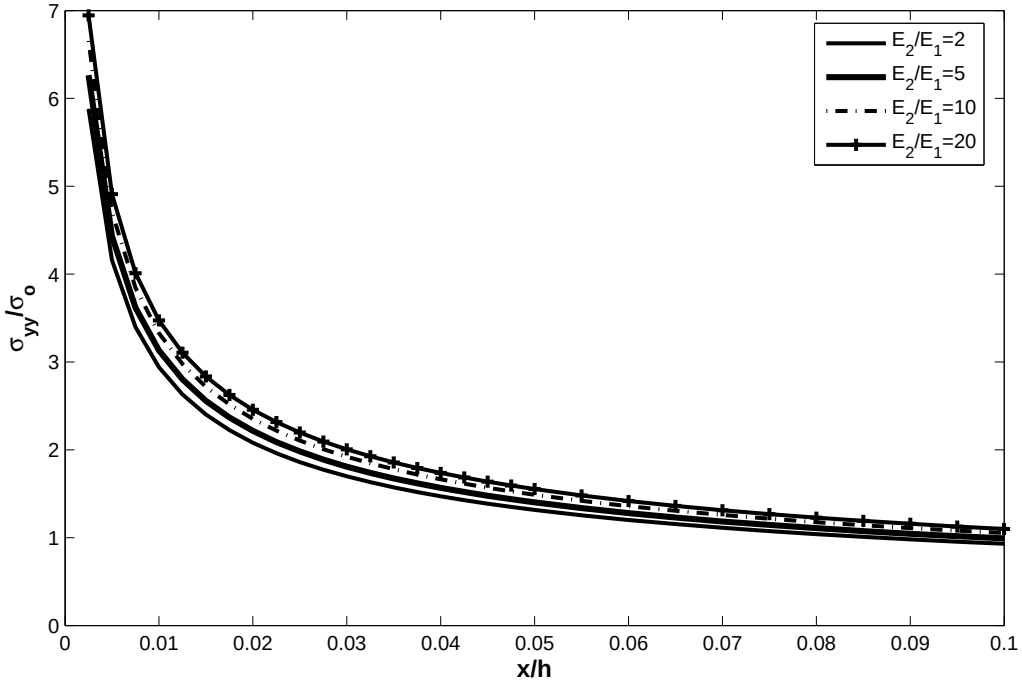

Figure 3.8. ASY results for σ_{yy}/σ_o vs distance from crack tip, $a/h = 0.3$, $\alpha = 15^o$ for different E_2/E_1 ratios

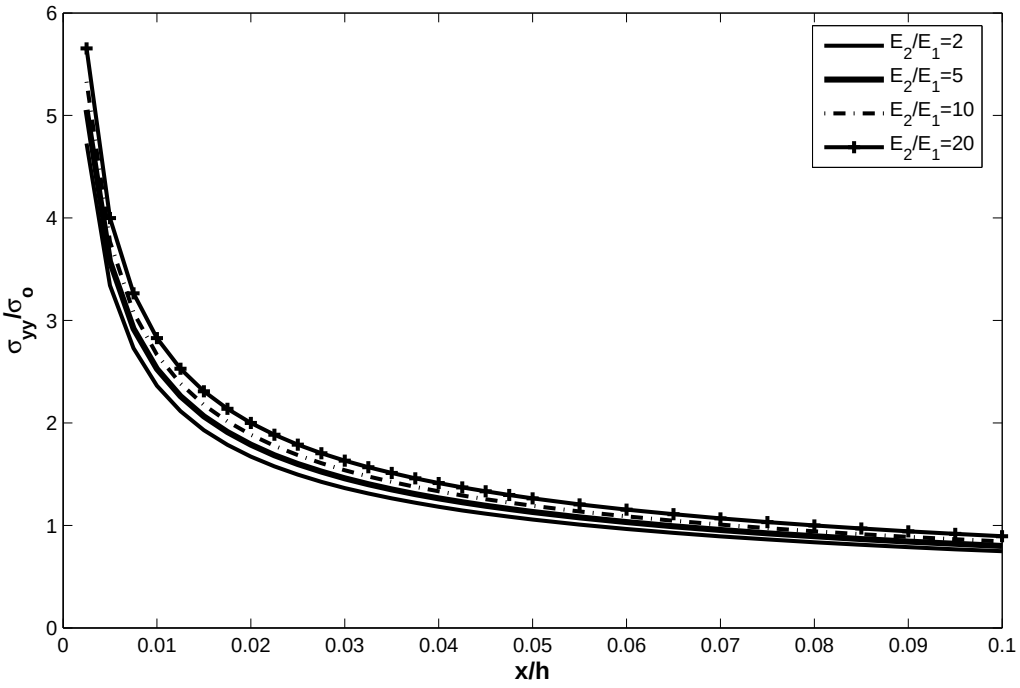

Figure 3.9. ASY results for σ_{yy}/σ_o vs distance from crack tip, $a/h = 0.3$, $\alpha = 30^o$ for different E_2/E_1 ratios

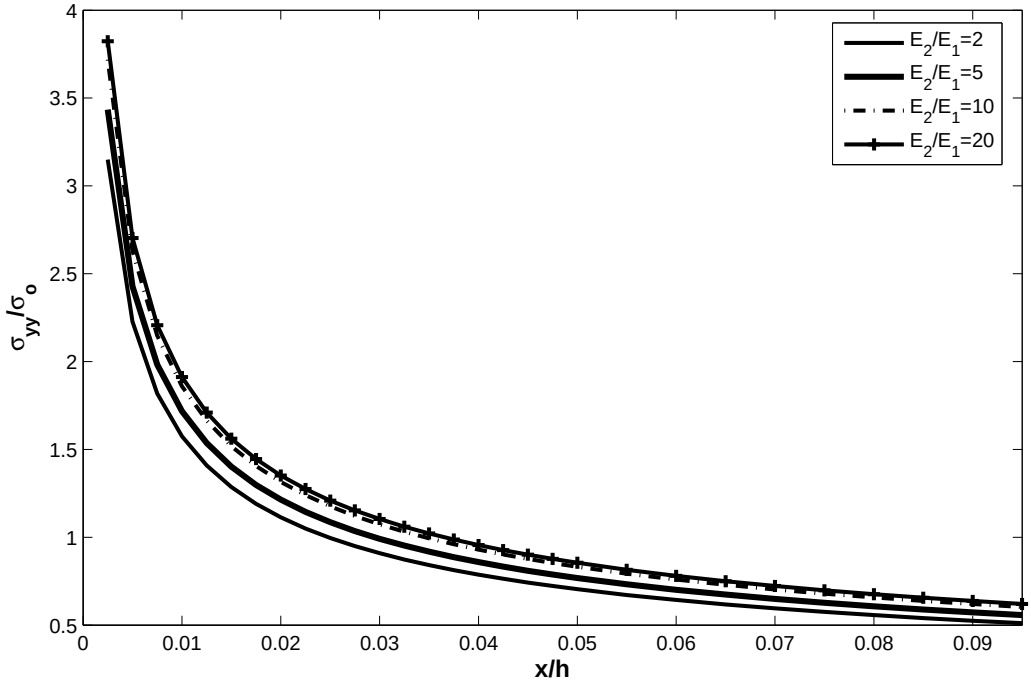

Figure 3.10. ASY results for σ_{yy}/σ_o vs distance from crack tip, $a/h = 0.3$, $\alpha = 45^o$ for different E_2/E_1 ratios

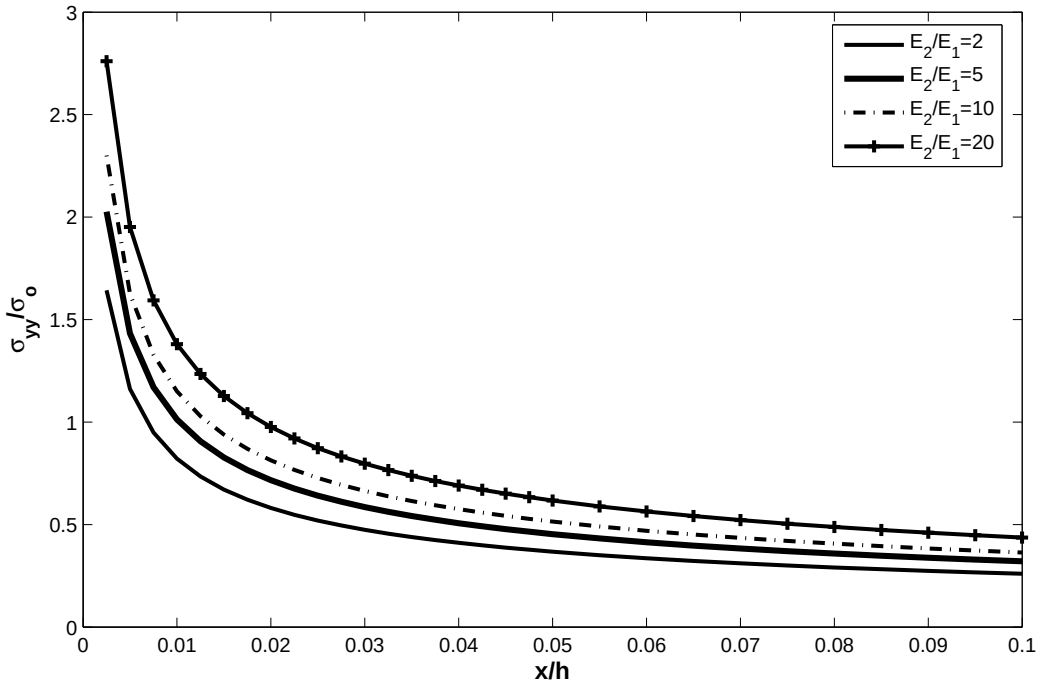

Figure 3.11. ASY results for σ_{yy}/σ_o vs distance from crack tip, $a/h = 0.3$, $\alpha = 60^o$ for different E_2/E_1 ratios

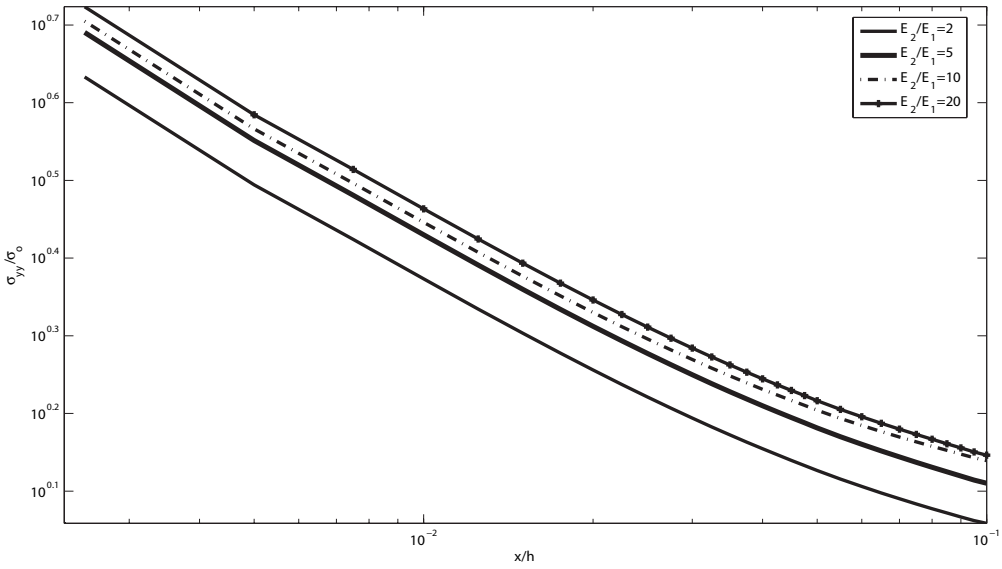

Figure 3.12. FE results for σ_{yy}/σ_o vs distance from crack tip, $a/h = 0.3$, $\alpha = 15^o$ for different E_2/E_1 ratios in log-log graph

Up to now plots of opening stress, σ_{yy}, are considered. However, the plots of σ_{yy} alone are not sufficient to find the extent and shape of the K-dominant region around the crack tip with different material nonhomogeneity. K-dominant region can only be found by comparing the asymptotic stress field around the crack tip to FE solutions. As a result, stress contours of σ_{yy} are plotted on two dimensional domain (x/h by y/h) near the right crack tip. Figures 3.13 - 3.28 show σ_{yy} stress contours for a/h = 0.2 with $\alpha = 15^o$, 30^o, 45^o and 60^o for different E_2/E_1 values. Each contour plot contains several contours for FE solution and ASY solution. Extent of K-dominant region increases when contours of FE and ASY solutions get closer to each other.

For the right tip of the crack, the material nonhomogeneity is increasing in the crack propagation direction. Thus, it is seen that the stress contours become larger for both finite element solution and asymptotic equation solution when the material nonhomogeneity increases. As a result, K-dominant region increases as the material nonhomogeneity increases for $a/h = 0.2$ and $\alpha = 15^o$, 30^o, 45^o and 60^o.

As it seen that FE curves are fluctuating at some points and they are not smooth. The reason for that is the finite elements' nodes are not always in line and sometimes they are spread since FE mesh does not have a definite shape in some region in the plate.

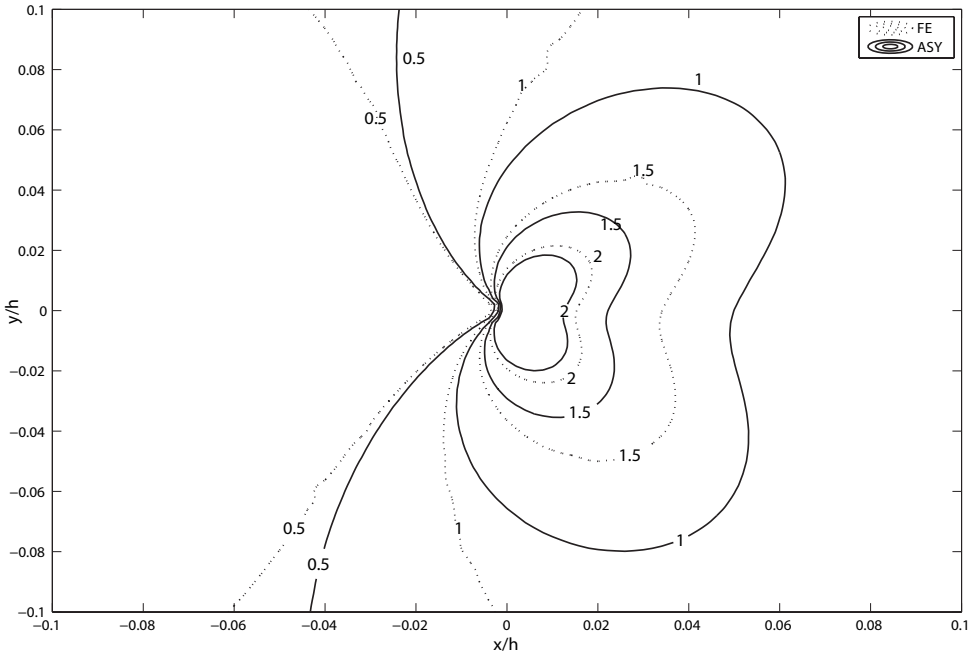

Figure 3.13. Contour plots of σ_{yy} for $E_2/E_1 = 2$, $\alpha = 15^o$ and a/h = 0.2 around right crack tip

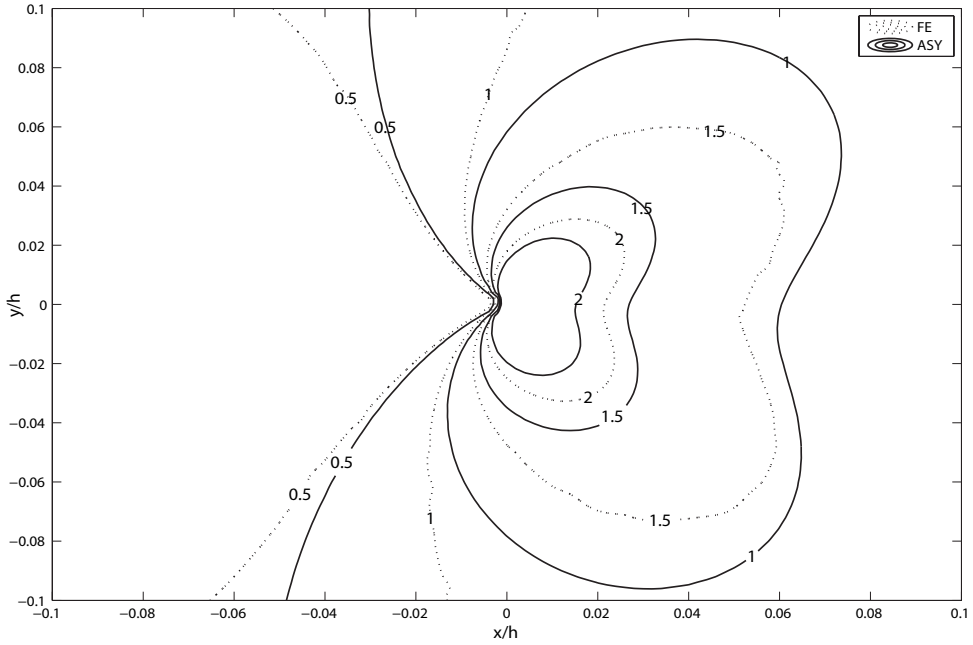

Figure 3.14. Contour plots of σ_{yy} for $E_2/E_1 = 5$, $\alpha = 15^o$ and a/h = 0.2 around right crack tip

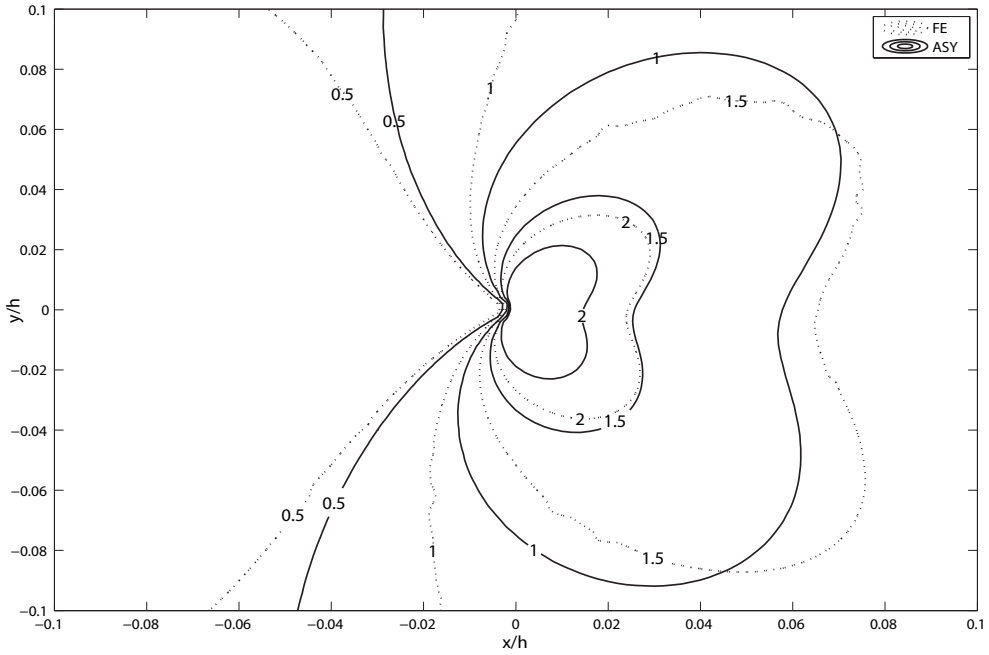

Figure 3.15. Contour plots of σ_{yy} for $E_2/E_1 = 10$, $\alpha = 15^o$ and a/h = 0.2 around right crack tip

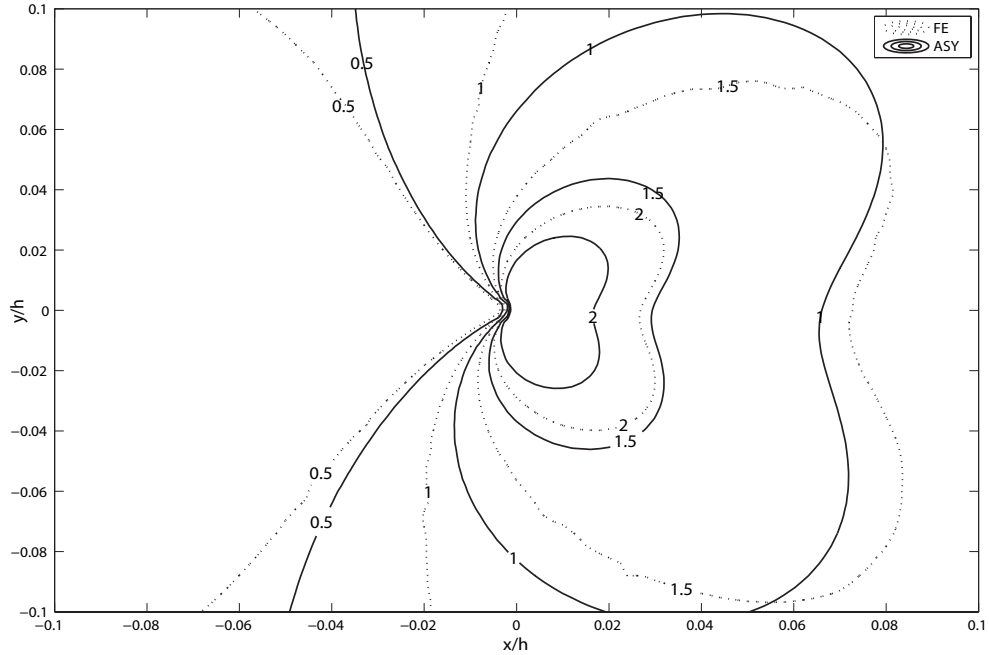

Figure 3.16. Contour plots of σ_{yy} for $E_2/E_1 = 20$, $\alpha = 15^o$ and a/h = 0.2 around right crack tip

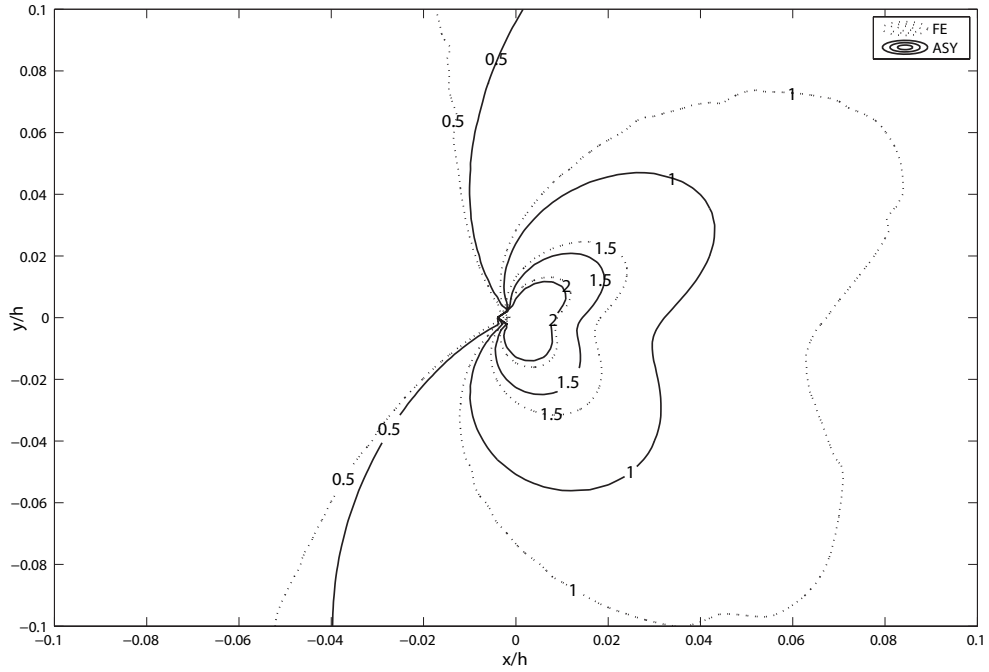

Figure 3.17. Contour plots of σ_{yy} for $E_2/E_1 = 2$, $\alpha = 30^o$ and a/h = 0.2 around right crack tip

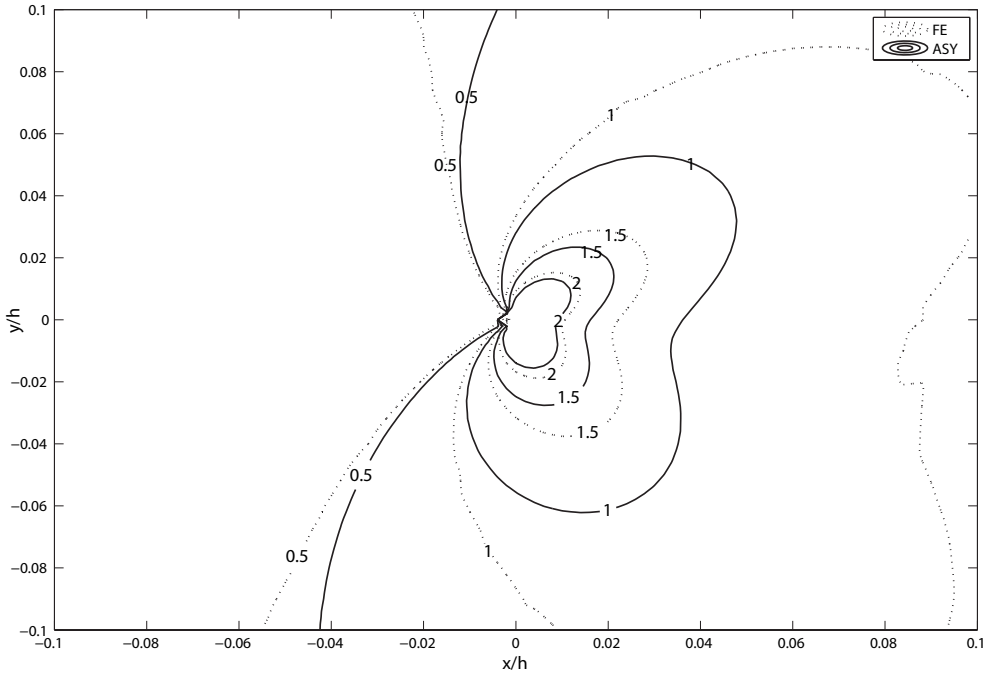

Figure 3.18. Contour plots of σ_{yy} for $E_2/E_1 = 5$, $\alpha = 30^o$ and a/h = 0.2 around right crack tip

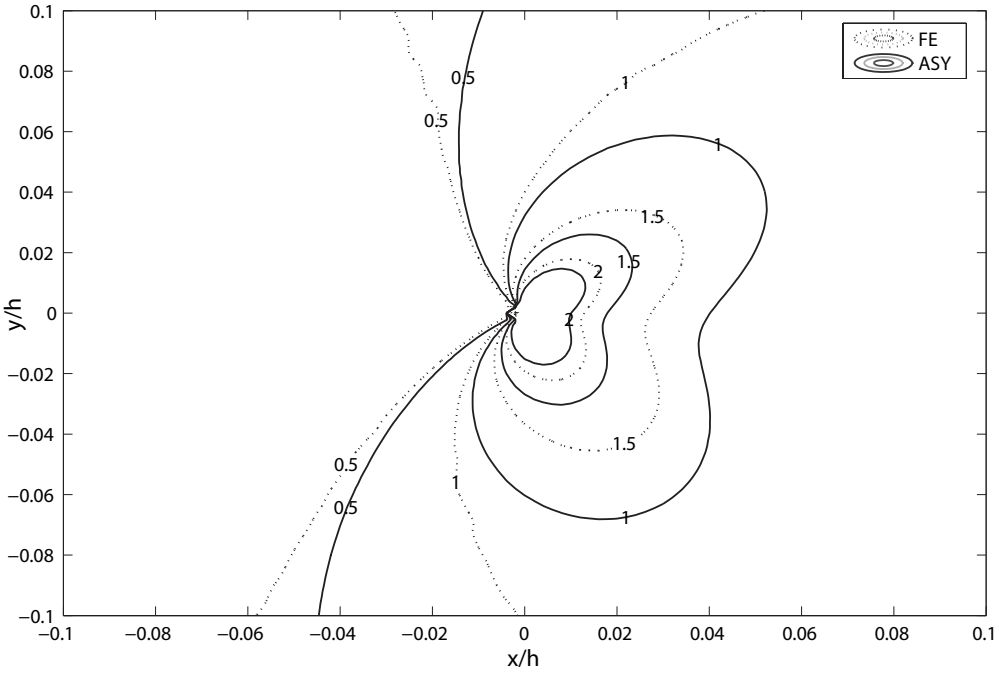

Figure 3.19. Contour plots of σ_{yy} for $E_2/E_1 = 10$, $\alpha = 30^o$ and a/h = 0.2 around right crack tip

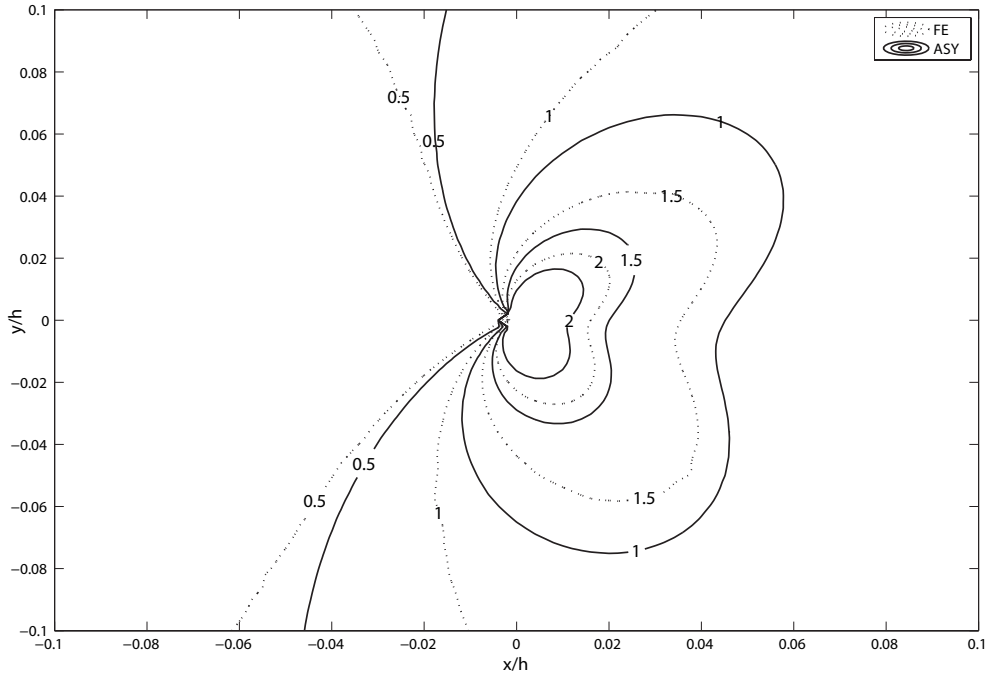

Figure 3.20. Contour plots of σ_{yy} for $E_2/E_1 = 20$, $\alpha = 30^o$ and a/h = 0.2 around right crack tip

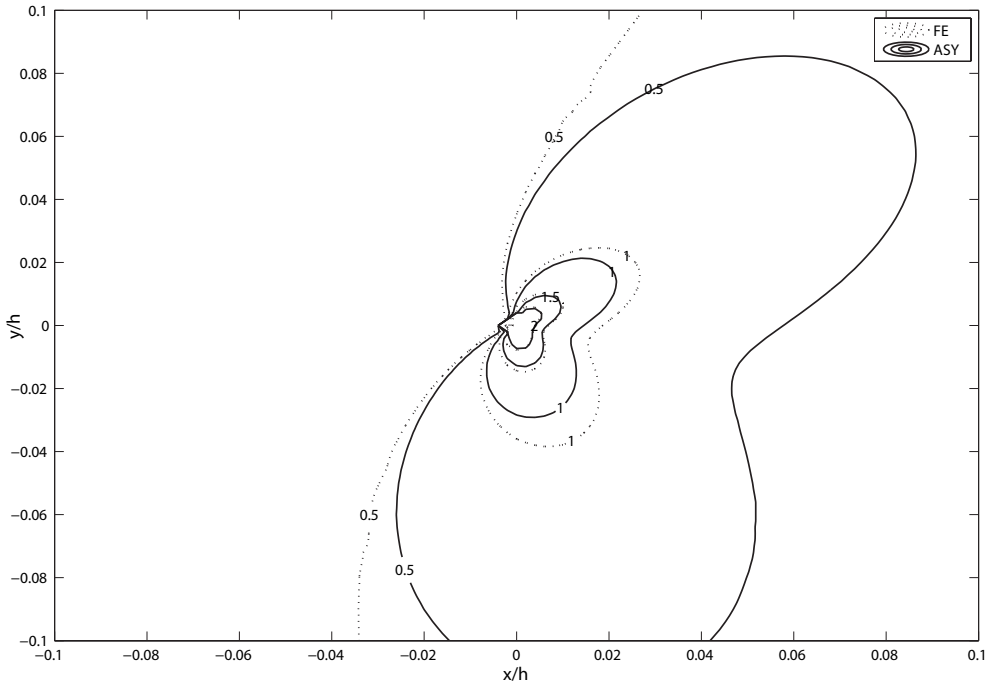

Figure 3.21. Contour plots of σ_{yy} for $E_2/E_1 = 2$, $\alpha = 45^o$ and a/h = 0.2 around right crack tip

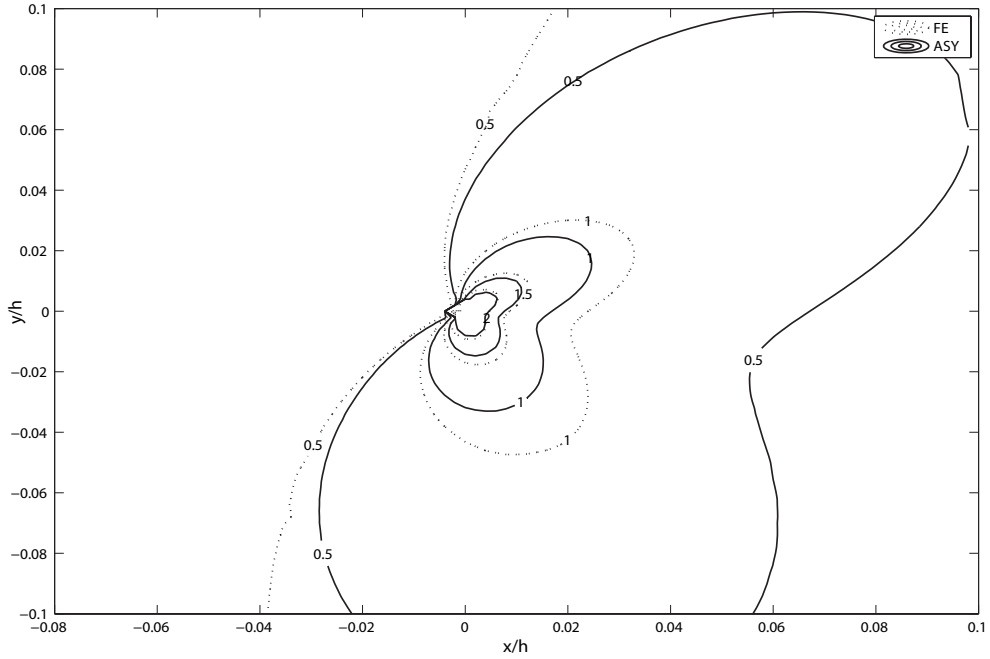

Figure 3.22. Contour plots of σ_{yy} for $E_2/E_1 = 5$, $\alpha = 45^o$ and a/h = 0.2 around right crack tip

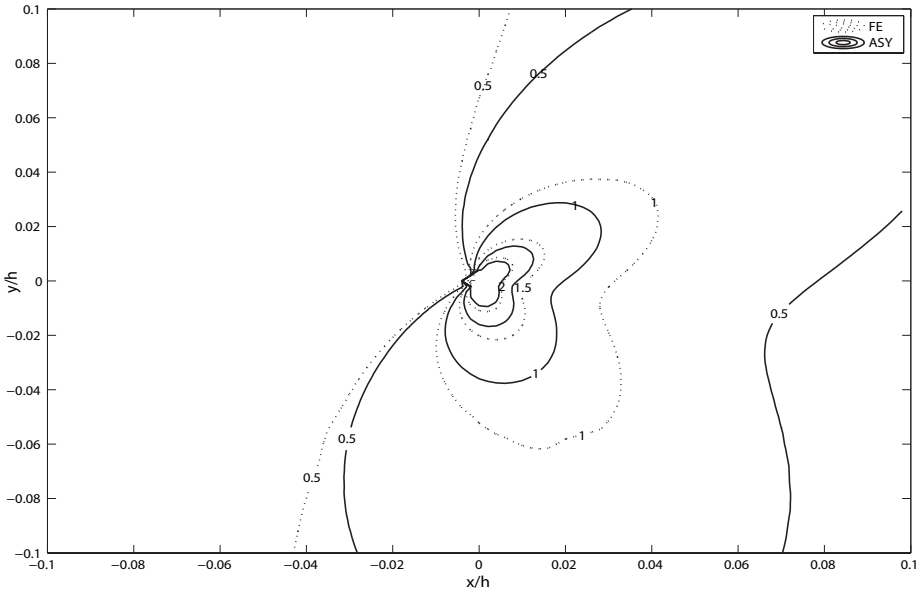

Figure 3.23. Contour plots of σ_{yy} for $E_2/E_1 = 10$, $\alpha = 45^o$ and a/h = 0.2 around right crack tip

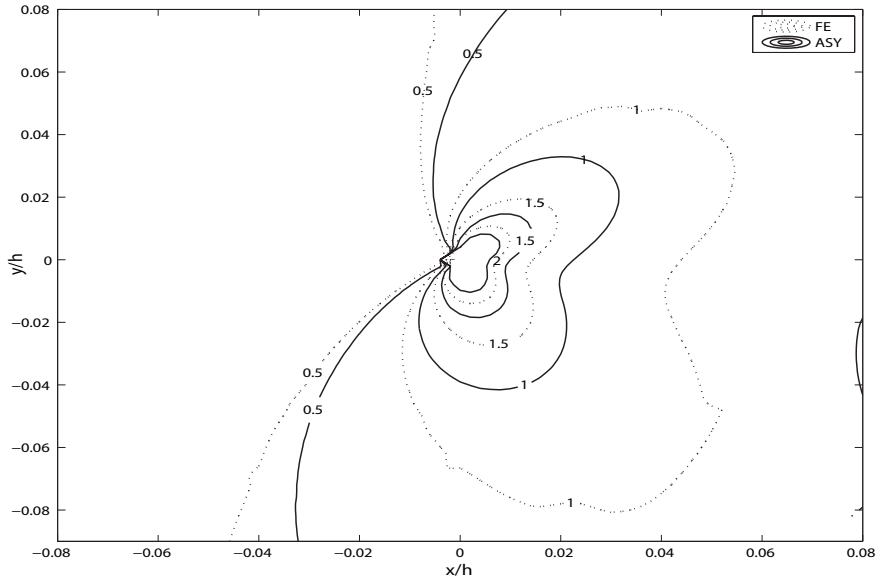

Figure 3.24. Contour plots of σ_{yy} for $E_2/E_1 = 20$, $\alpha = 45^o$ and a/h = 0.2 around right crack tip

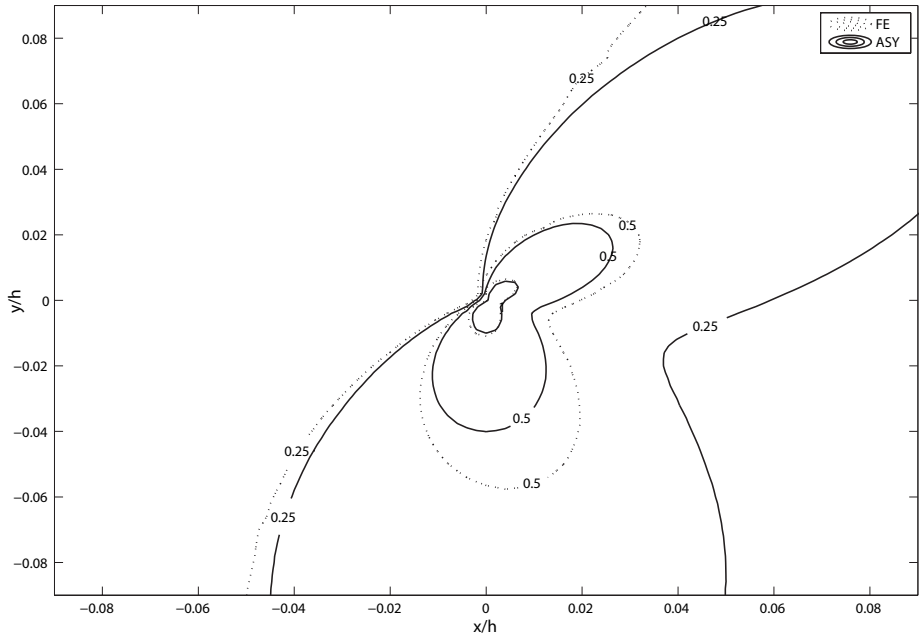

Figure 3.25. Contour plots of σ_{yy} for $E_2/E_1 = 2$, $\alpha = 60^o$ and a/h = 0.2 around right crack tip

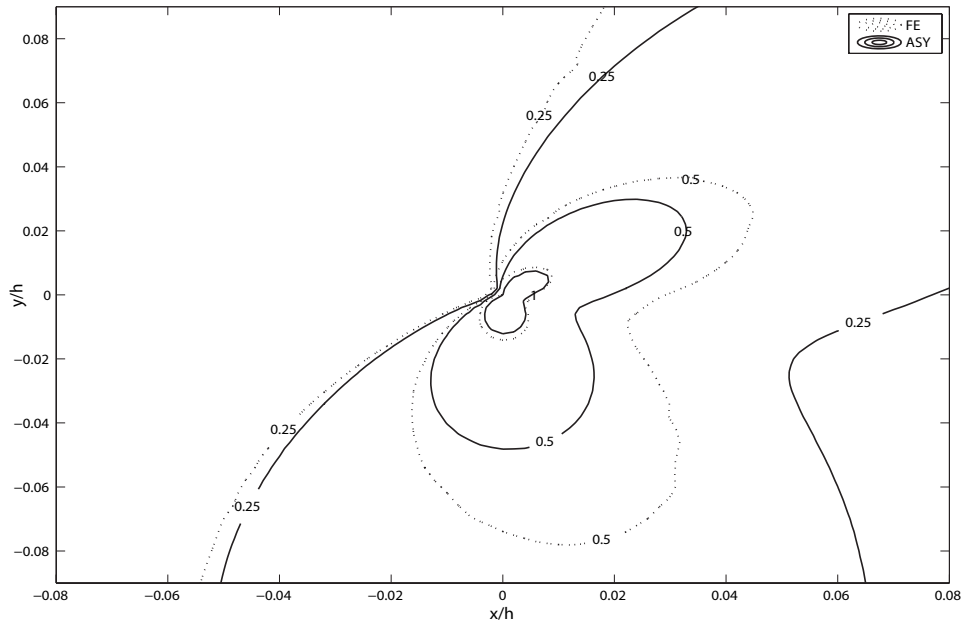

Figure 3.26. Contour plots of σ_{yy} for $E_2/E_1 = 5$, $\alpha = 60^o$ and a/h = 0.2 around right crack tip

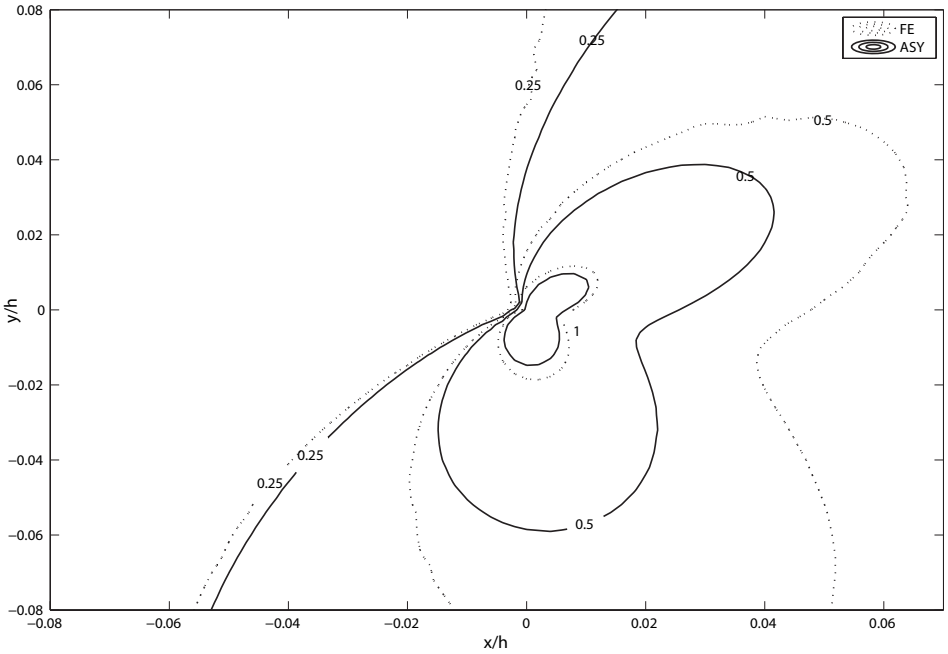

Figure 3.27. Contour plots of σ_{yy} for $E_2/E_1 = 10$, $\alpha = 60^o$ and a/h = 0.2 around right crack tip

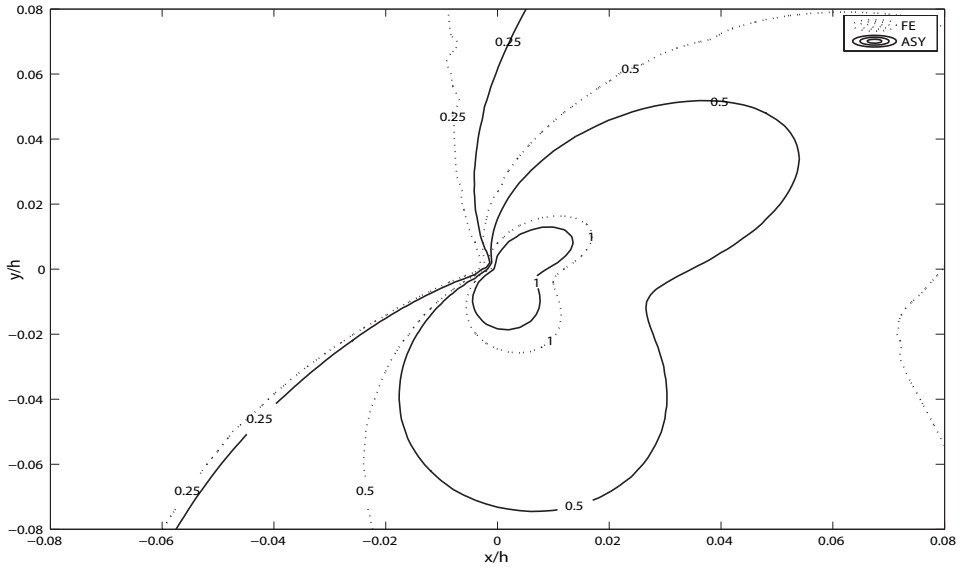

Figure 3.28. Contour plots of σ_{yy} for $E_2/E_1 = 20$, $\alpha = 60^o$ and a/h = 0.2 around right crack tip

A further analysis of the extent of K-dominant region can be better done by using error contours. Although differences between stress values of both solutions can be seen from figures of stress contours the difference and therefore the K-dominant region can be quantified at each point in the field by an error parameter [24];

$$e = \sqrt{\frac{(\sigma_{ij}^F - \sigma_{ij}^A)(\sigma_{ij}^F - \sigma_{ij}^A)}{\sigma_{ij}^A \sigma_{ij}^A}} \tag{3.1}$$

For error contours the plots cover x/h by y/h region, and the crack tip is located at $x/h = 0$. Figure 3.30 gives error contour for $\alpha = 0^o$ and $a/h = 0.2$ around right crack tip. It can be easily seen that K-dominant region is changing with changing nonhomogeneity. The error contours cover the smallest area for the homogeneous case and as E_2/E_1 increases contours cover larger area. Thus, as it is discussed with the stress contours K-dominant zone gets larger as material nonhomogeneity increases for the right crack tip. Similar observation are made for $\alpha = 15^o$, 30^o which are given in Figures 3.30 - 3.31. Again the K-dominant region grows as the material nonhomogenenity increases.

In all models, the elastic modulus increases in the crack propogation direction. It means that the right edge is stiffer than the left edge of the plate. The case where the elastic modulus decreases in the crack propogation direction is not given in this study. However, it can be said that investigating the behaviour around left crack tip can simulate such behavior. Thus, similar error contours are plotted for left crack tip in Figures 3.32 - 3.34. As it is expected, this time, the error contour is larger for homogeneous case, $E_2/E_1 = 1$, and the area covered diminishes as the material nonhomogeneity increases.

It can be concluded that if nonhomogeneity increases in the crack propogation direction, and if the material gradient is high near the crack tip, K-dominant region increases with increasing nonhomogeneity.

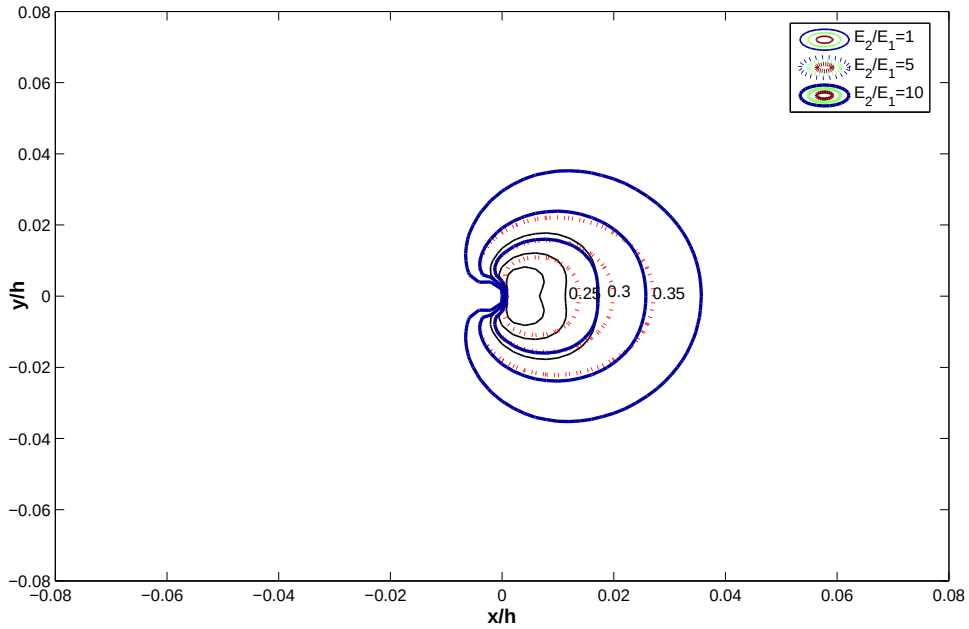

Figure 3.29. Error contours for different E_2/E_1 ratios, $a/h = 0.2$ and $\alpha = 0^o$ around right crack tip

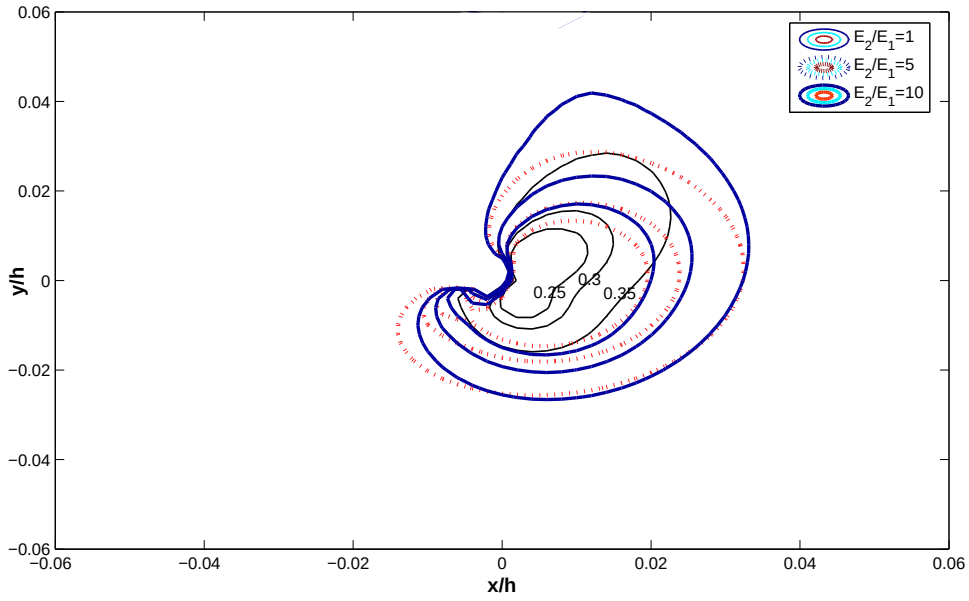

Figure 3.30. Error contours for different E_2/E_1 ratios, $a/h = 0.2$ and $\alpha = 15^o$ around right crack tip

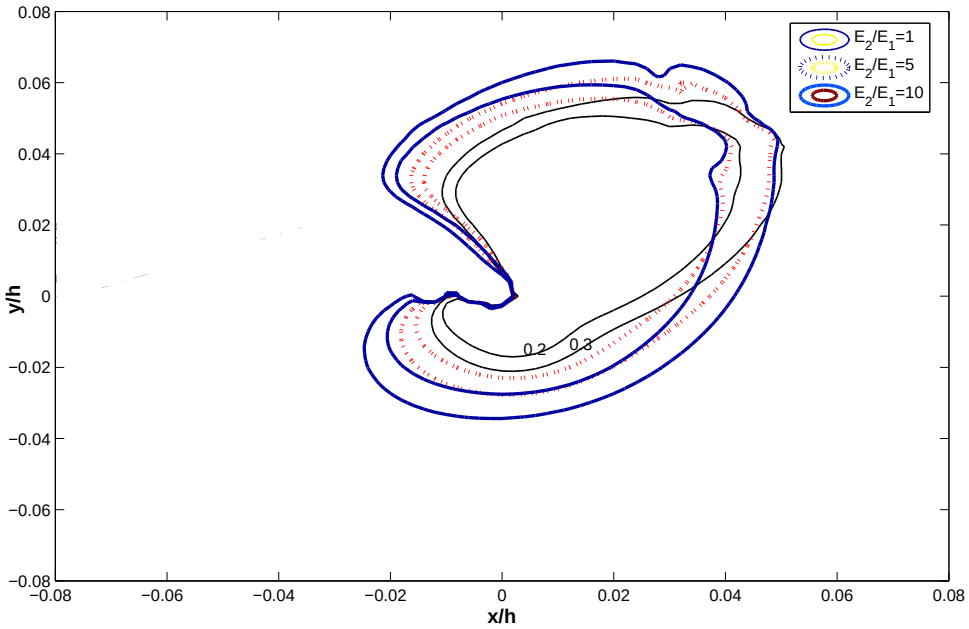

Figure 3.31. Error contours for different E_2/E_1 ratios, $a/h = 0.2$ and $\alpha = 30^o$ around right crack tip

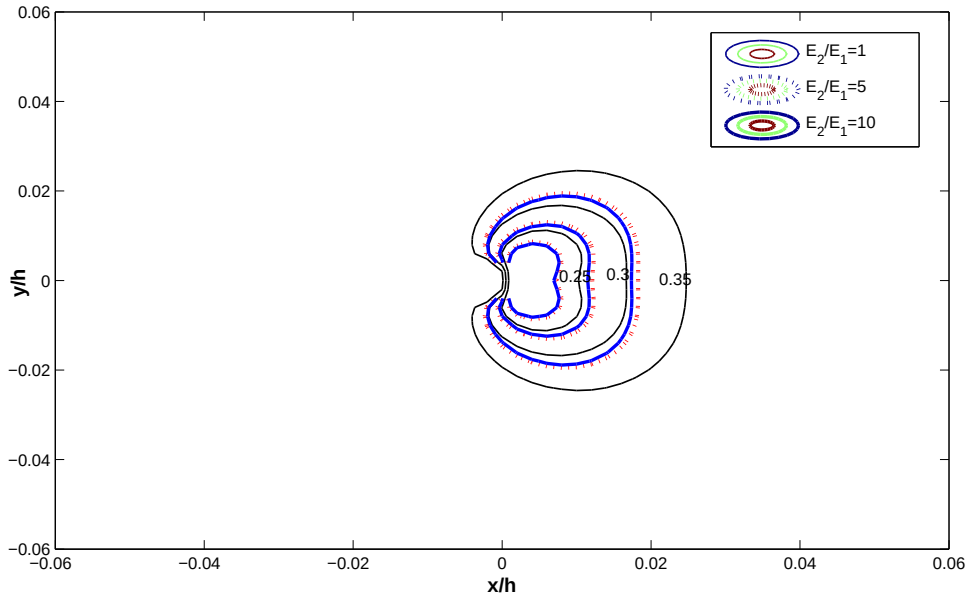

Figure 3.32. Error contours for different E_2/E_1 ratios, $a/h = 0.2$ and $\alpha = 0^o$ around left crack tip

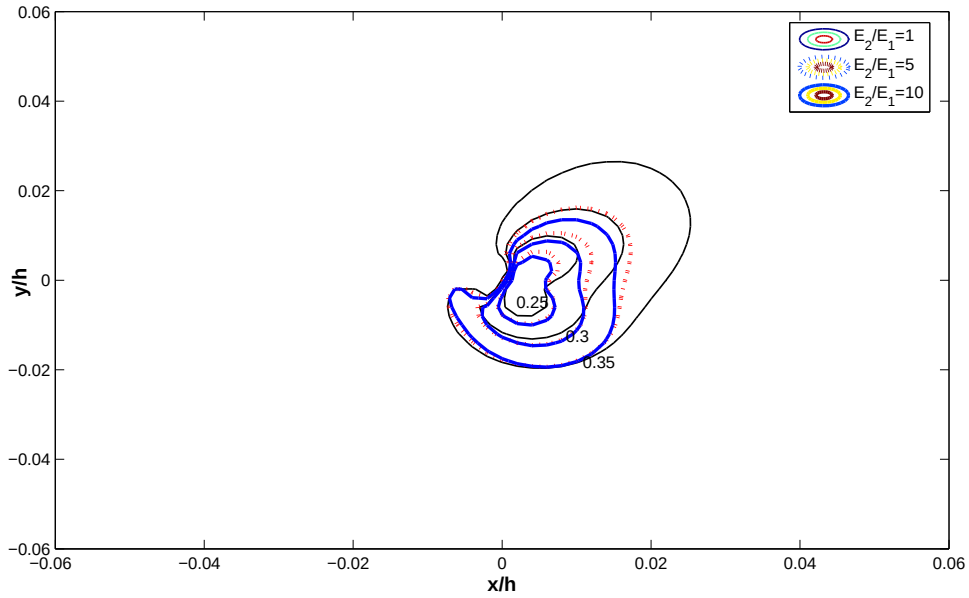

Figure 3.33. Error contours for different E_2/E_1 ratios, $a/h = 0.2$ and $\alpha = 15^o$ around left crack tip

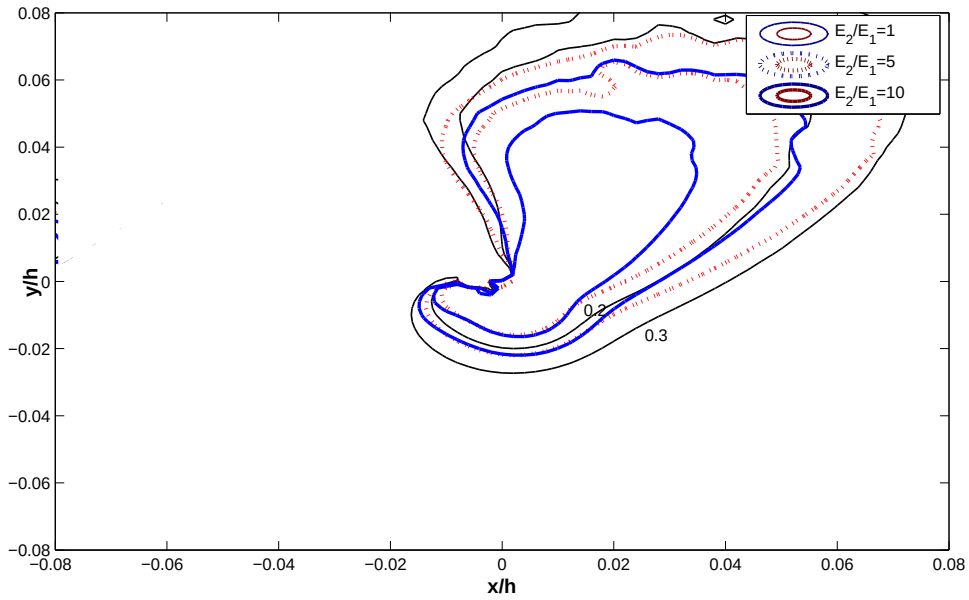

Figure 3.34. Error contours for different E_2/E_1 ratios, $a/h = 0.2$ and $\alpha = 30^o$ around left crack tip

3.3.2. Effect of Crack Angle on Extent of K-dominant Region

The opening stress, σ_{yy}, along the crack is analyzed for different crack angles. FE and ASY stress curves are plotted separately from $\alpha = 15^o$ to $\alpha = 60^o$ for $a/h = 0.3$ with $E_2/E_1 = 2, 5, 10, 20$ in Figures 3.35 - 3.42. Both left and right crack tips are considered. The origin seen on the graphs is the common origin for the left and right halves of the domain, and it represents both of the two crack tips. From ASY and FE results, it is understood that as the crack angle increases σ_{yy} decreases. In all the plots, ASY stress values underestimate FE stress values. Besides, stress values along right crack tip to right edge of the plate are higher than the values along the left crack tip to left edge of the plate.

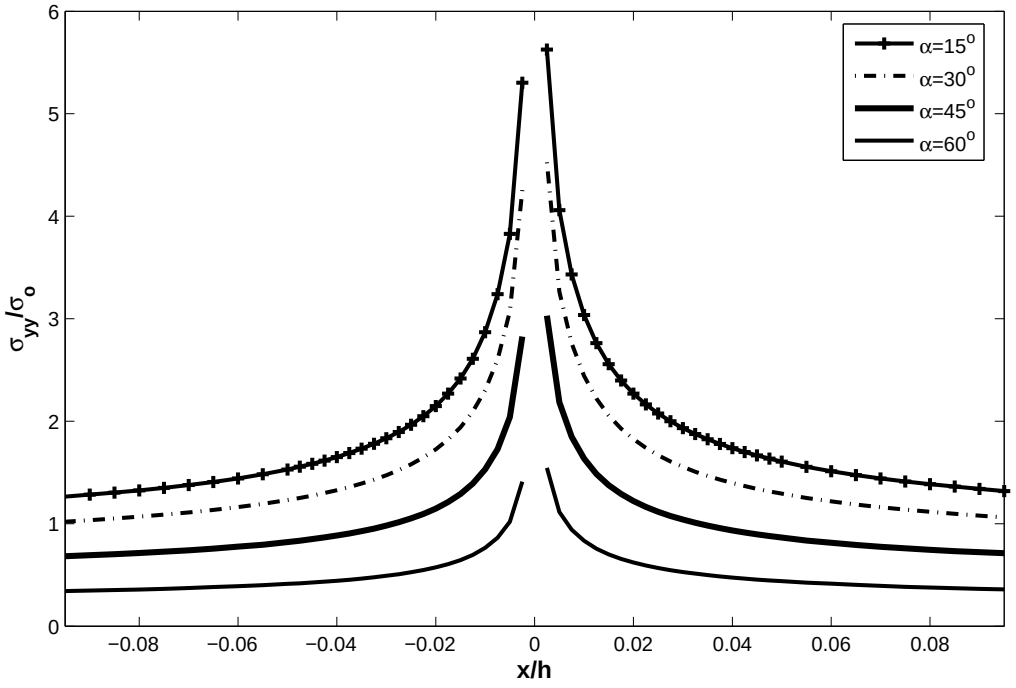

Figure 3.35. FE results for σ_{yy}/σ_o vs. distance from crack tip, $a/h = 0.3$, $E_2/E_1 = 2$ for different crack angles

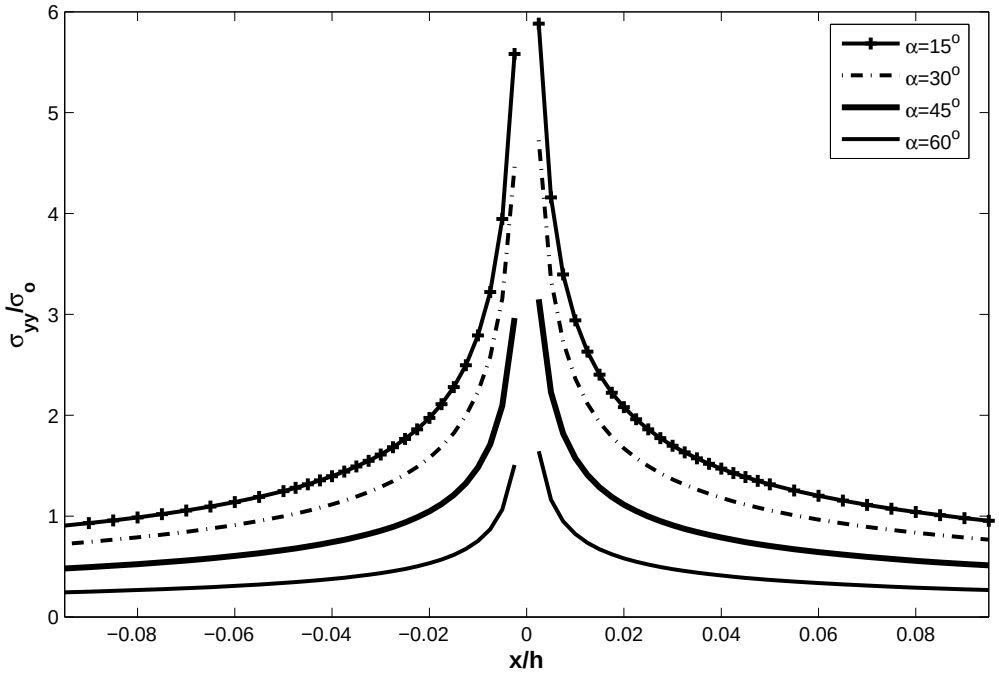

Figure 3.36. ASY results for σ_{yy}/σ_o vs. distance from crack tip, $a/h = 0.3$, $E_2/E_1 = 2$ for different crack angles

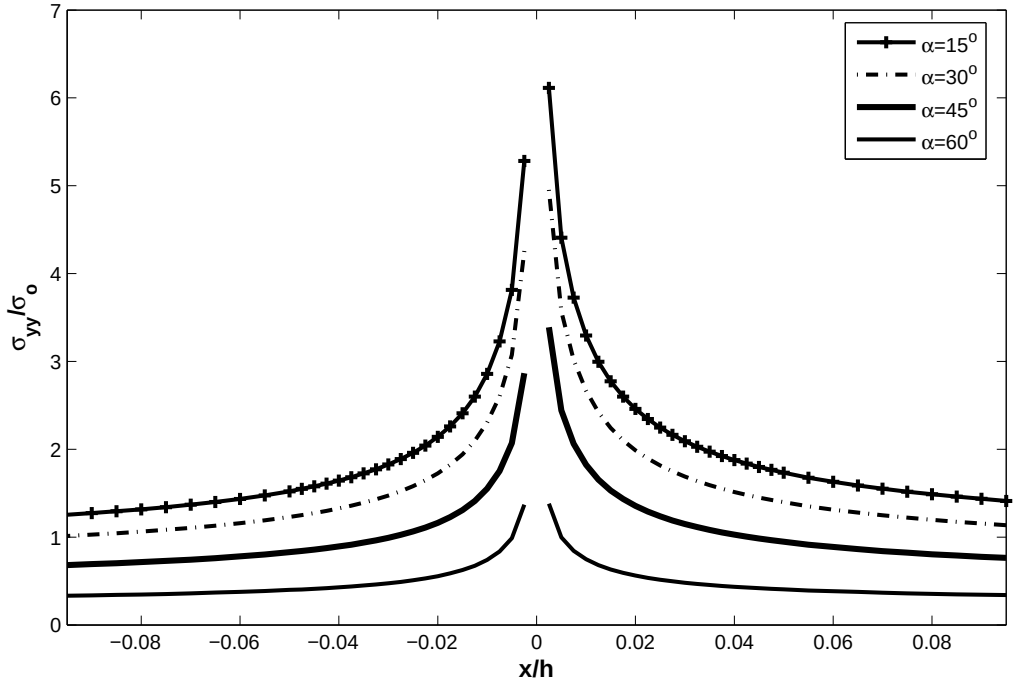

Figure 3.37. FE results for σ_{yy}/σ_o vs. distance from crack tip, $a/h = 0.3$, $E_2/E_1 = 5$ for different crack angles

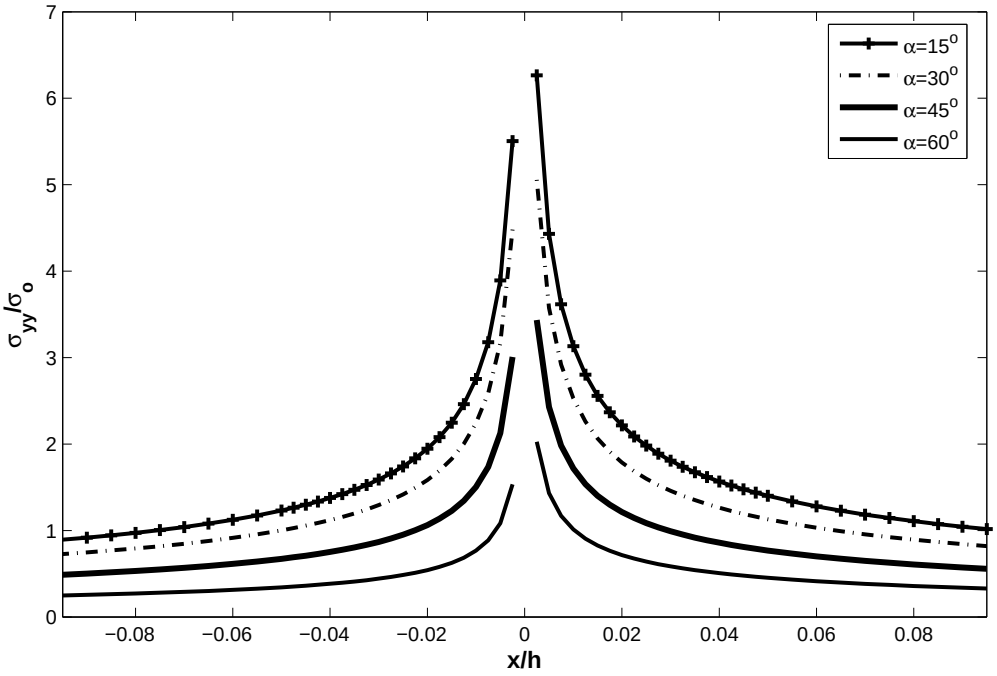

Figure 3.38. ASY results for σ_{yy}/σ_o vs. distance from crack tip, $a/h = 0.3$, $E_2/E_1 = 5$ for different crack angles

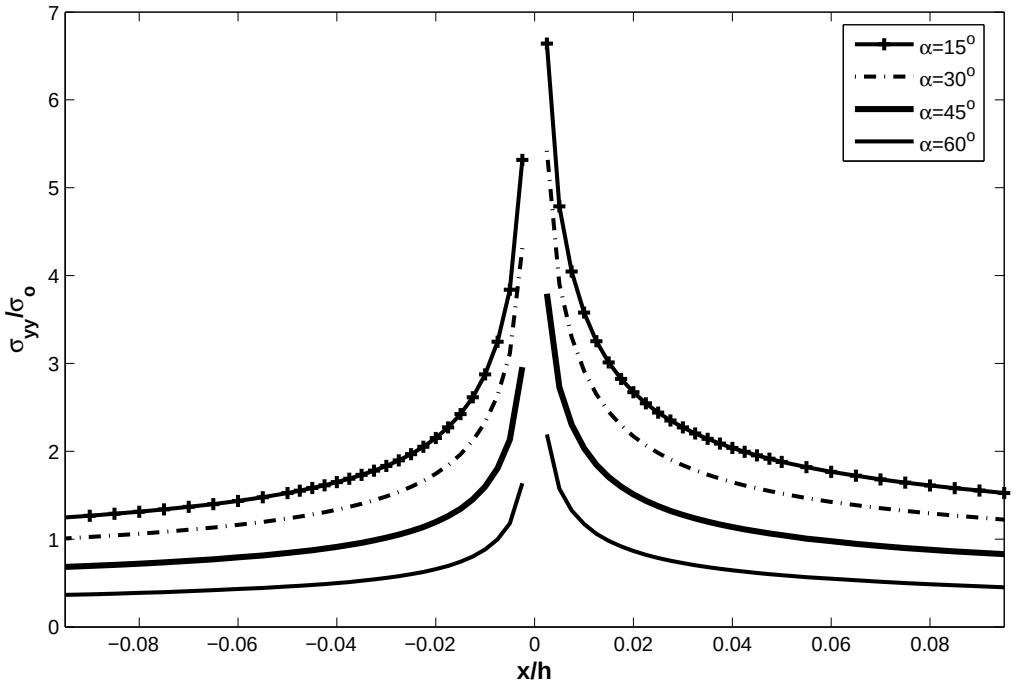

Figure 3.39. FE results for σ_{yy}/σ_o vs distance from crack tip, $a/h = 0.3$, $E_2/E_1 = 10$ for different crack angles

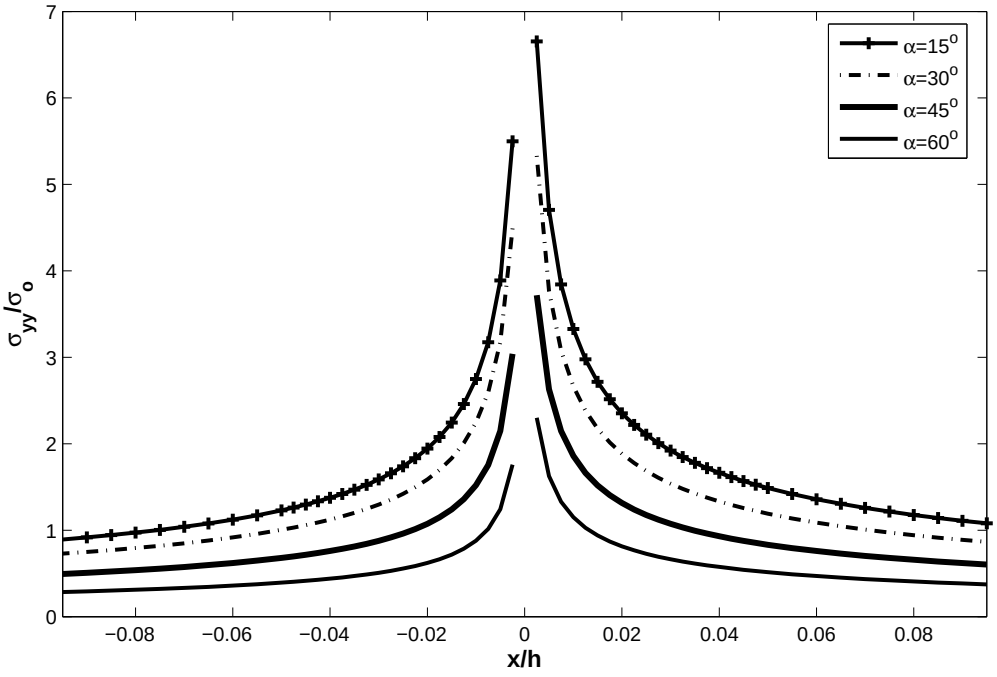

Figure 3.40. ASY results for σ_{yy}/σ_o vs. distance from crack tip, $a/h = 0.3$, $E_2/E_1 = 10$ for different crack angles

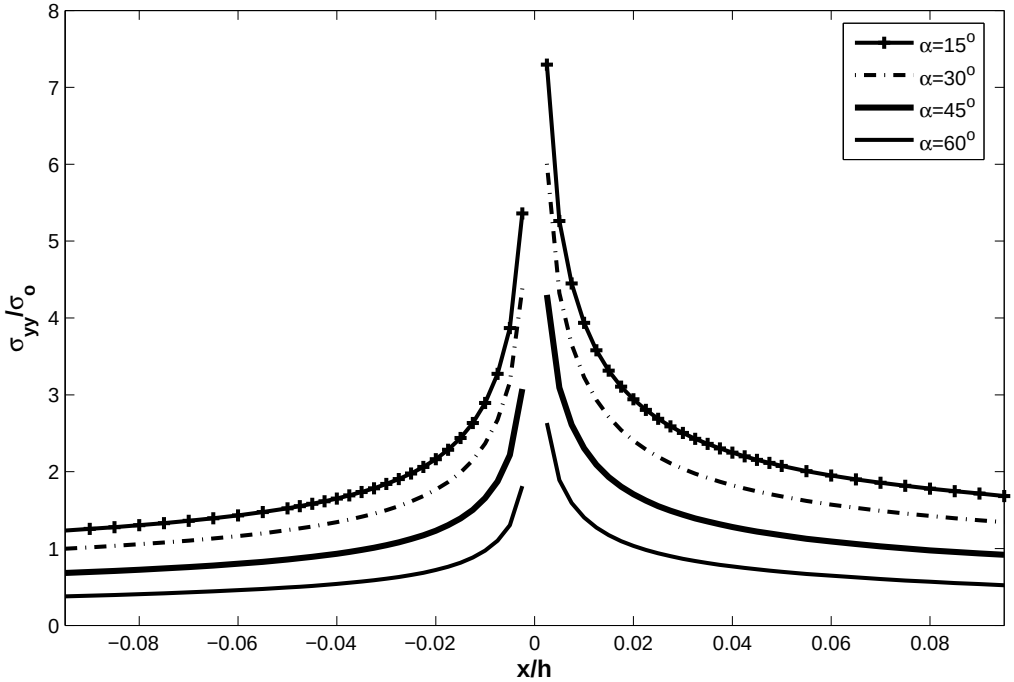

Figure 3.41. FE results for σ_{yy}/σ_o vs. distance from crack tip, $a/h = 0.3$, $E_2/E_1 = 20$ for different crack angles

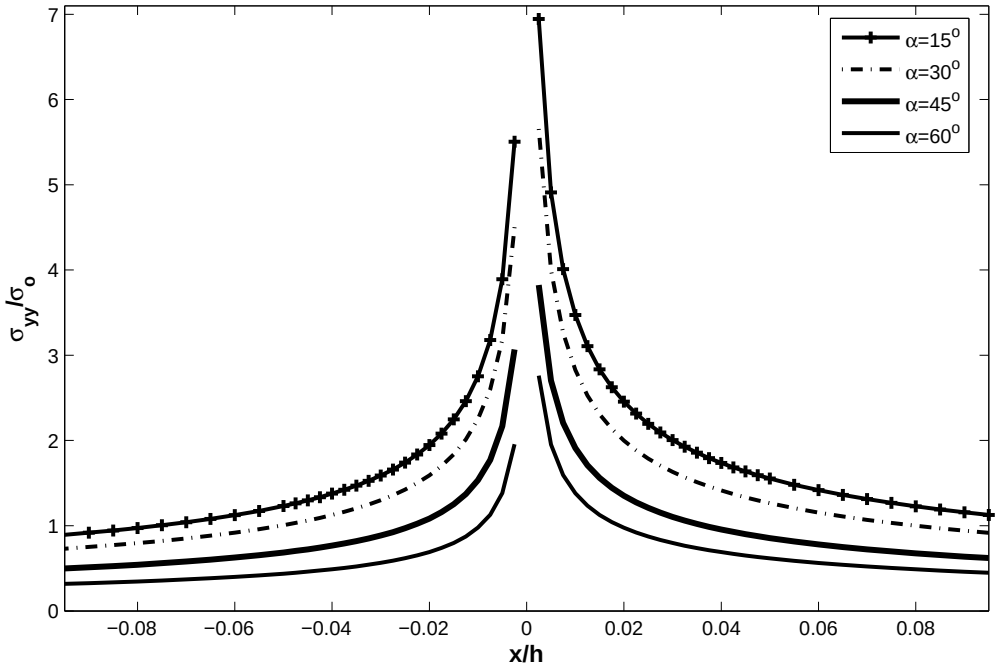

Figure 3.42. ASY results for σ_{yy}/σ_o vs. distance from crack tip, $a/h = 0.3$, $E_2/E_1 = 20$ for different crack angles

Second, the stress contours are plotted to investigate the effect of angle change on K-dominant region. Figures 3.43 - 3.74 show stress contours for $a/h = 0.3$ with $E_2/E_1 = 2$, 5, 10, 20 for different crack angle values. The graphs are plotted for stress fields around the right and left crack tips separately.

It is seen that as the crack angle increases stress contours of FE and ASY solution stress curves are getting closer to each other. The extent of K-dominant region increases as the crack angle increases for each E_2/E_1 value. Beside that the shape of the stress contours for both ASY and FE solutions change. The shape of the stress contours get narrow and rotate slightly while α increases. The stress contours around right and left crack tip have similar trend.

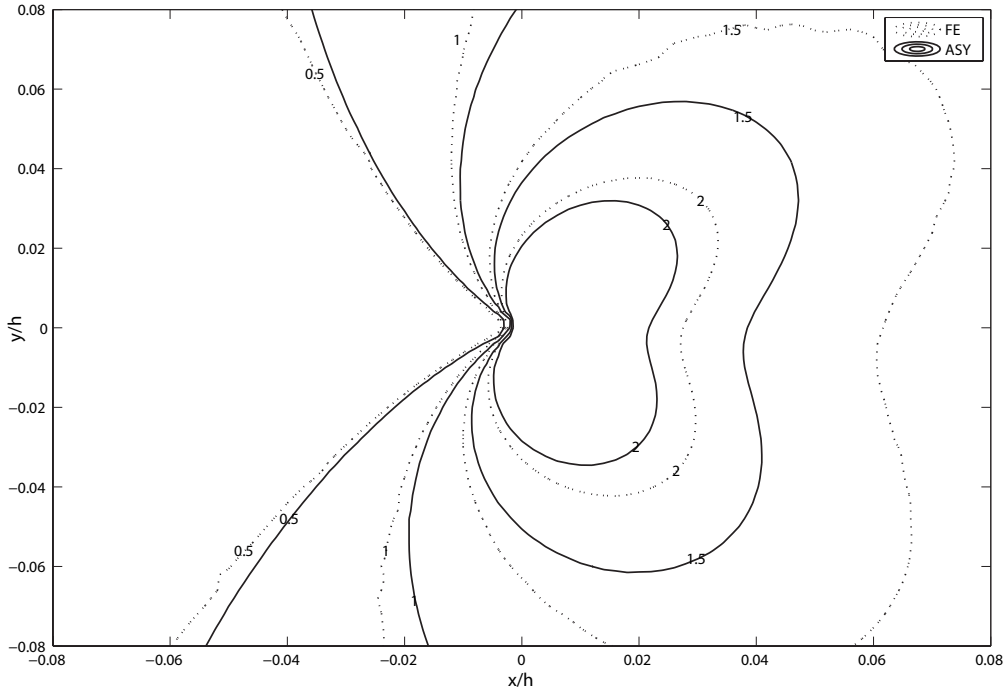

Figure 3.43. Contour plot of σ_{yy} for $E_2/E_1 = 2$, $a/h = 0.3$ and $\alpha = 15^o$ around right crack tip

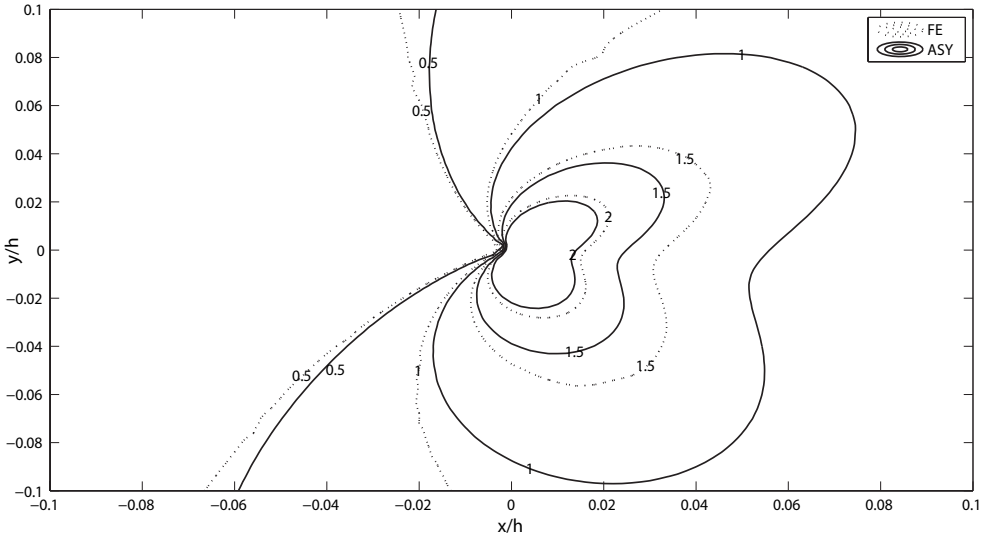

Figure 3.44. Contour plot of σ_{yy} for $E_2/E_1 = 2$, $a/h = 0.3$ and $\alpha = 30^o$ around right crack tip

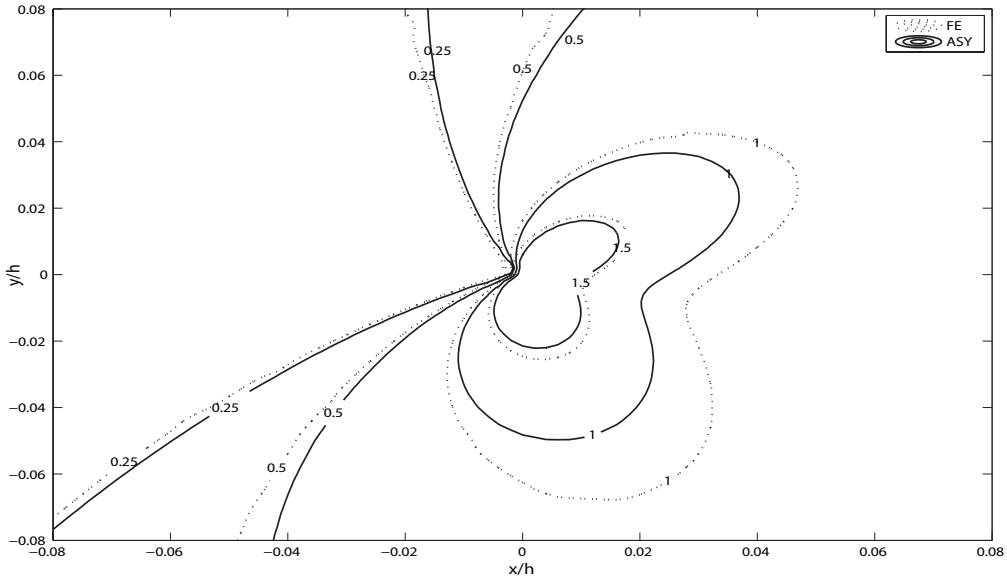

Figure 3.45. Contour plot of σ_{yy} for $E_2/E_1 = 2$, $a/h = 0.3$ and $\alpha = 45^o$ around right crack tip

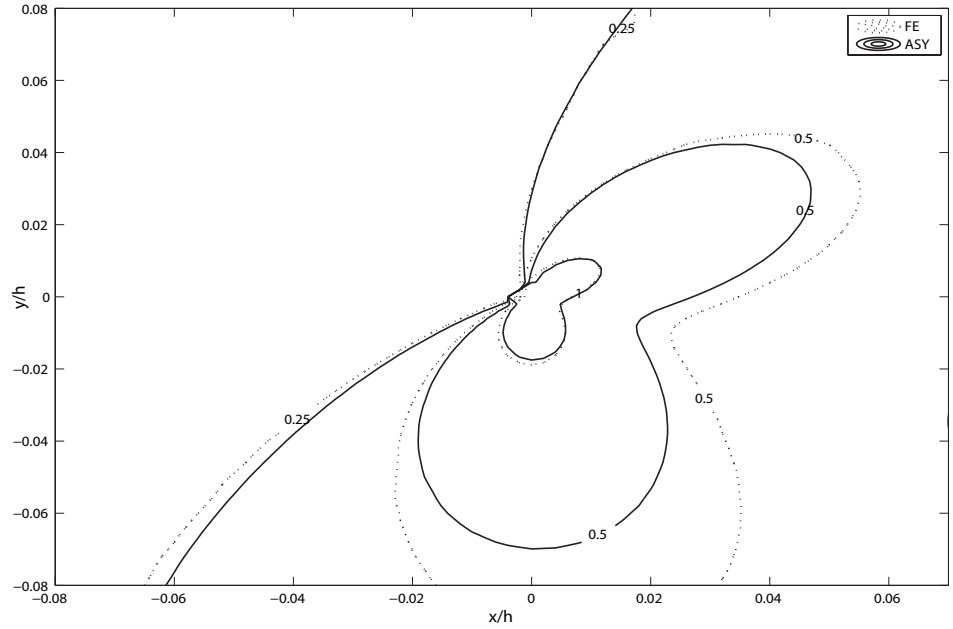

Figure 3.46. Contour plot of σ_{yy} for $E_2/E_1 = 2$, $a/h = 0.3$ and $\alpha = 60^o$ around right crack tip

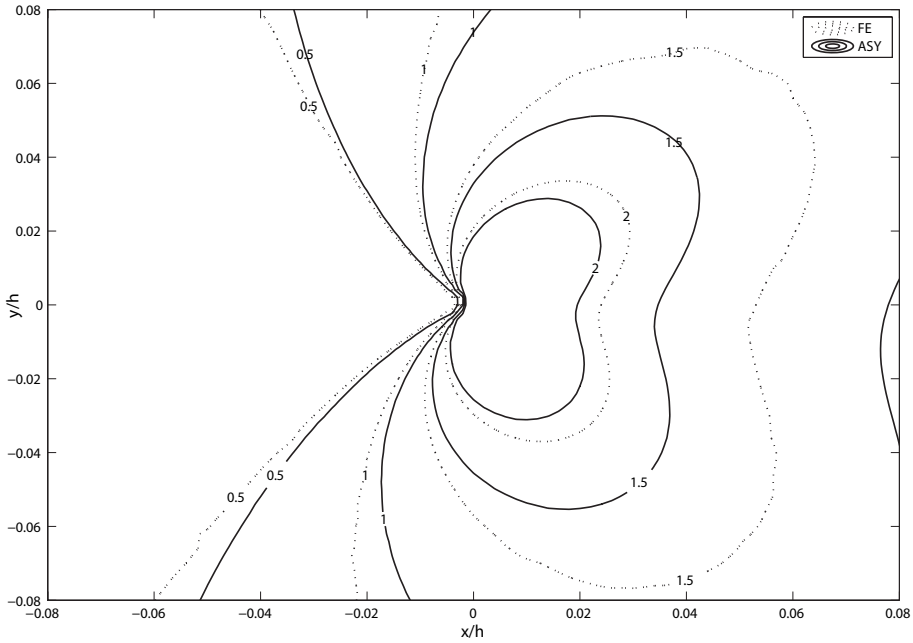

Figure 3.47. Contour plot of σ_{yy} for $E_2/E_1 = 2$, $a/h = 0.3$ and $\alpha = 15^o$ around left crack tip

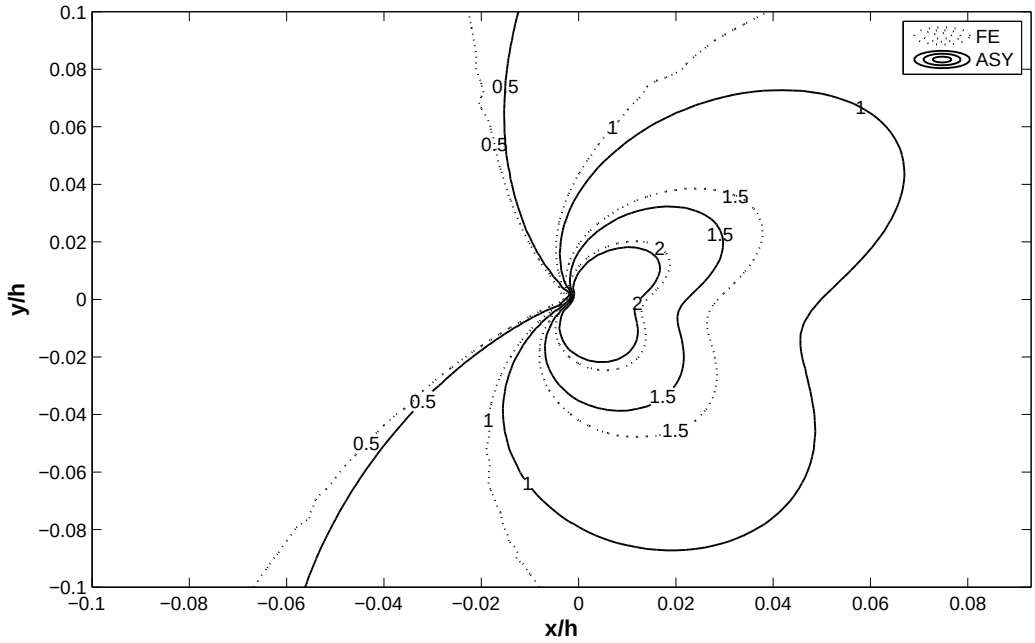

Figure 3.48. Contour plot of σ_{yy} for $E_2/E_1 = 2$, $a/h = 0.3$ and $\alpha = 30^o$ around left crack tip

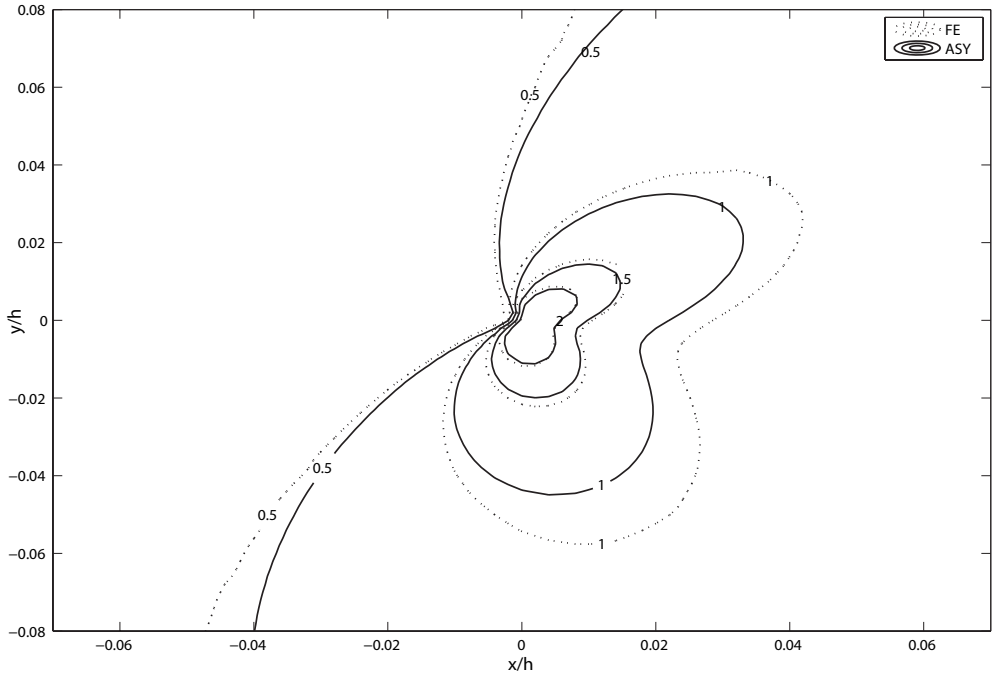

Figure 3.49. Contour plot of σ_{yy} for $E_2/E_1 = 2$, $a/h = 0.3$ and $\alpha = 45^o$ around left crack tip

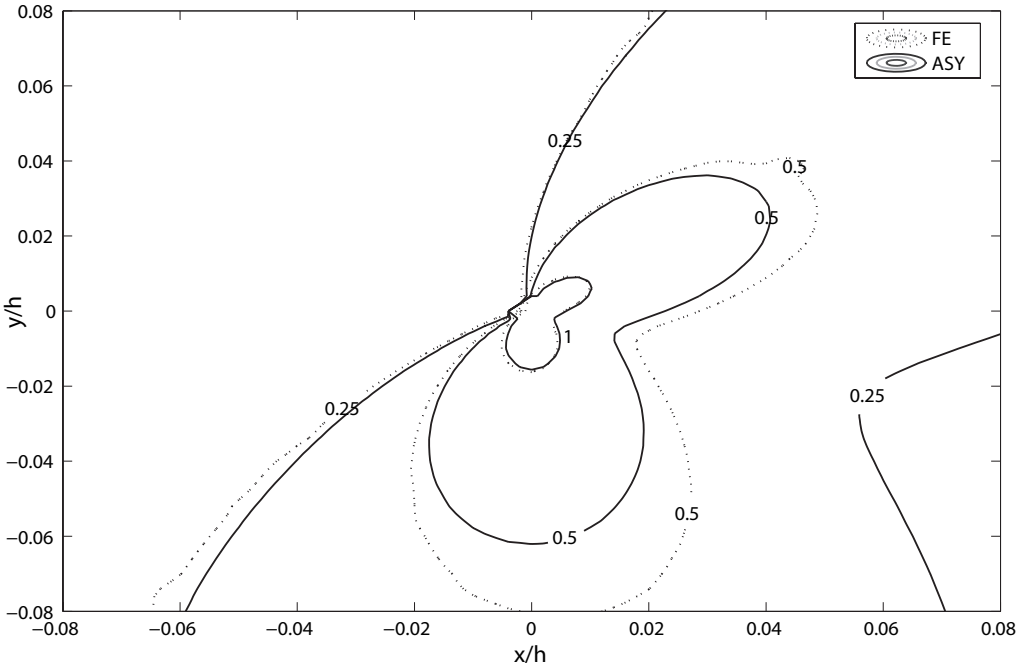

Figure 3.50. Contour plot of σ_{yy} for $E_2/E_1 = 2$, $a/h = 0.3$ and $\alpha = 60^o$ around left crack tip

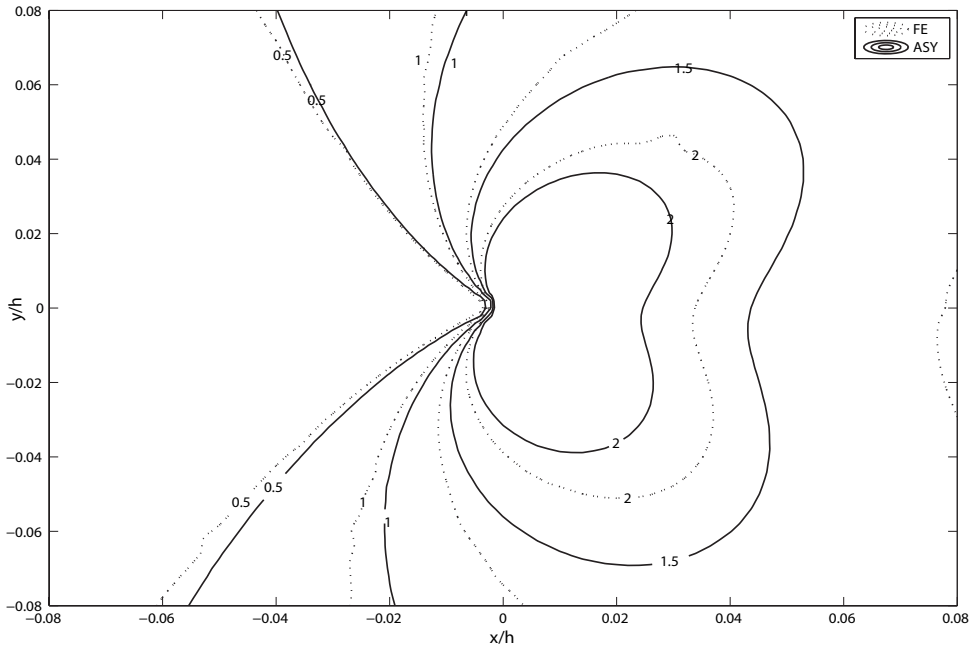

Figure 3.51. Contour plot of σ_{yy} for $E_2/E_1 = 5$, $a/h = 0.3$ and $\alpha = 15^o$ around right crack tip

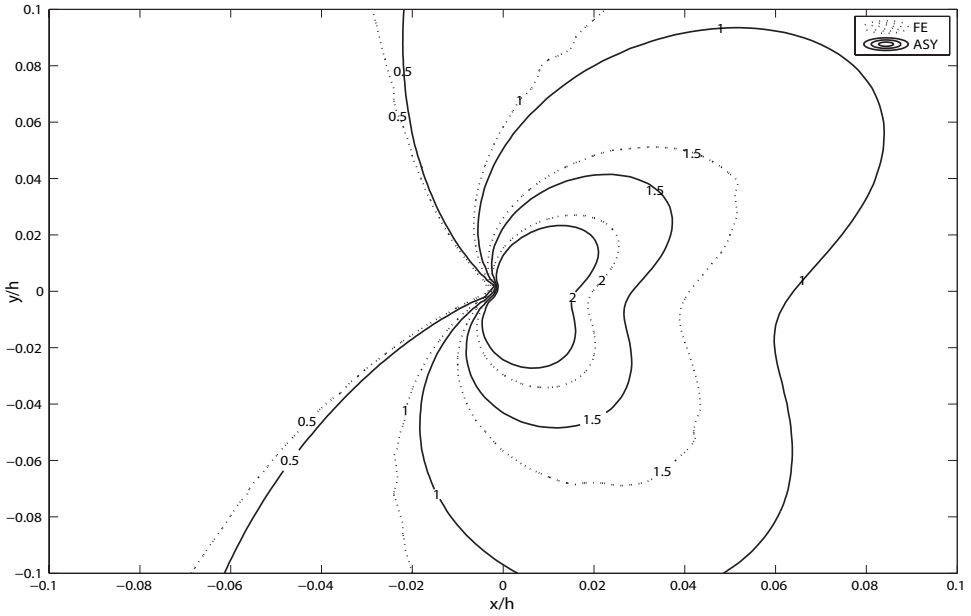

Figure 3.52. Contour plot of σ_{yy} for $E_2/E_1 = 5$, $a/h = 0.3$ and $\alpha = 30^o$ around right crack tip

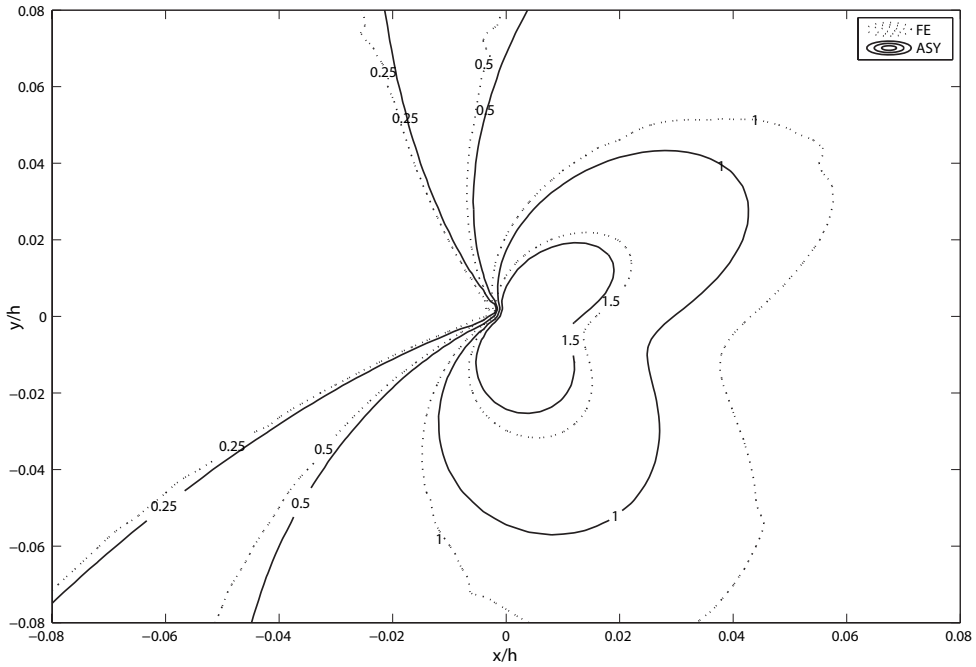

Figure 3.53. Contour plot of σ_{yy} for $E_2/E_1 = 5$, $a/h = 0.3$ and $\alpha = 45^o$ around right crack tip

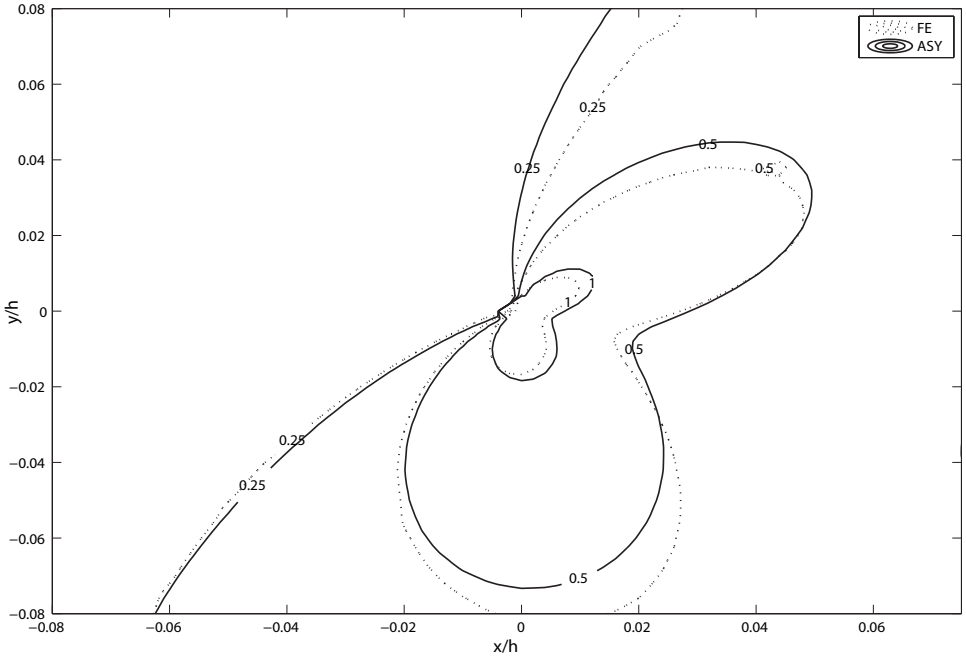

Figure 3.54. Contour plot of σ_{yy} for $E_2/E_1 = 5$, $a/h = 0.3$ and $\alpha = 60^o$ around right crack tip

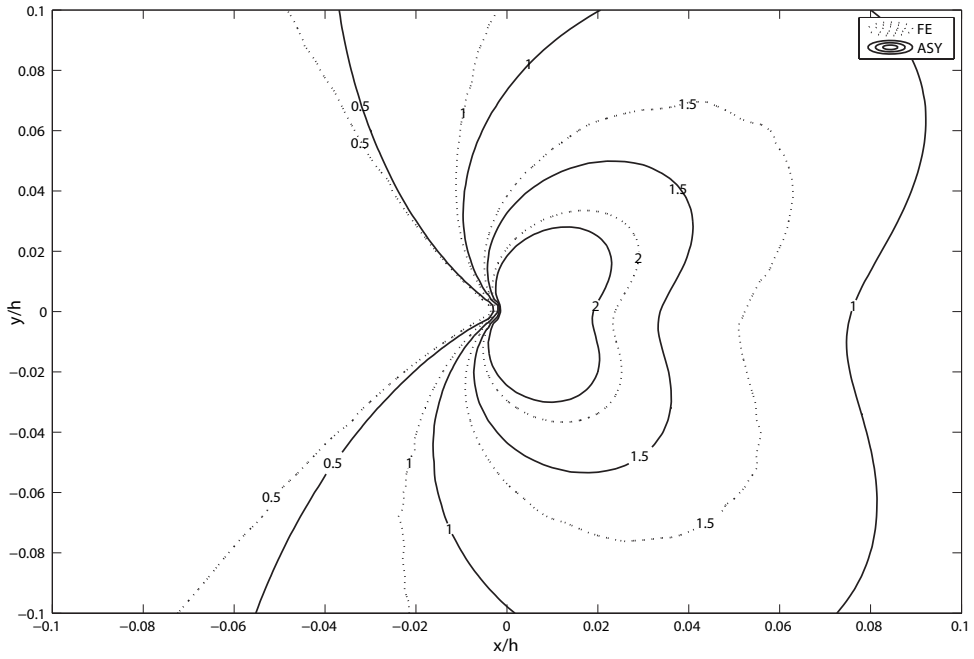

Figure 3.55. Contour plot of σ_{yy} for $E_2/E_1 = 5$, $a/h = 0.3$ and $\alpha = 15^o$ around left crack tip

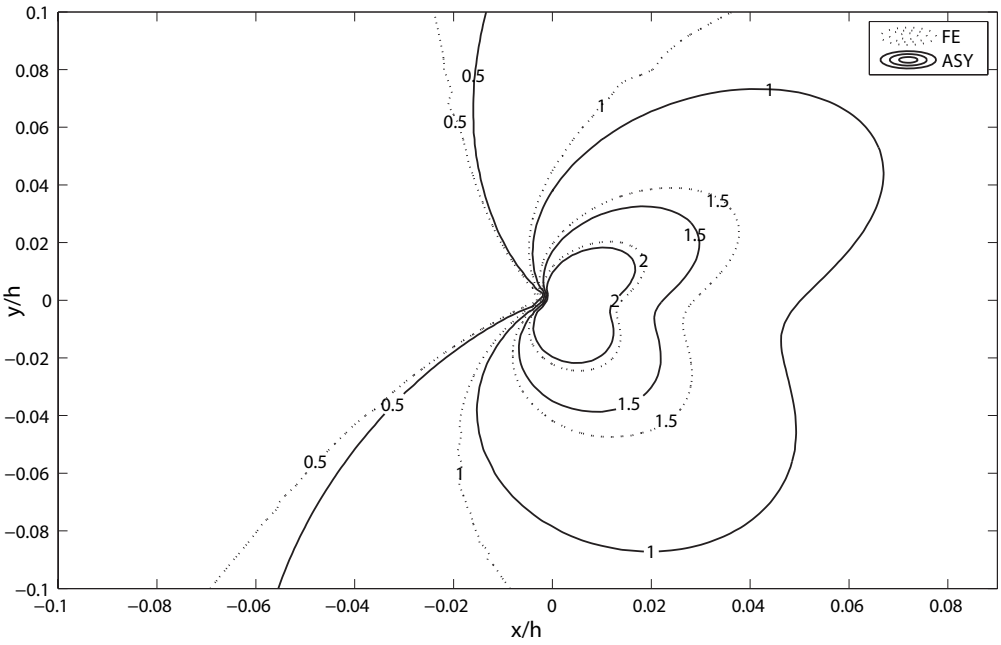

Figure 3.56. Contour plot of σ_{yy} for $E_2/E_1 = 5$, $a/h = 0.3$ and $\alpha = 30^o$ around left crack tip

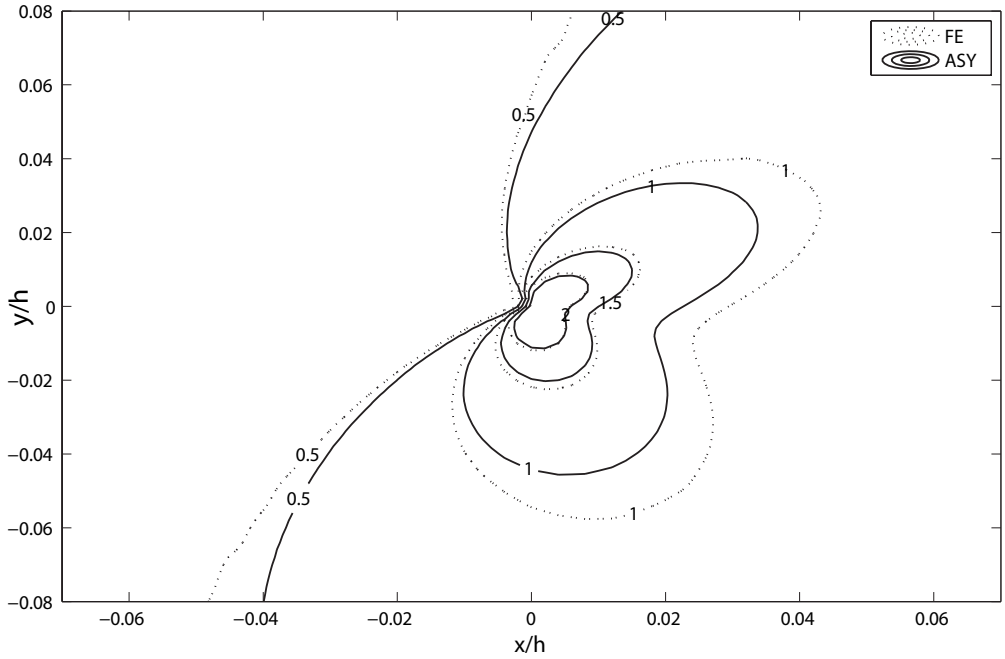

Figure 3.57. Contour plot of σ_{yy} for $E_2/E_1 = 5$, $a/h = 0.3$ and $\alpha = 45^o$ around left crack tip

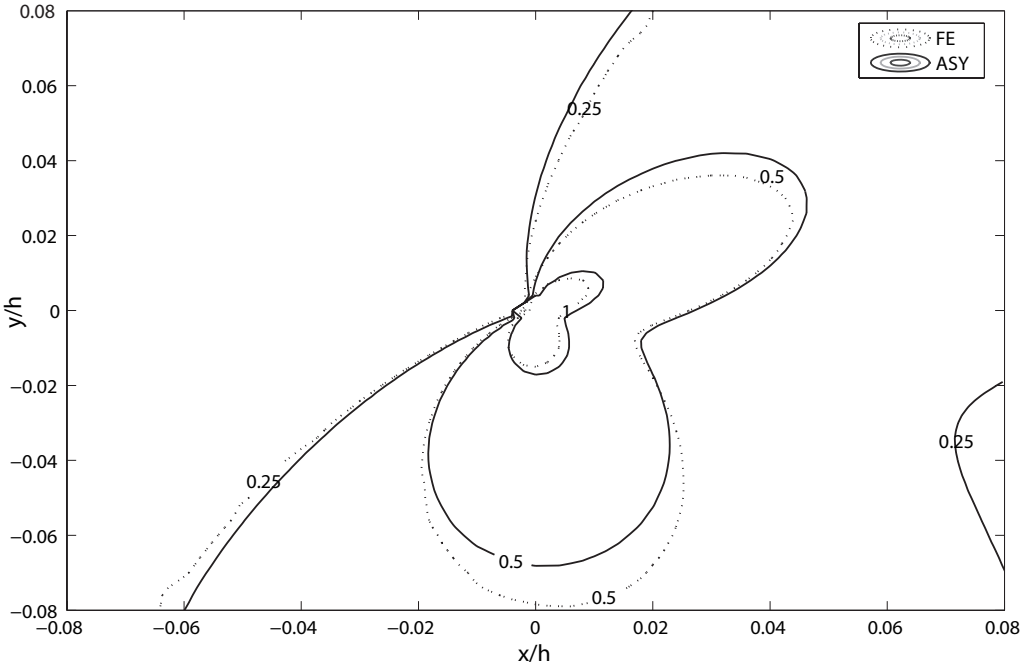

Figure 3.58. Contour plot of σ_{yy} for $E_2/E_1 = 5$, $a/h = 0.3$ and $\alpha = 60^o$ around left crack tip

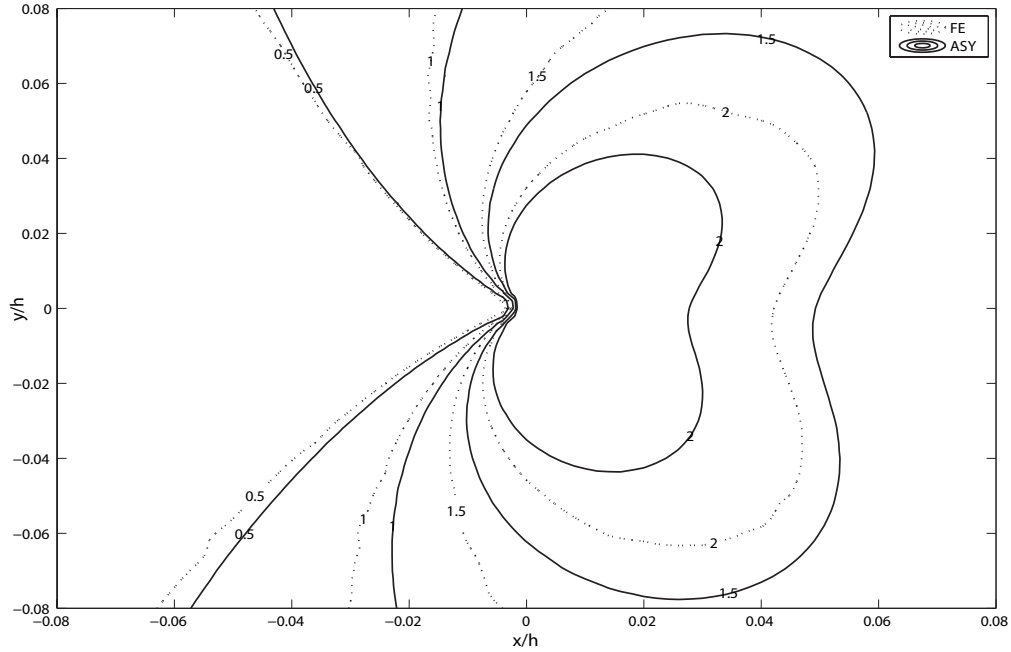

Figure 3.59. Contour plot of σ_{yy} for $E_2/E_1 = 10$, $a/h = 0.3$ and $\alpha = 15^o$ around right crack tip

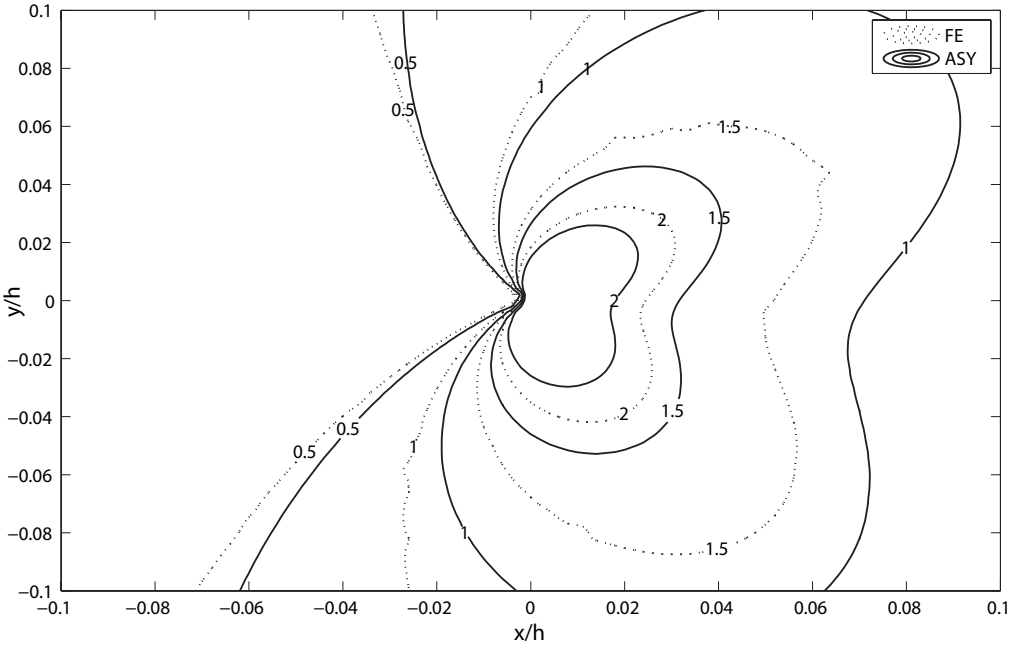

Figure 3.60. Contour plot of σ_{yy} for $E_2/E_1 = 10$, $a/h = 0.3$ and $\alpha = 30^o$ around right crack tip

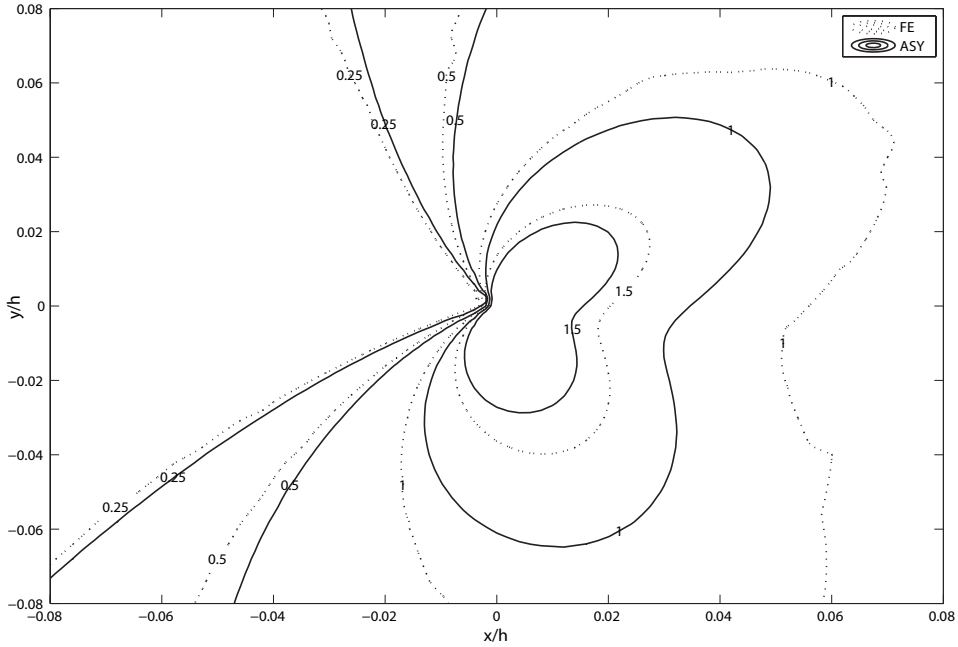

Figure 3.61. Contour plot of σ_{yy} for $E_2/E_1 = 10$, $a/h = 0.3$ and $\alpha = 45^o$ around right crack tip

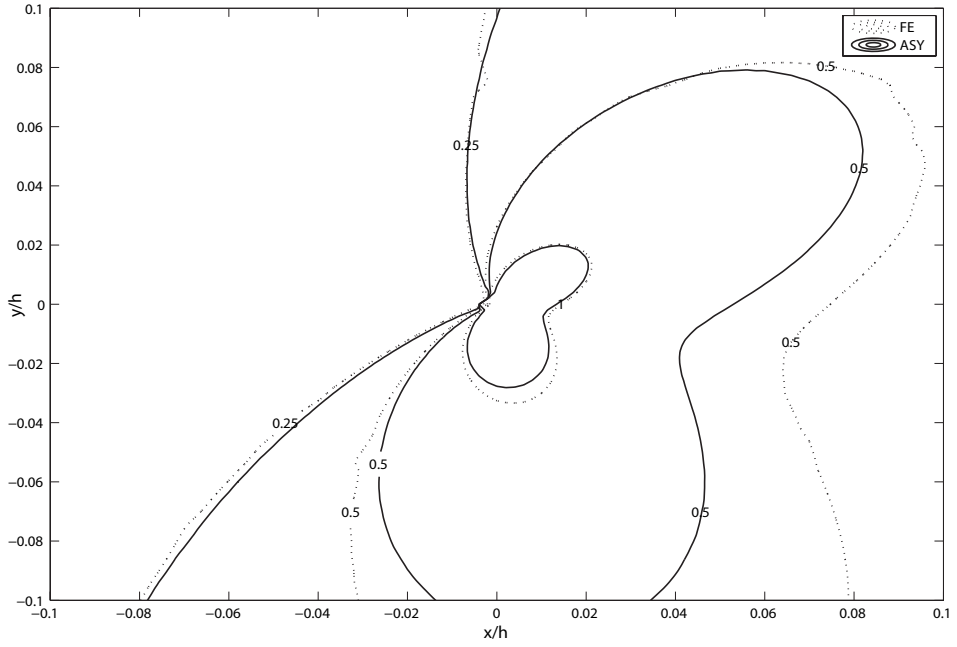

Figure 3.62. Contour plot of σ_{yy} for $E_2/E_1 = 10$, $a/h = 0.3$ and $\alpha = 60^o$ around right crack tip

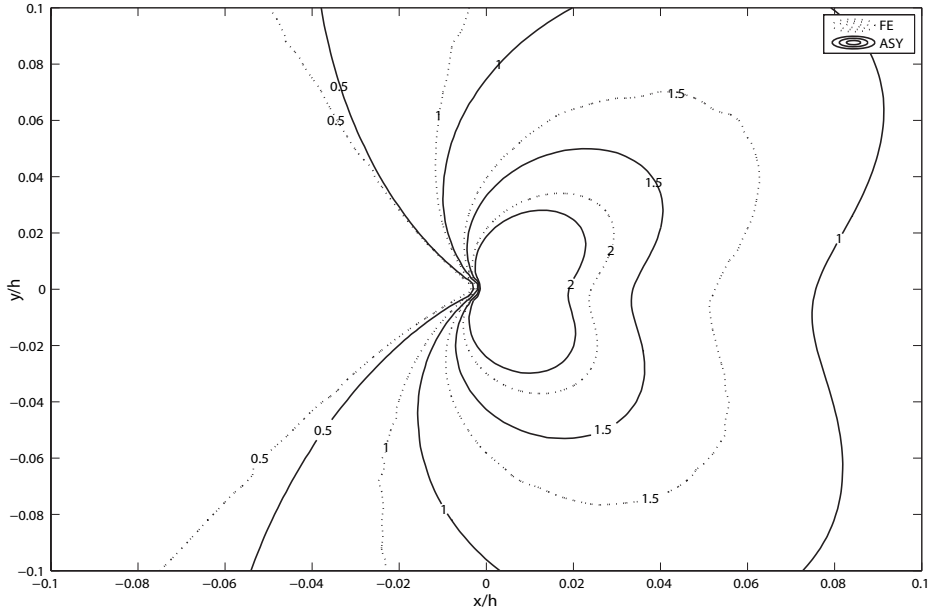

Figure 3.63. Contour plot of σ_{yy} for $E_2/E_1 = 10$, $a/h = 0.3$ and $\alpha = 15^o$ around left crack tip

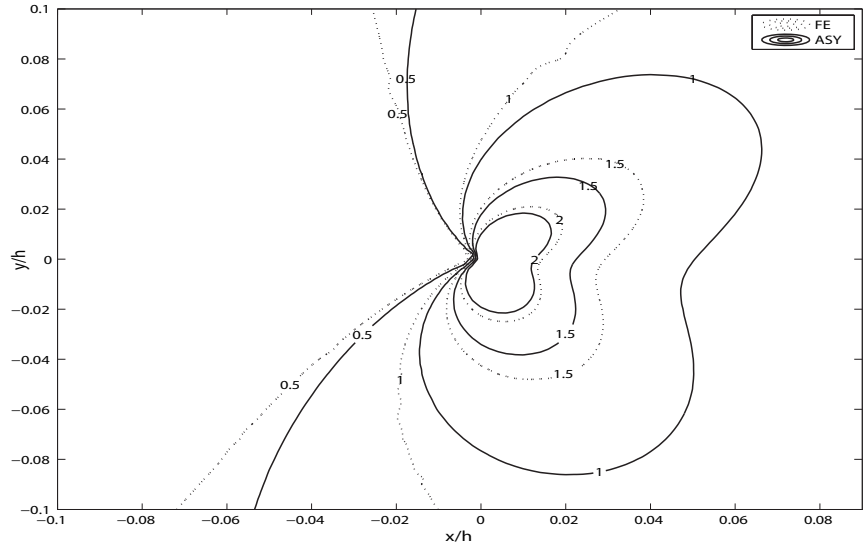

Figure 3.64. Contour plot of σ_{yy} for $E_2/E_1 = 10$, $a/h = 0.3$ and $\alpha = 30^o$ around left crack tip

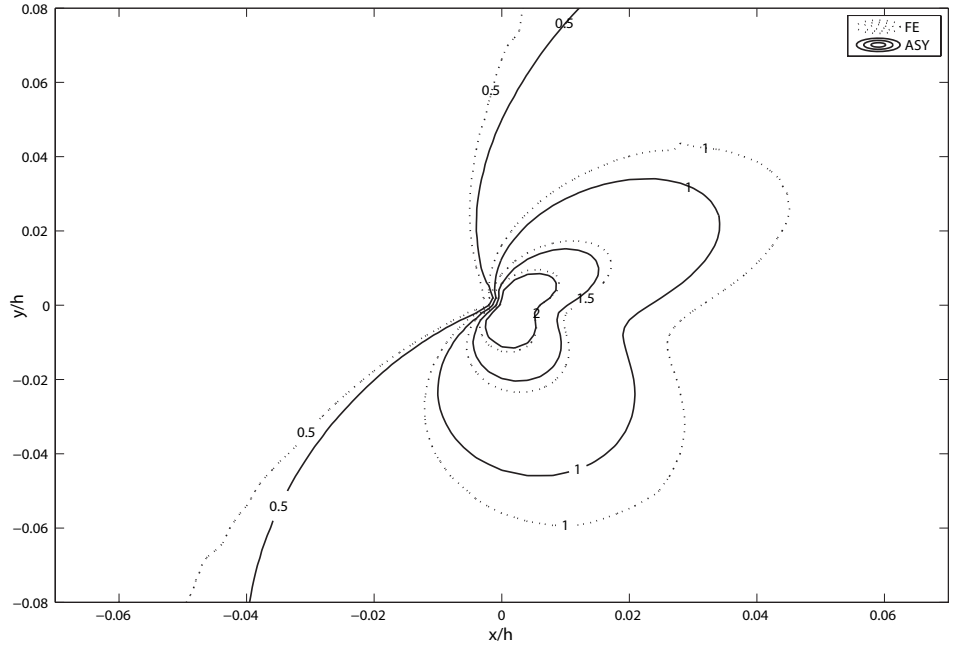

Figure 3.65. Contour plot of σ_{yy} for $E_2/E_1 = 10$, $a/h = 0.3$ and $\alpha = 45^o$ around left crack tip

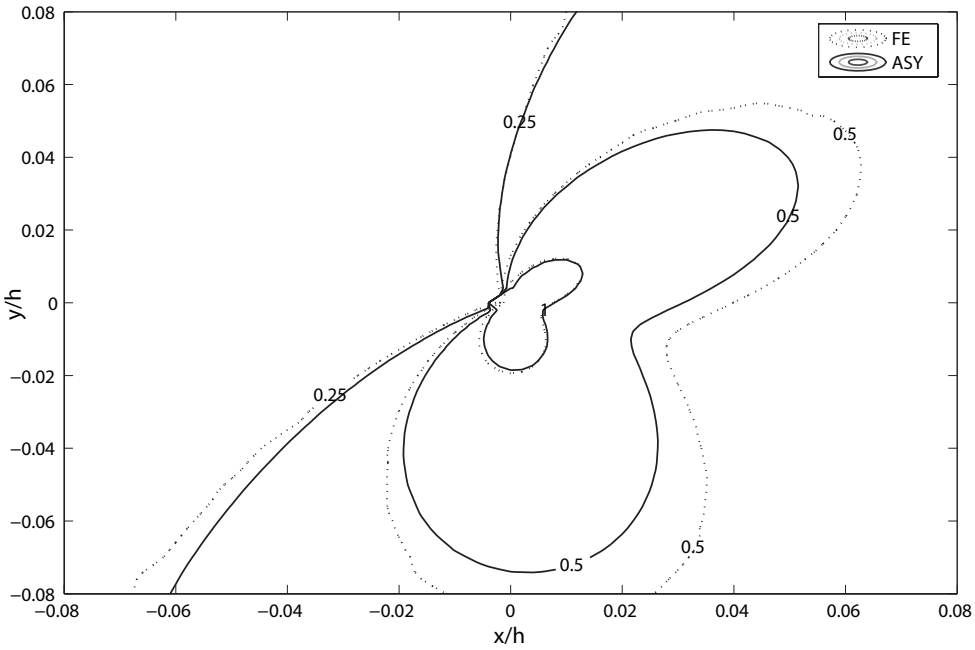

Figure 3.66. Contour plot of σ_{yy} for $E_2/E_1 = 10$, $a/h = 0.3$ and $\alpha = 60^o$ around left crack tip

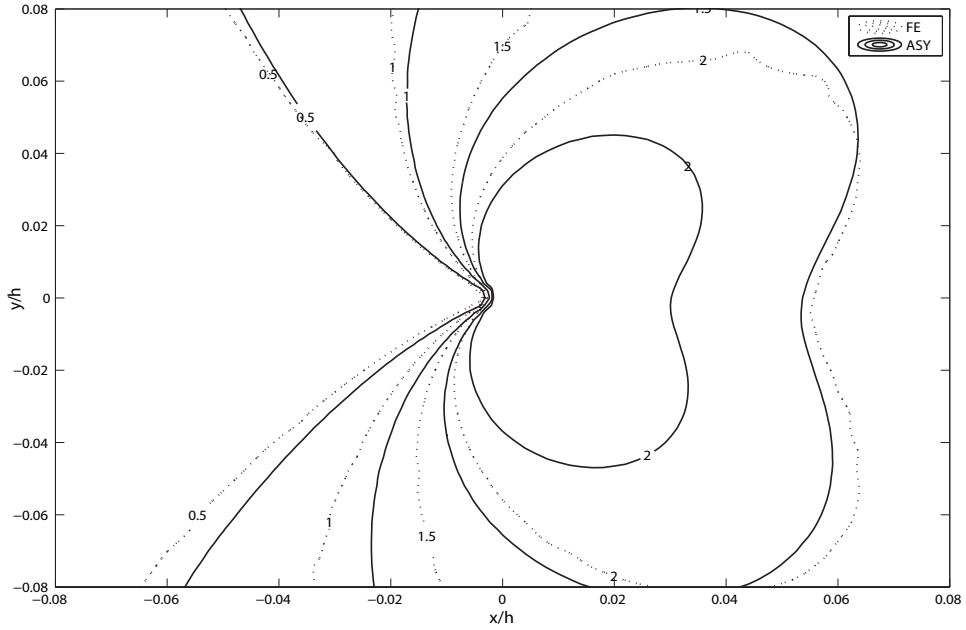

Figure 3.67. Contour plot of σ_{yy} for $E_2/E_1 = 20$, $a/h = 0.3$ and $\alpha = 15^o$ around right crack tip

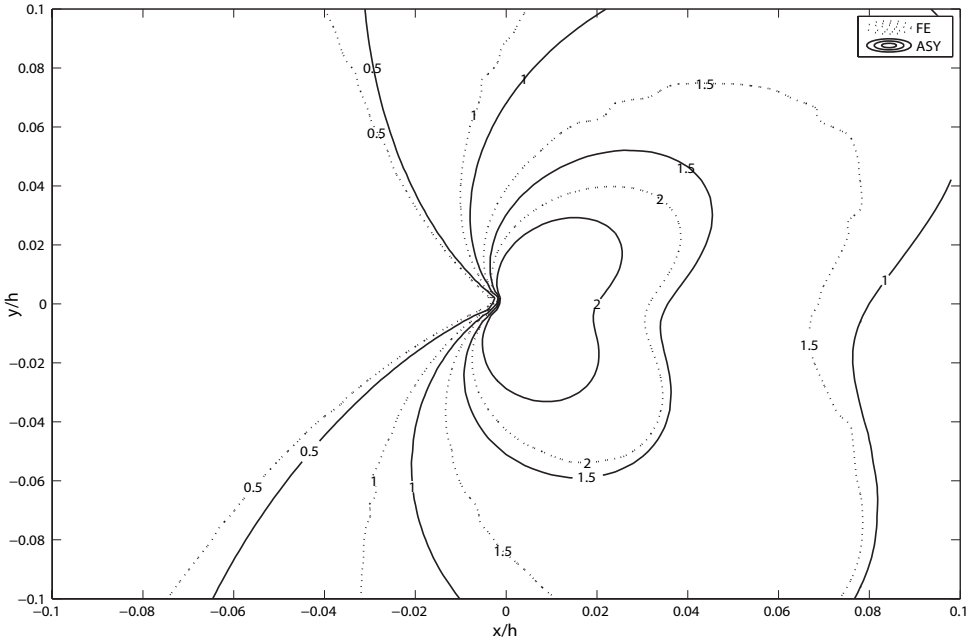

Figure 3.68. Contour plot of σ_{yy} for $E_2/E_1 = 20$, $a/h = 0.3$ and $\alpha = 30^o$ around right crack tip

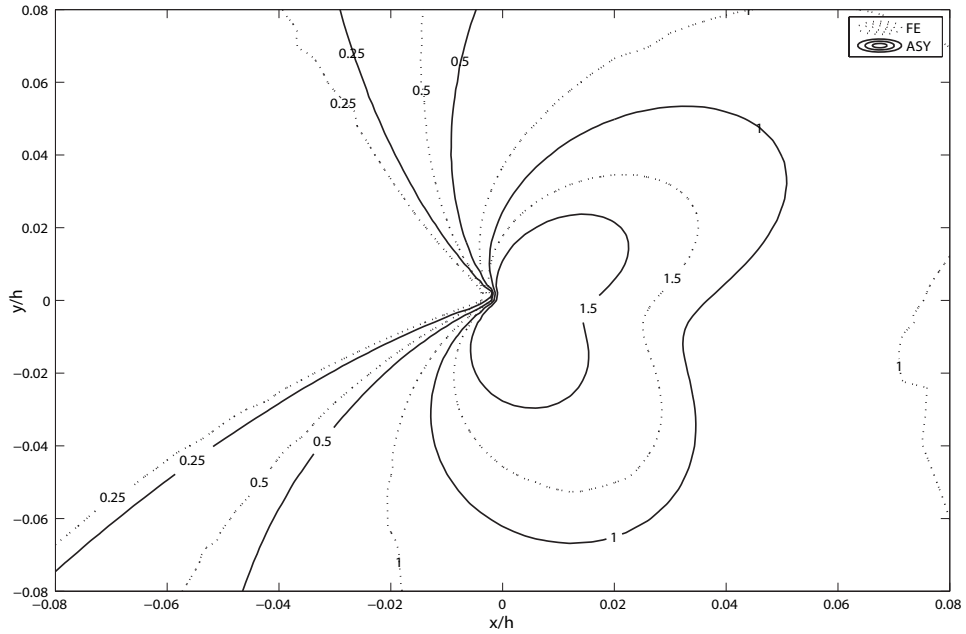

Figure 3.69. Contour plot of σ_{yy} for $E_2/E_1 = 20$, $a/h = 0.3$ and $\alpha = 45^o$ around right crack tip

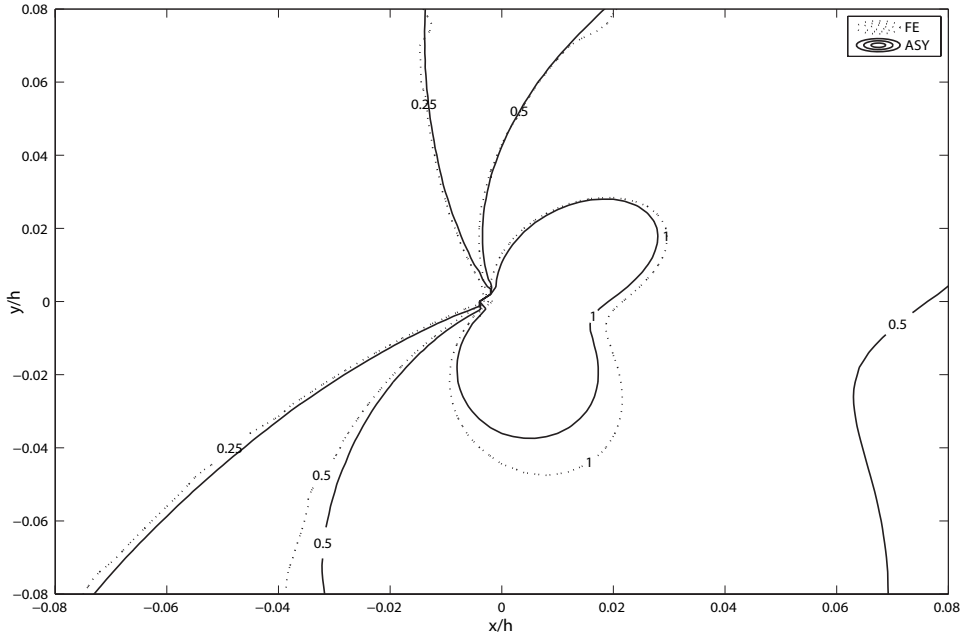

Figure 3.70. Contour plot of σ_{yy} for $E_2/E_1 = 20$, $a/h = 0.3$ and $\alpha = 60^o$ around right crack tip

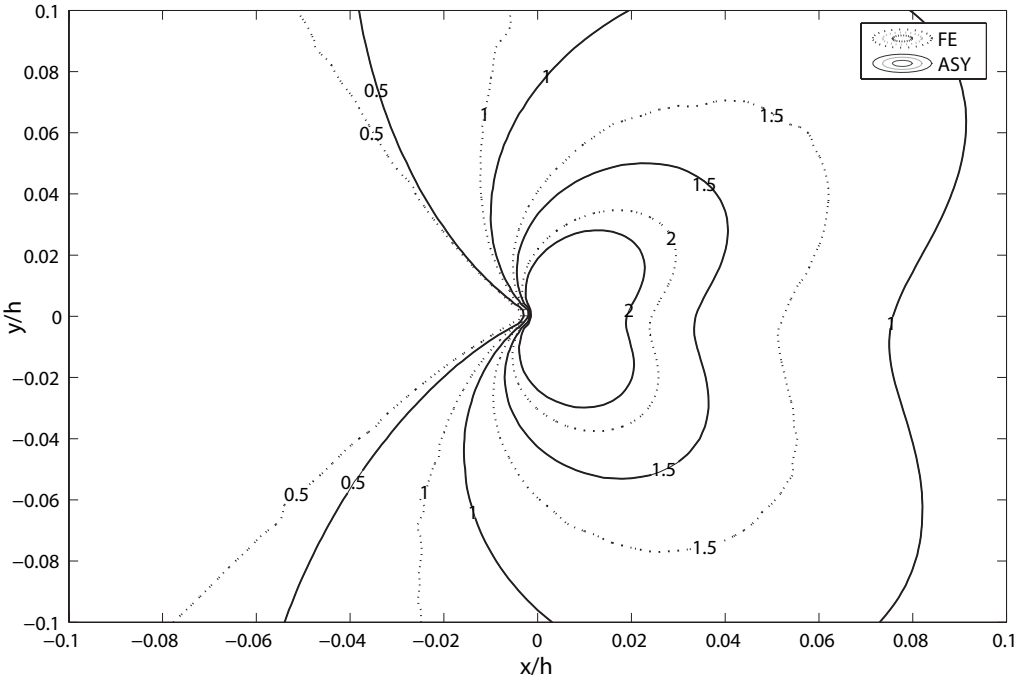

Figure 3.71. Contour plot of σ_{yy} for $E_2/E_1 = 20$, $a/h = 0.3$ and $\alpha = 15^o$ around left crack tip

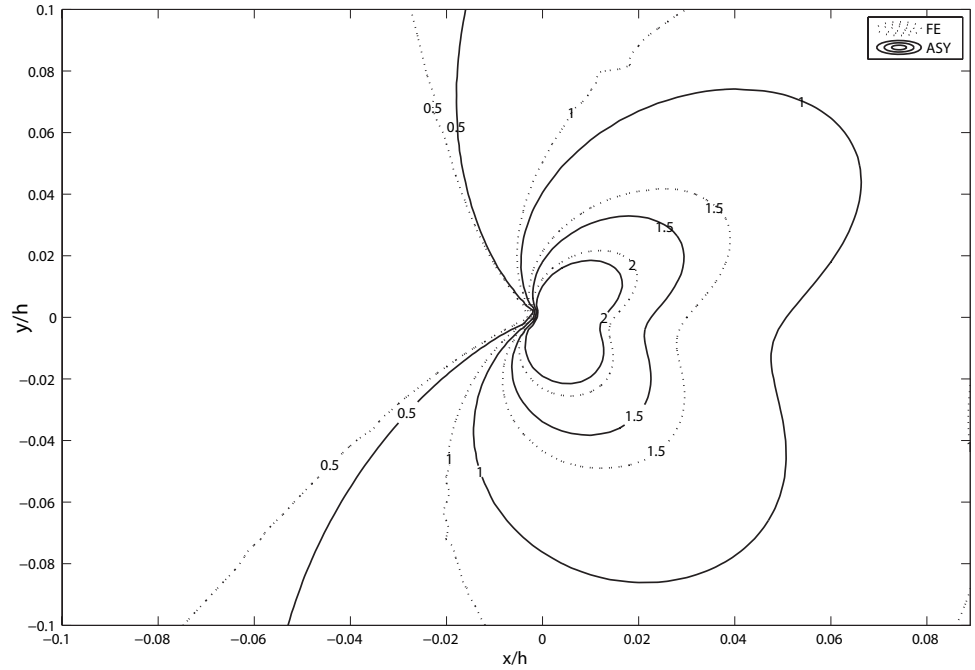

Figure 3.72. Contour plot of σ_{yy} for $E_2/E_1 = 20$, $a/h = 0.3$ and $\alpha = 30^o$ around left crack tip

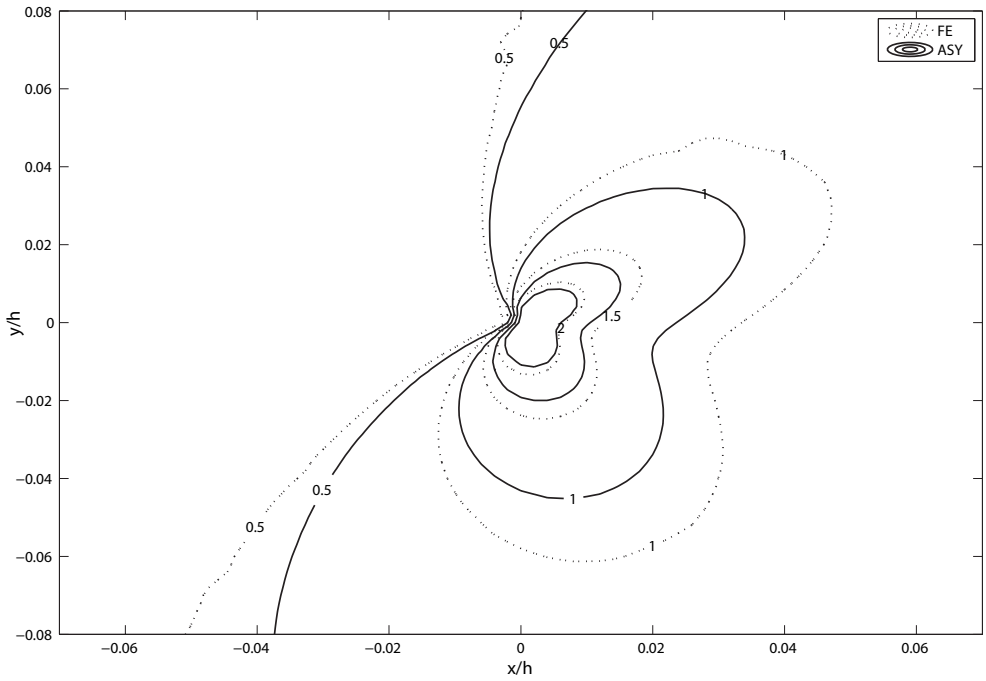

Figure 3.73. Contour plot of σ_{yy} for $E_2/E_1 = 20$, $a/h = 0.3$ and $\alpha = 45^o$ around left crack tip

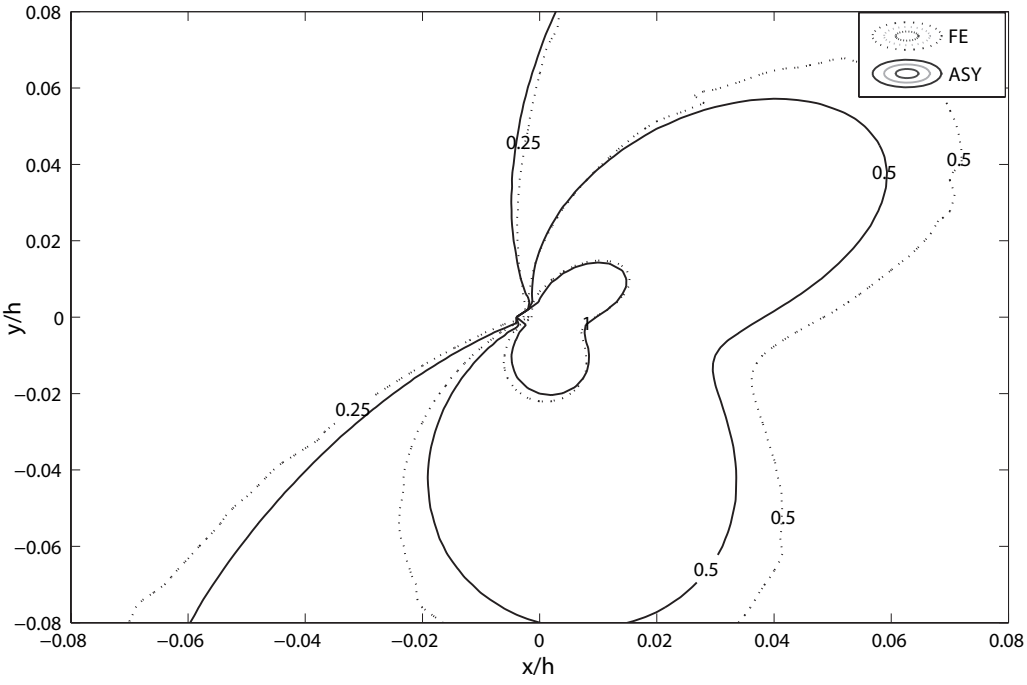

Figure 3.74. Contour plot of σ_{yy} for $E_2/E_1 = 20$, $a/h = 0.3$ and $\alpha = 60^o$ around left crack tip

After the stress contours are plotted, the extent of K-dominant region with the change of crack angle is investigated by using error contours. Error contours are plotted for $a/h = 0.3$ and $E_2/E_1 = 2$, 5, 10 with $\alpha = 0^o$, 15^o, 30^o in Figures 3.75 - 3.80. Both right and left crack tips are considered separately.

It is seen that the area covered by error contour increases dramatically as the crack angle increases. It means that the K-dominant region is larger for higher crack angle values ($\alpha = 30^o$) around both left and right crack tip. Furthermore, the contours around the right crack tip cover larger areas. That means extent of K-dominance is better around the right crack tip.

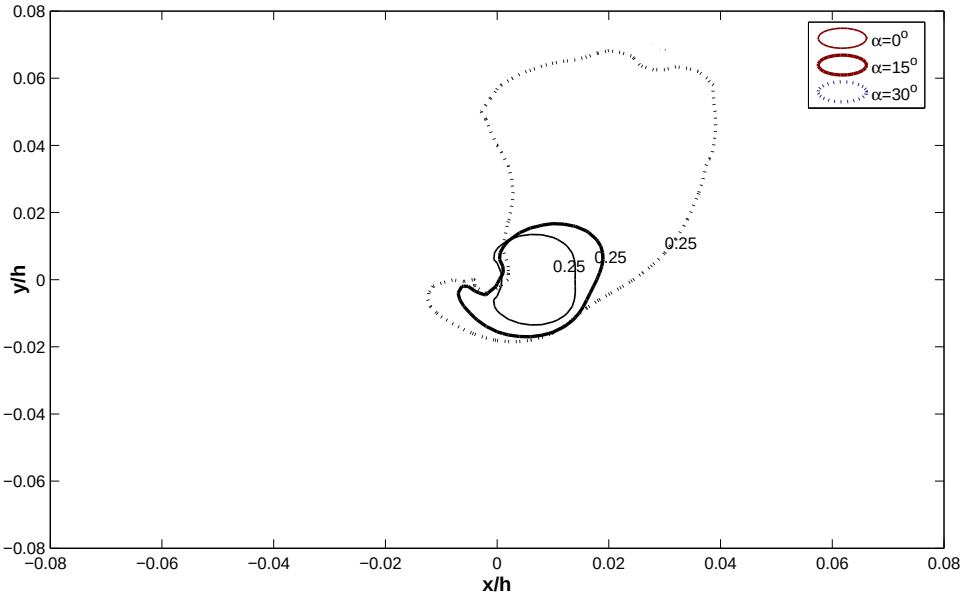

Figure 3.75. Error contours for $a/h = 0.3$ and $E_2/E_1 = 2$ with different crack angles around right crack tip

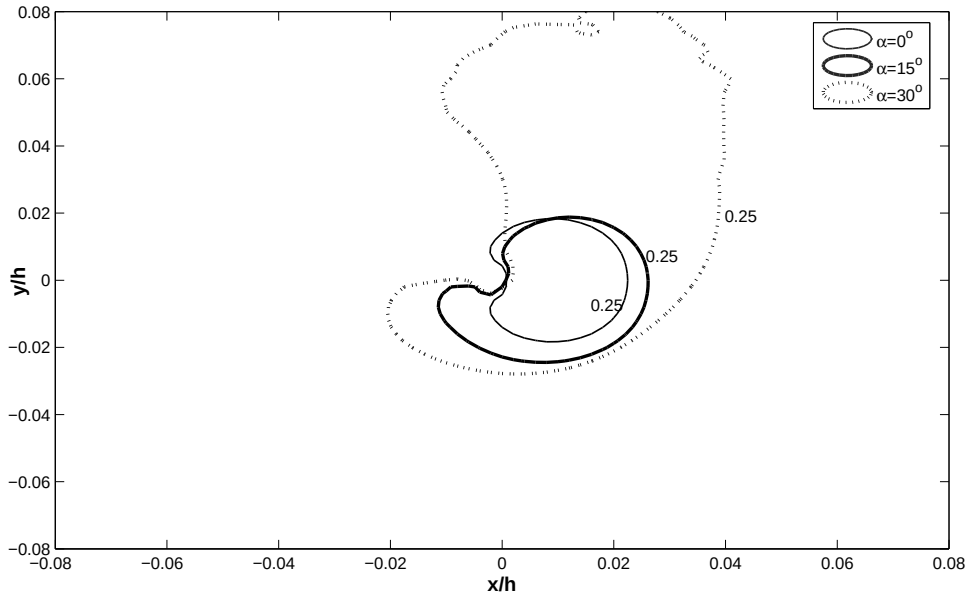

Figure 3.76. Error contours for $a/h = 0.3$ and $E_2/E_1 = 5$ with different crack angles around right crack tip

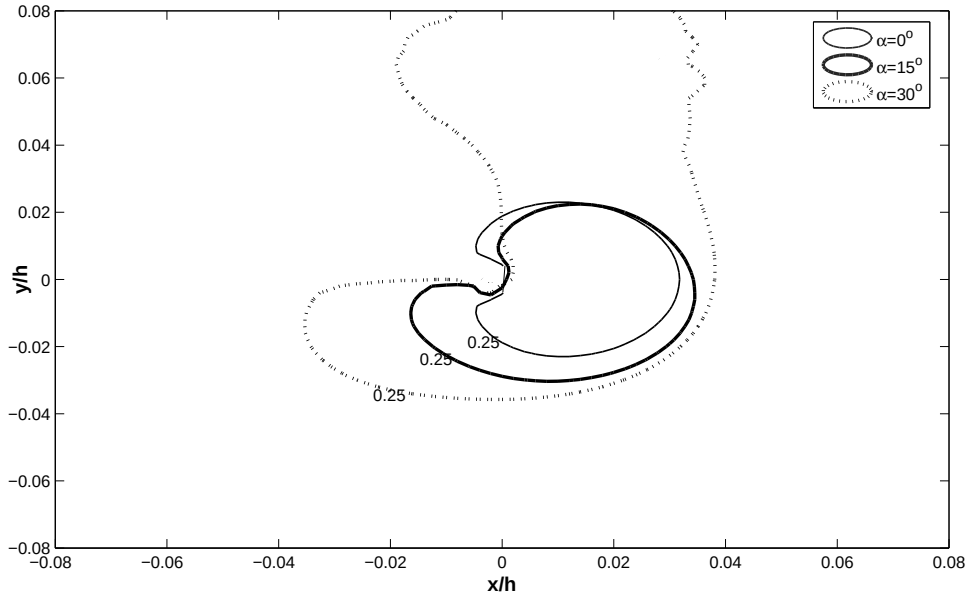

Figure 3.77. Error contours for $a/h = 0.3$ and $E_2/E_1 = 10$ with different crack angles around right crack tip

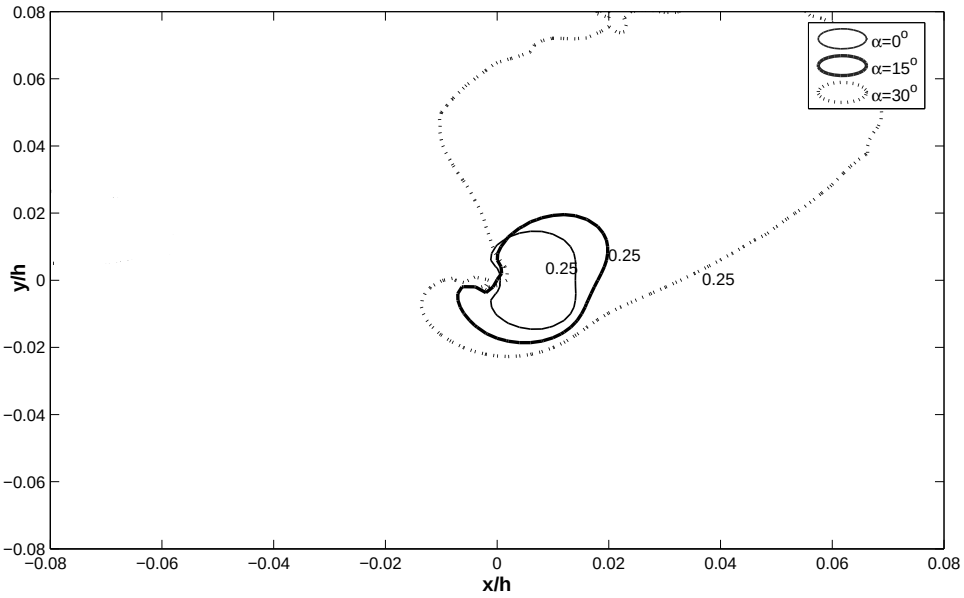

Figure 3.78. Error contours for $a/h = 0.3$ and $E_2/E_1 = 2$ with different crack angles around left crack tip

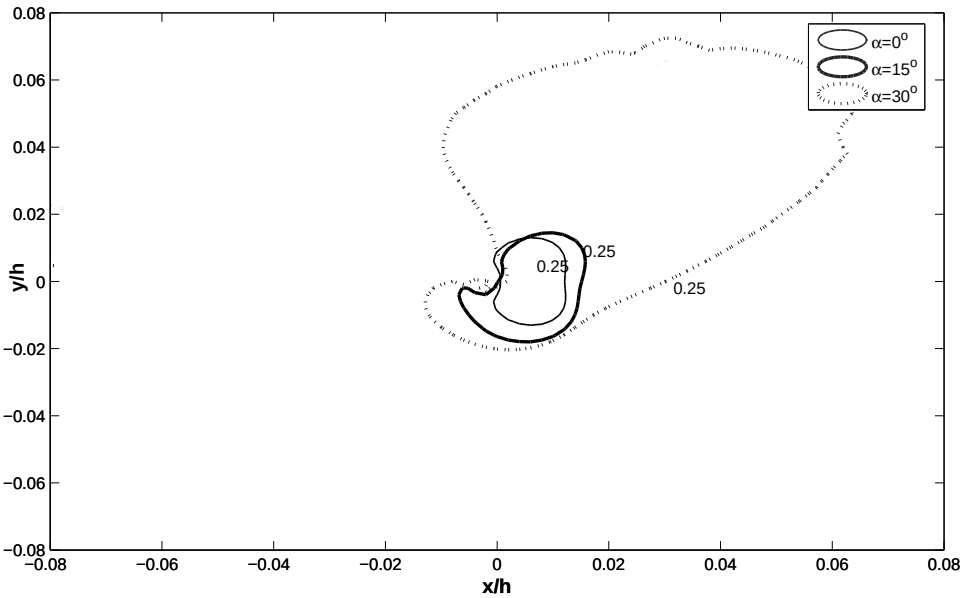

Figure 3.79. Error contours for $a/h = 0.3$ and $E_2/E_1 = 5$ with different crack angles around left crack tip

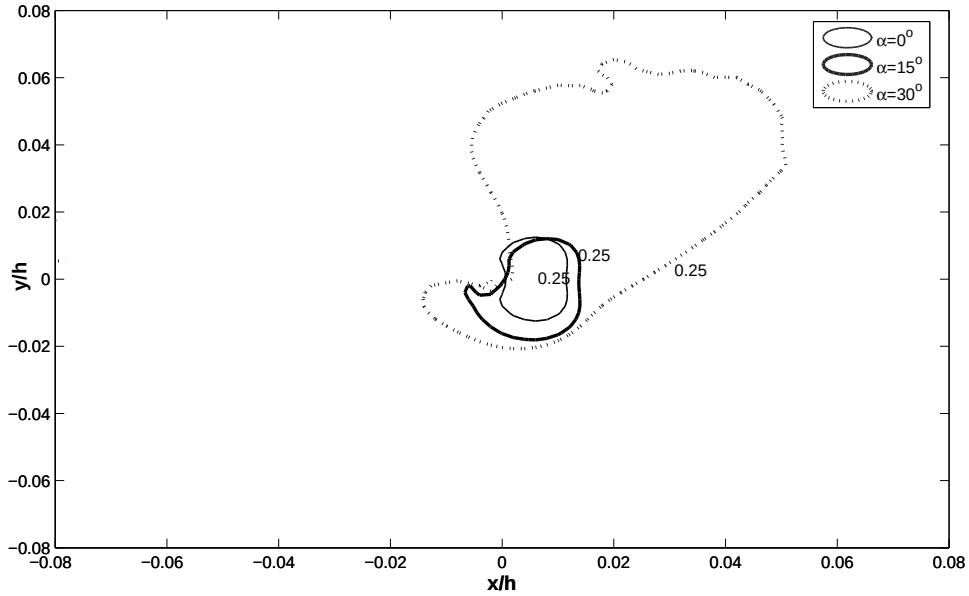

Figure 3.80. Error contours for $a/h = 0.3$ and $E_2/E_1 = 10$ with different crack angles around left crack tip

3.3.3. Effect of Crack Length on Extent of K-dominant Region

First analysis is to investigate the stress field in y-direction along the crack for different crack lengths. The analysis is done for $E_2/E_1 = 2$ with $\alpha = 15^o$, 30^o, 45^o, 60^o. FE and ASY solution of σ_{yy} are given separately. The results are plotted in Figures 3.81 - 3.86 for the right crack tip.

It is seen that as crack length increases both finite element and asymptotic stress values increase. For all the crack lengths, FE stress values are higher than ASY stress values. Besides, for longer crack the opening stress is higher at the crack tip and drops dramatically towards the right edge. In other words, the stress curve has high-slope. The reason is that there are more compressive stresses near the right edge form for longer cracks.

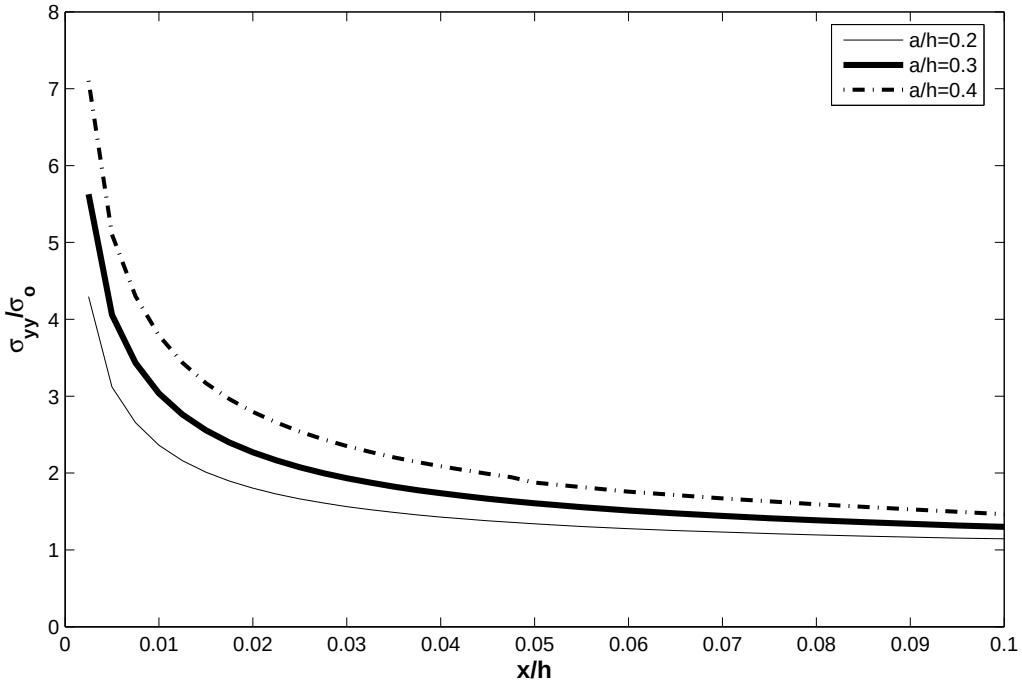

Figure 3.81. FE results for σ_{yy}/σ_o vs x/h, $\alpha = 15^o$, $E_2/E_1 = 2$ for different crack lengths

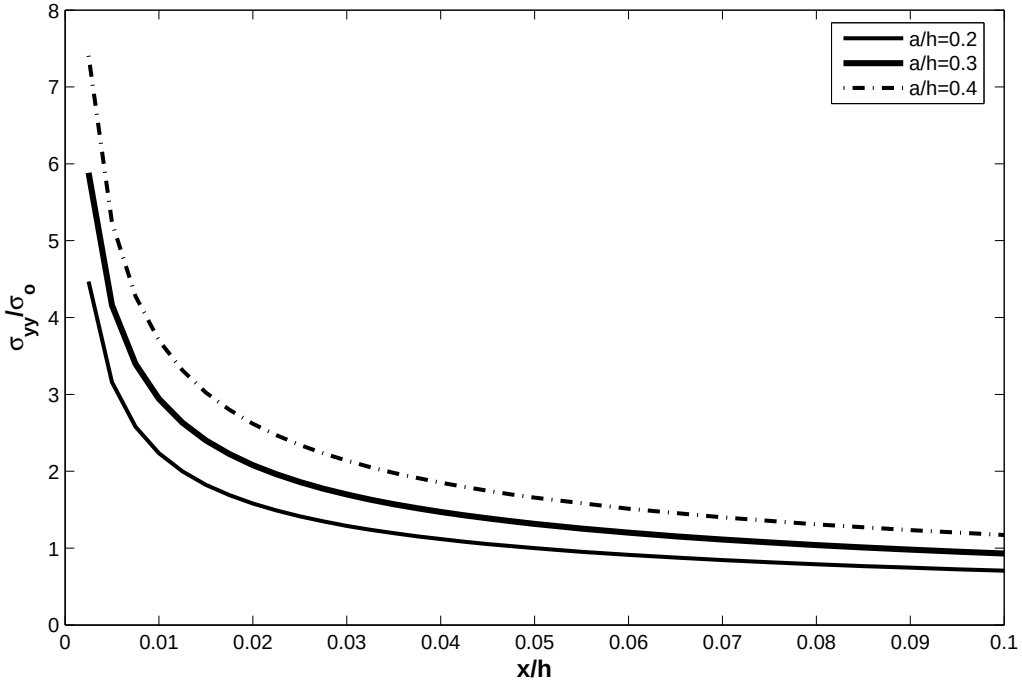

Figure 3.82. ASY results for σ_{yy}/σ_o vs x/h $\alpha = 15^o$, $E_2/E_1 = 2$ for different crack lengths

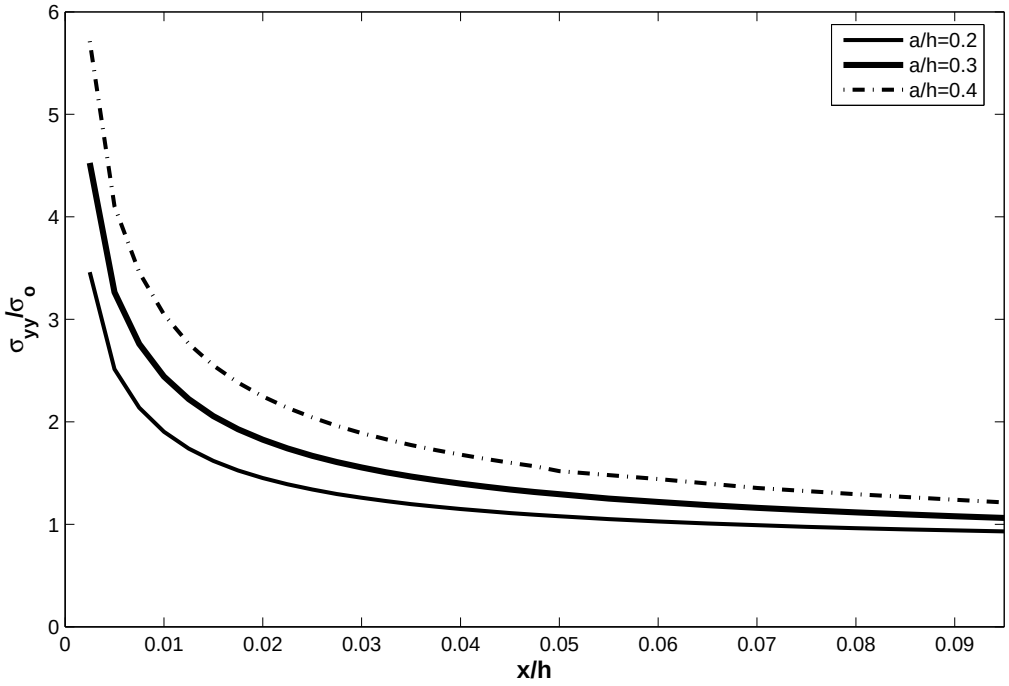

Figure 3.83. FE results for σ_{yy}/σ_o vs x/h, $\alpha = 30^o$, $E_2/E_1 = 2$ for different crack lengths

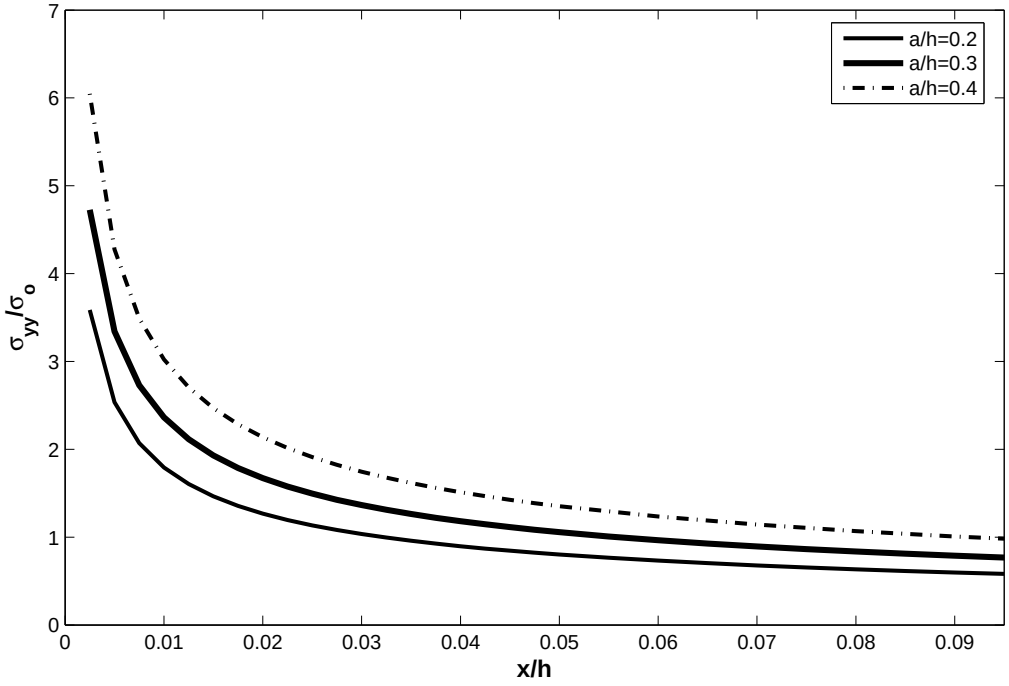

Figure 3.84. ASY results for σ_{yy}/σ_o vs x/h, $\alpha = 30^o$, $E_2/E_1 = 2$ for different crack lengths

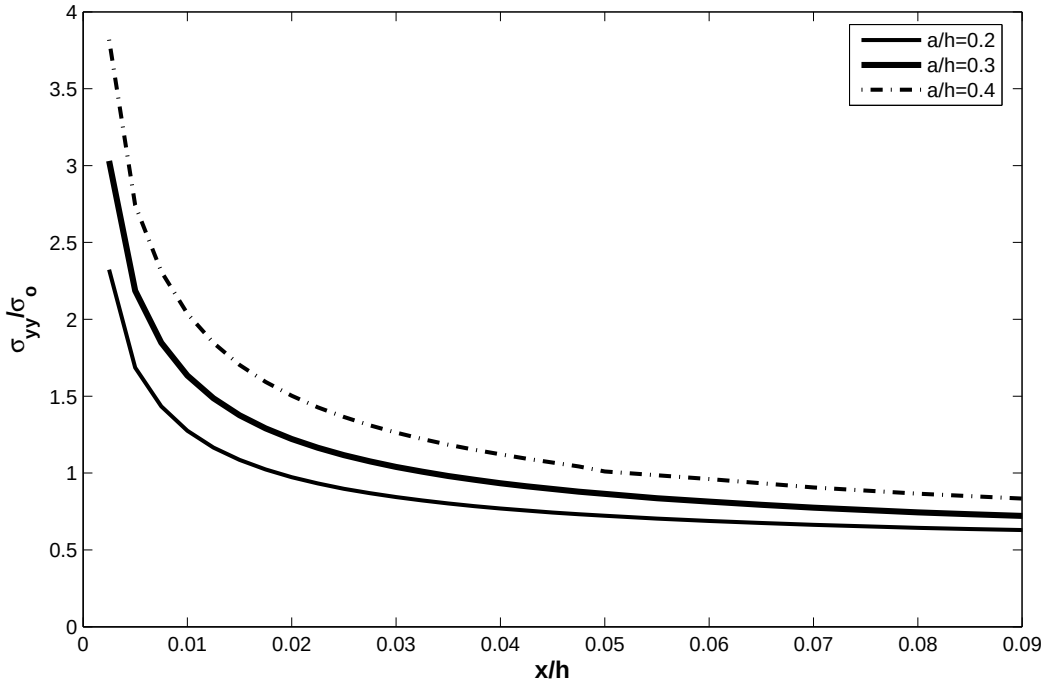

Figure 3.85. FE results for σ_{yy}/σ_o vs x/h, $\alpha = 45^o$, $E_2/E_1 = 2$ for different crack lengths

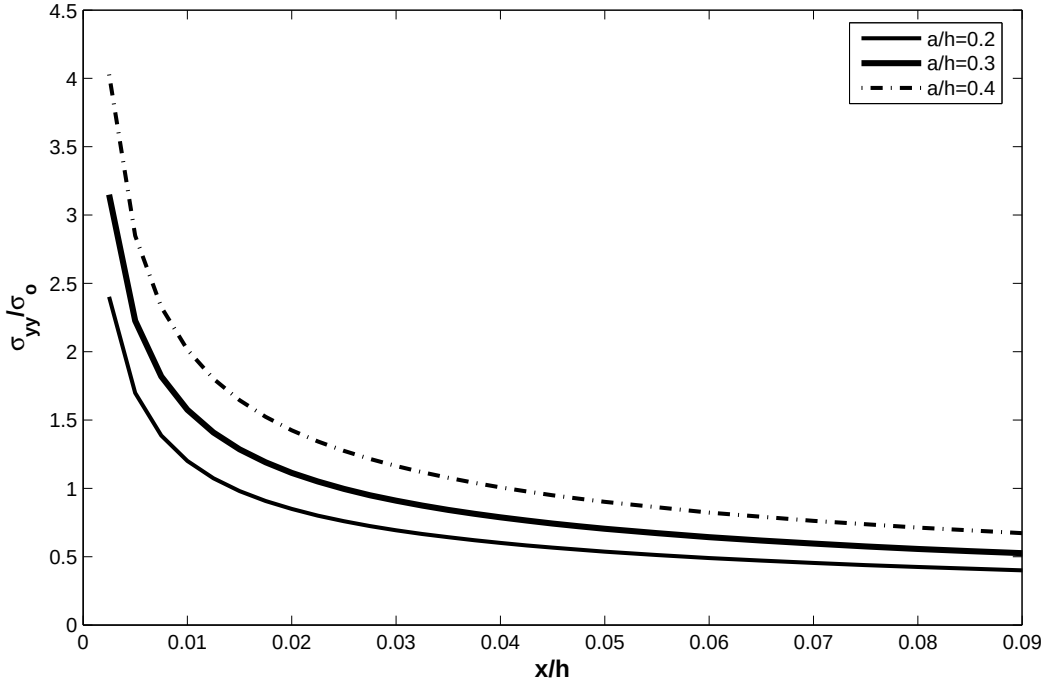

Figure 3.86. ASY results for σ_{yy}/σ_o vs x/h, $\alpha = 45^o$, $E_2/E_1 = 2$ for different crack lengths

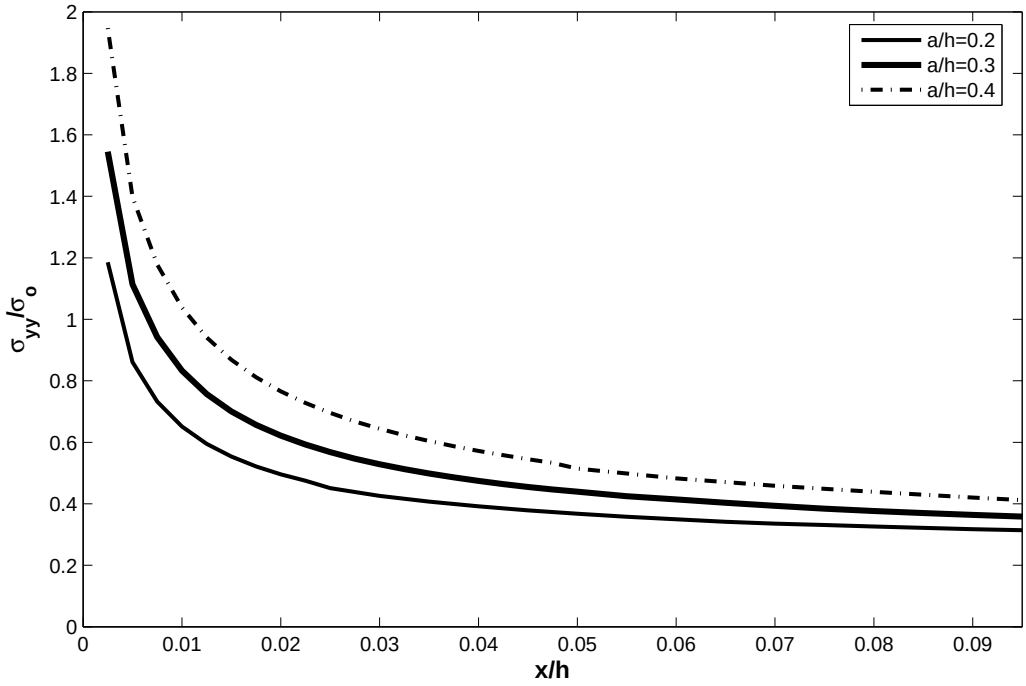

Figure 3.87. FE results for σ_{yy}/σ_o vs x/h, $\alpha = 60^o$, $E_2/E_1 = 2$ for different crack lengths

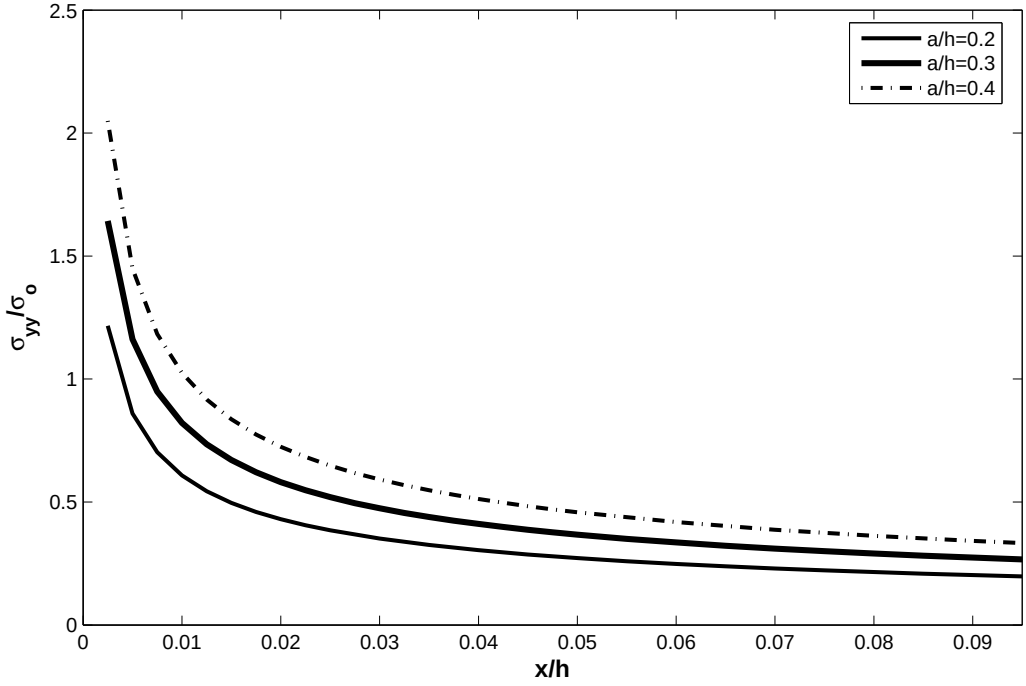

Figure 3.88. ASY results for σ_{yy}/σ_o vs x/h, $\alpha = 60^o$, $E_2/E_1 = 2$ for different crack lengths

Besides, a comparison between FE solution and ASY solution is done by plotting FE and ASY curves on the same graph. In Figure 3.89, the plot is given for $a/h = 0.2$, $\alpha = 15^o$ and $E_2/E_1 = 2$. FE solution gives higher stress values than ASY for this crack length and σ_{yy} value decreases towards the right edge because compressive stresses are formed. As the crack length increases to $a/h = 0.3$ and $a/h = 0.4$ with fixed crack angle ($\alpha = 15^o$), both FE and ASY stress values increase. As crack length gets longer, compressive effect becomes dominant and it causes ASY and FE curves to get closer to each other so they agree well. Similar graphs are plotted in Figures 3.92 - 3.94 for $\alpha = 30^o$. Same behavior is also seen here.

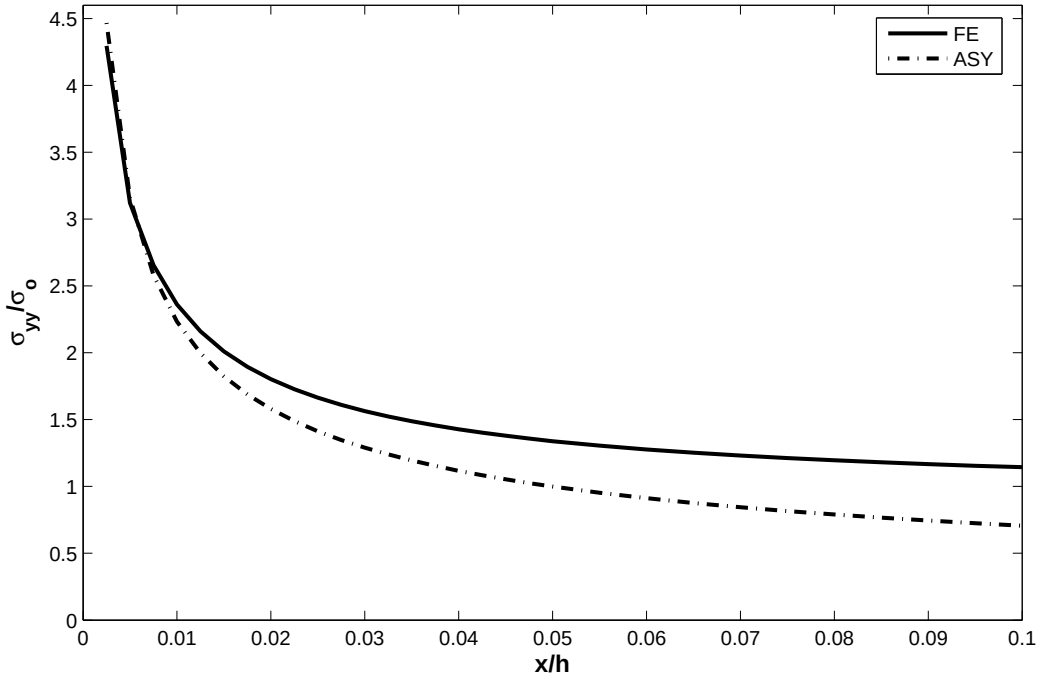

Figure 3.89. σ_{yy}/σ_o vs x/h for $a/h = 0.2$, $\alpha = 15^o$ and $E_2/E_1 = 2$ around right crack tip

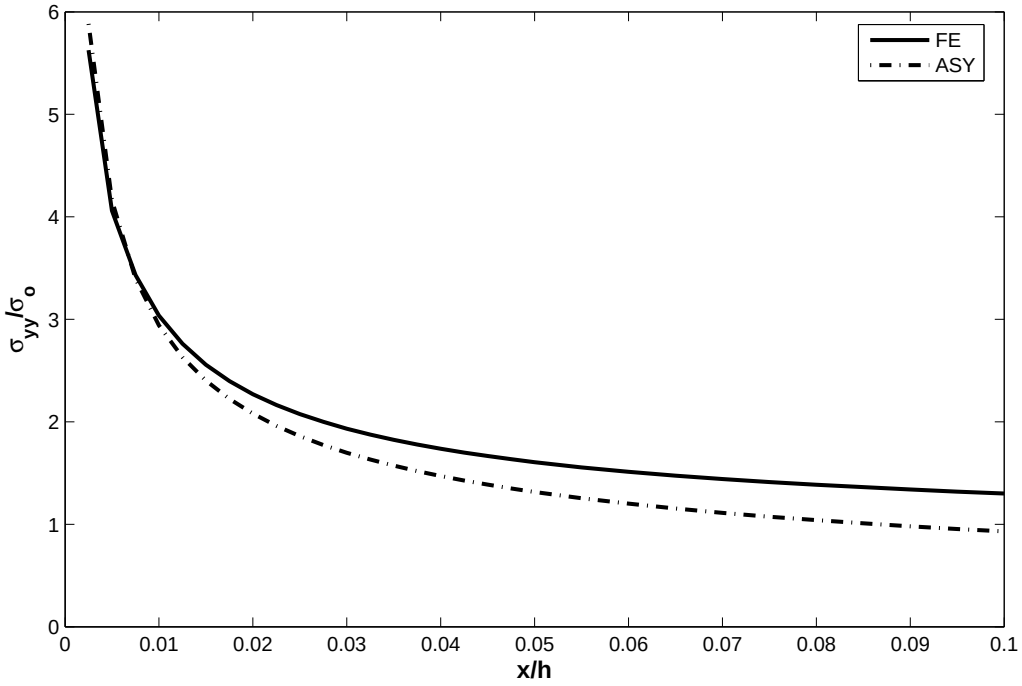

Figure 3.90. σ_{yy}/σ_o vs x/h for $a/h = 0.3$, $\alpha = 15^o$ and $E_2/E_1 = 2$ around right crack tip

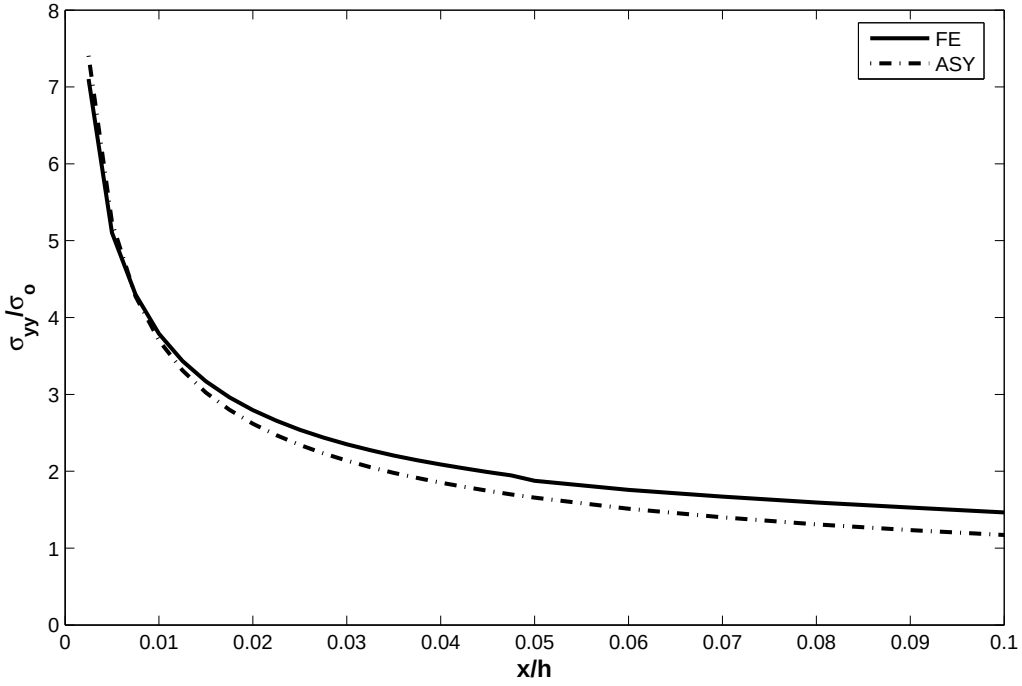

Figure 3.91. σ_{yy}/σ_o vs x/h for $a/h = 0.4$, $\alpha = 15^o$ and $E_2/E_1 = 2$ around right crack tip

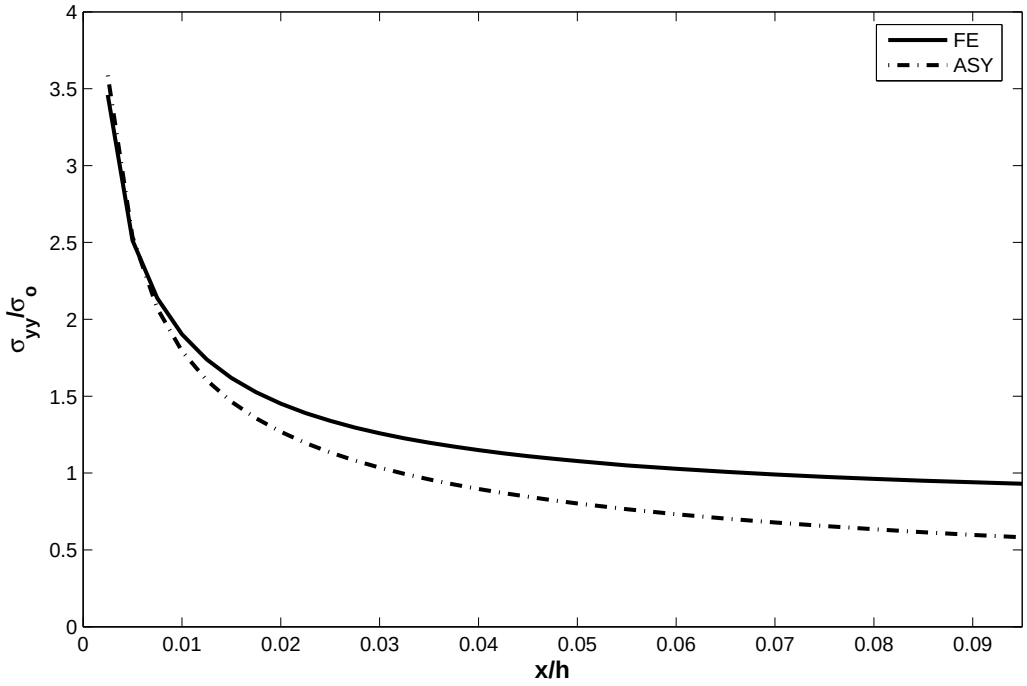

Figure 3.92. σ_{yy}/σ_o vs x/h for $a/h = 0.2$, $\alpha = 30^o$ and $E_2/E_1 = 2$ around right crack tip

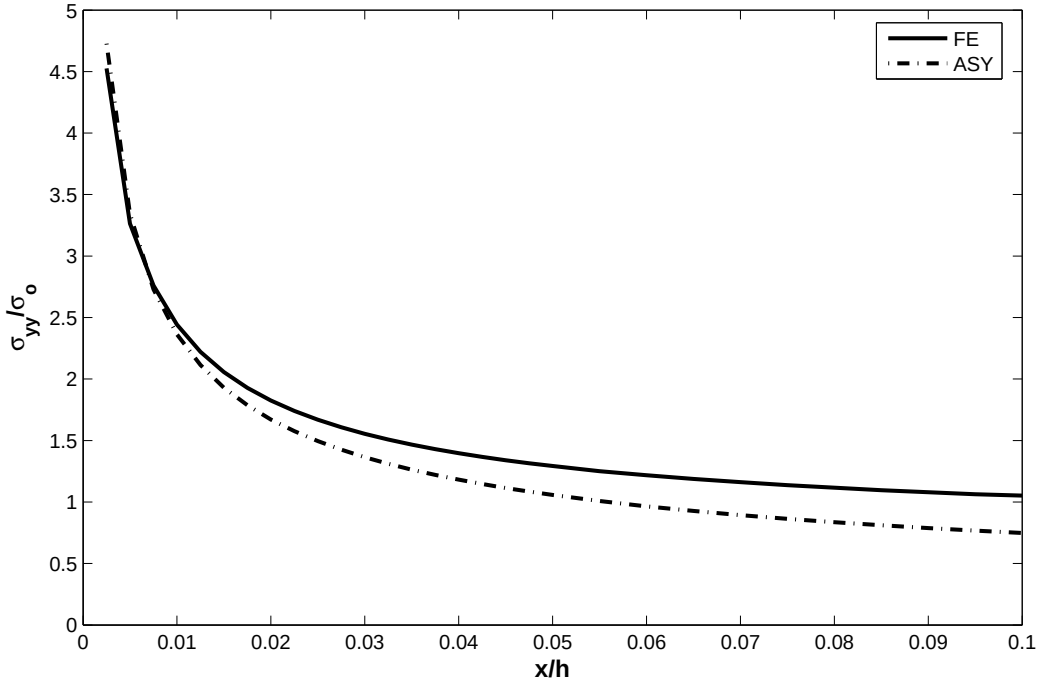

Figure 3.93. σ_{yy}/σ_o vs x/h for $a/h = 0.3$ $\alpha = 30^o$ and $E_2/E_1 = 2$ around right crack tip

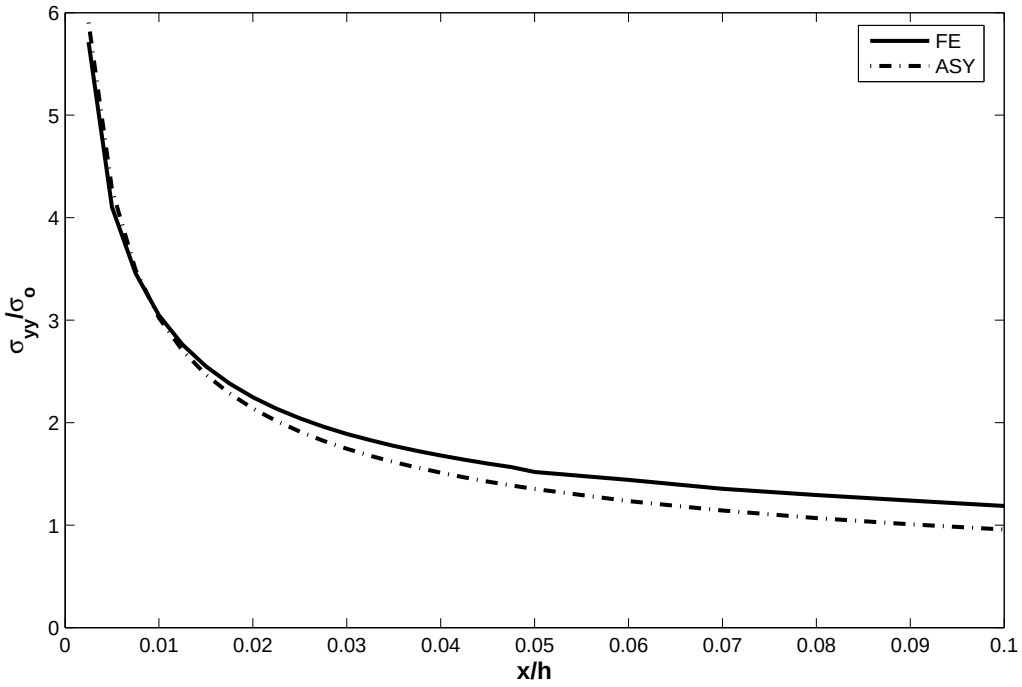

Figure 3.94. σ_{yy}/σ_o vs x/h for $a/h = 0.4$ $\alpha = 30^o$ and $E_2/E_1 = 2$ around right crack tip

In sections 3.3.1 and 3.3.2, the stress contours for $a/h = 0.2$ and 0.3 are given for $E_2/E_1 = 2$, 5, 10, 20 with $\alpha = 15^o$, 30^o, 45^o. The stress contours for $a/h = 0.4$ are given in Figures 3.95 - 3.106 around right crack tip. The effect of crack length on σ_{yy} can be investigated on the K-dominant region. Observation of the figures shows that both FE and ASY stress values increase as the crack length increases. Since compressive stresses become more effective at the longer crack lengths, σ_{yy} for FE can not increase as much as ASY solution. Thus, the stress contours get closer to each other as the crack length increases which means that K-dominant region increases with an increase in the crack length.

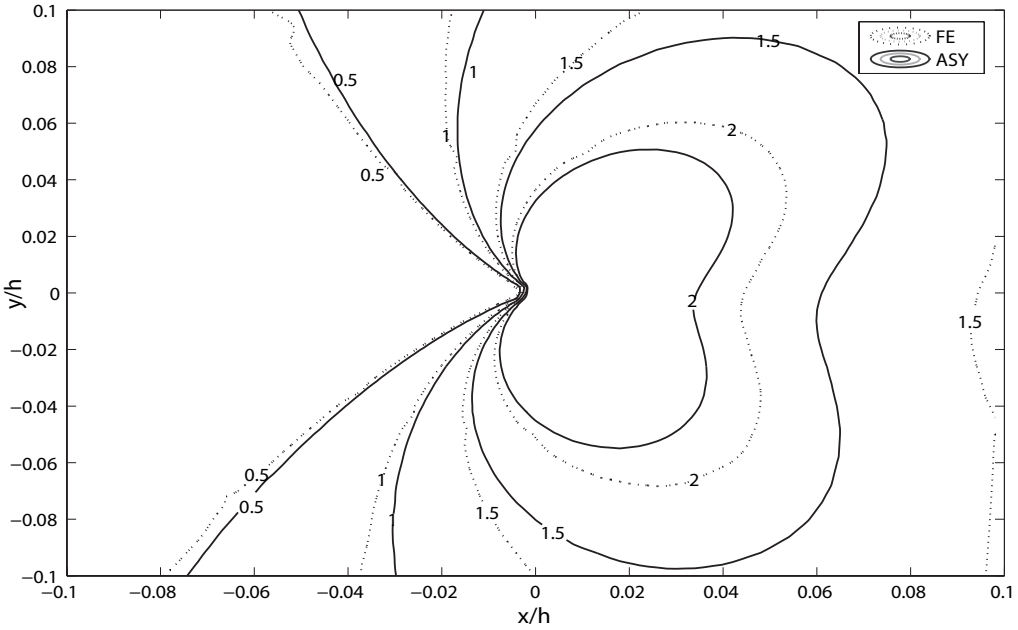

Figure 3.95. Contour plot of σ_{yy} for $E_2/E_1 = 2$, $a/h = 0.4$ and $\alpha = 15^o$ around right crack tip

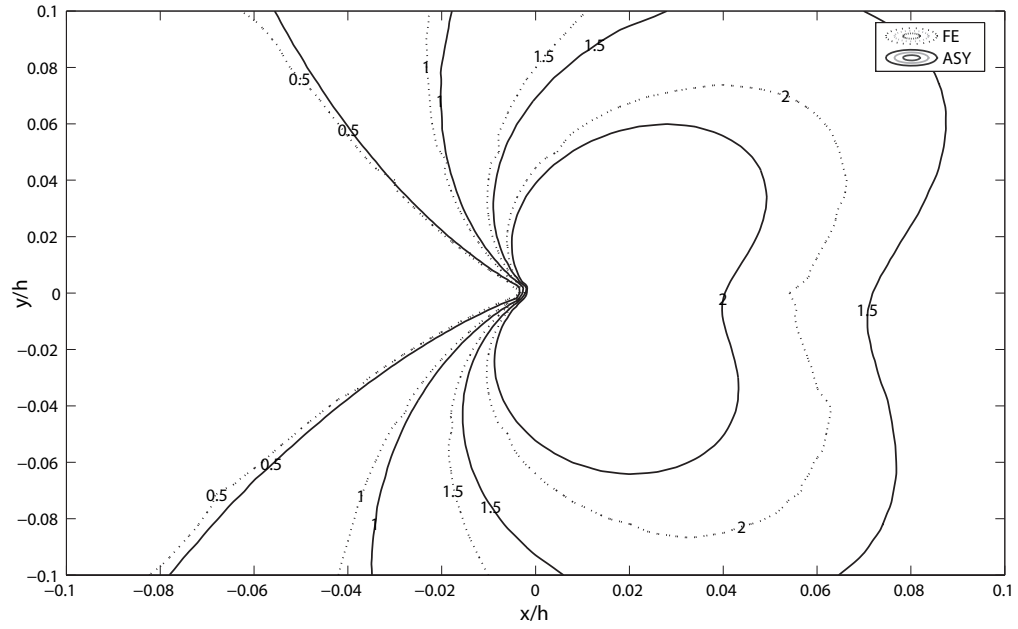

Figure 3.96. Contour plot of σ_{yy} for $E_2/E_1 = 5$, $a/h = 0.4$ and $\alpha = 15^o$ around right crack tip

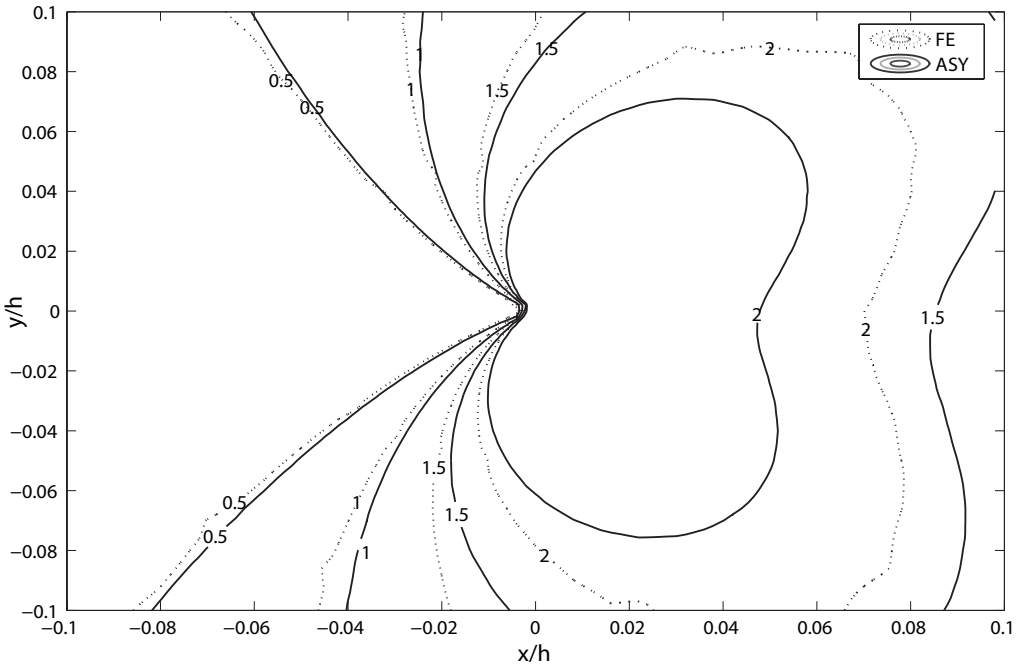

Figure 3.97. Contour plot of σ_{yy} for $E_2/E_1 = 2$, $a/h = 0.4$ and $\alpha = 15^o$ around right crack tip

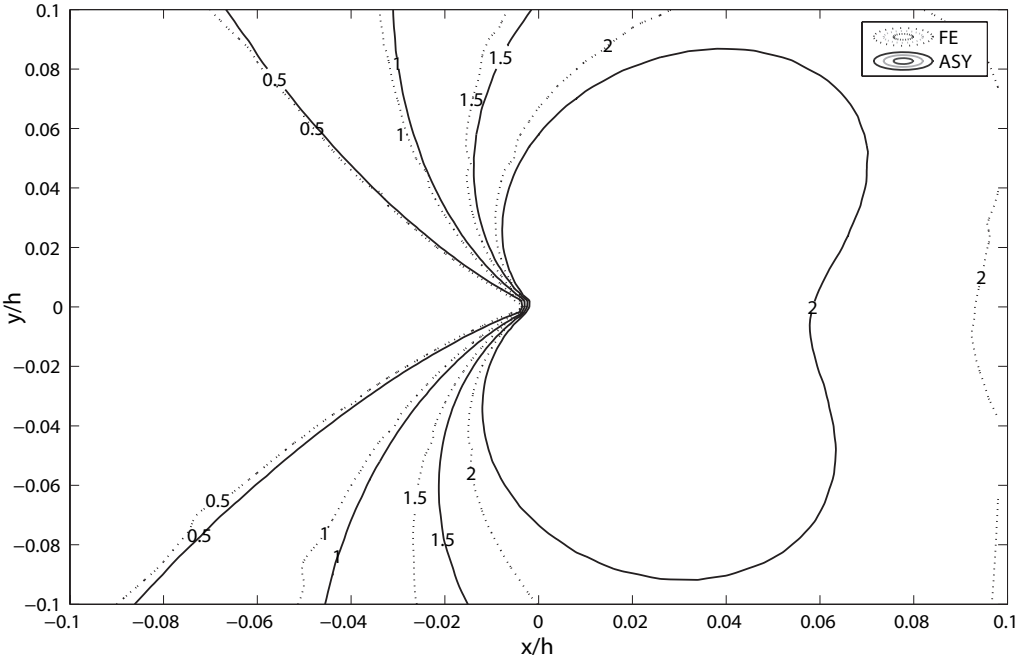

Figure 3.98. Contour plot of σ_{yy} for $E_2/E_1 = 20$, $a/h = 0.4$ and $\alpha = 15^o$ around right crack tip

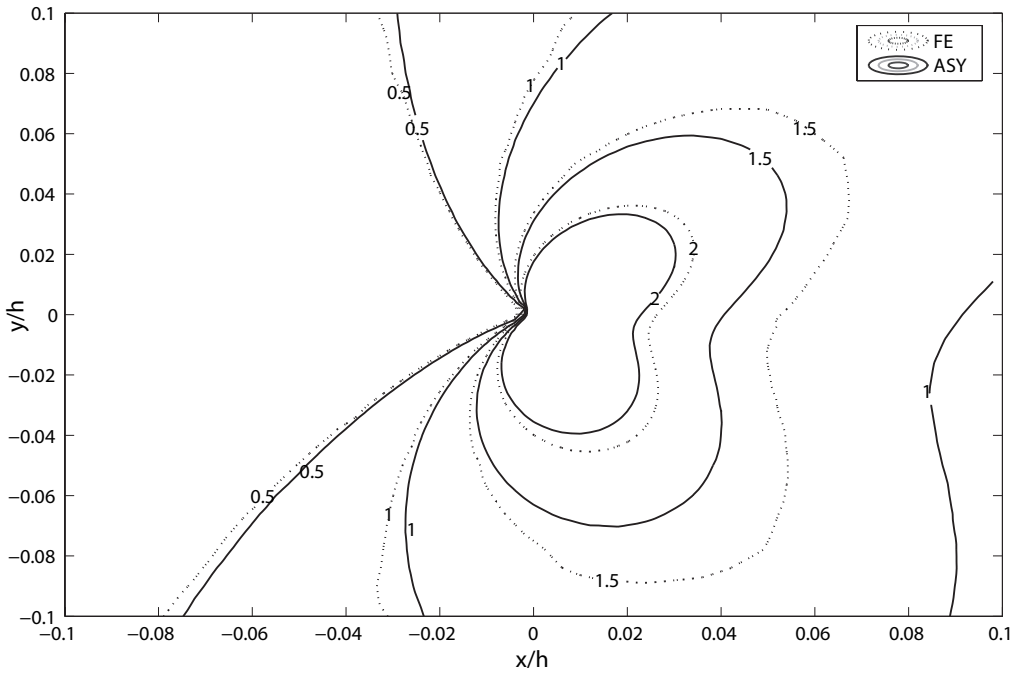

Figure 3.99. Contour plot of σ_{yy} for $E_2/E_1 = 2$, $a/h = 0.4$ and $\alpha = 30^o$ around right crack tip

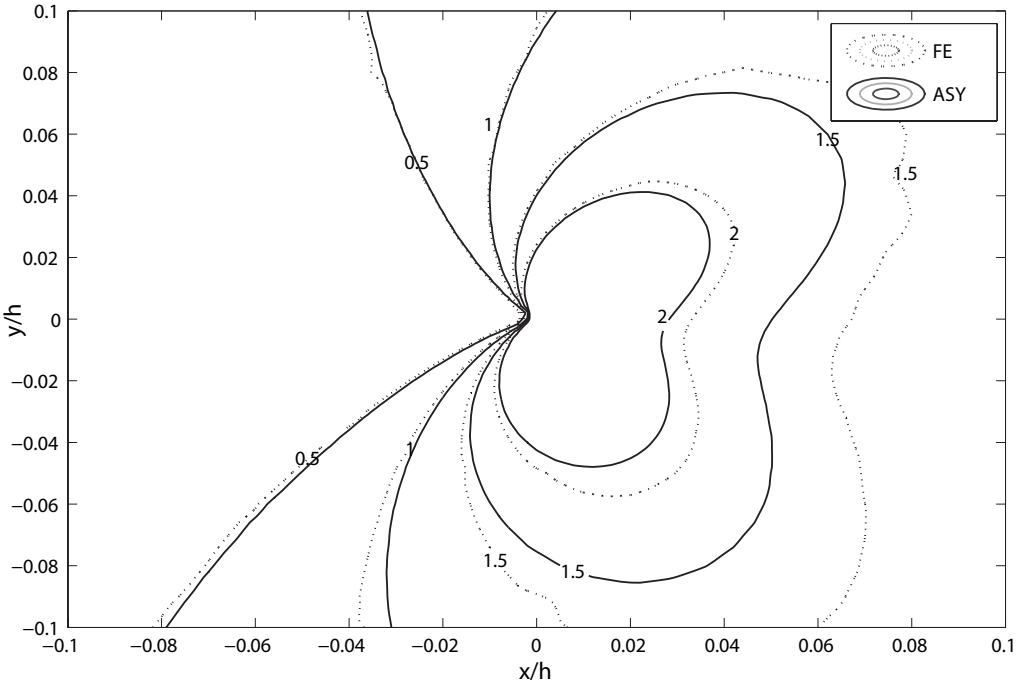

Figure 3.100. Contour plot of σ_{yy} for $E_2/E_1 = 5$, $a/h = 0.4$ and $\alpha = 30^o$ around right crack tip

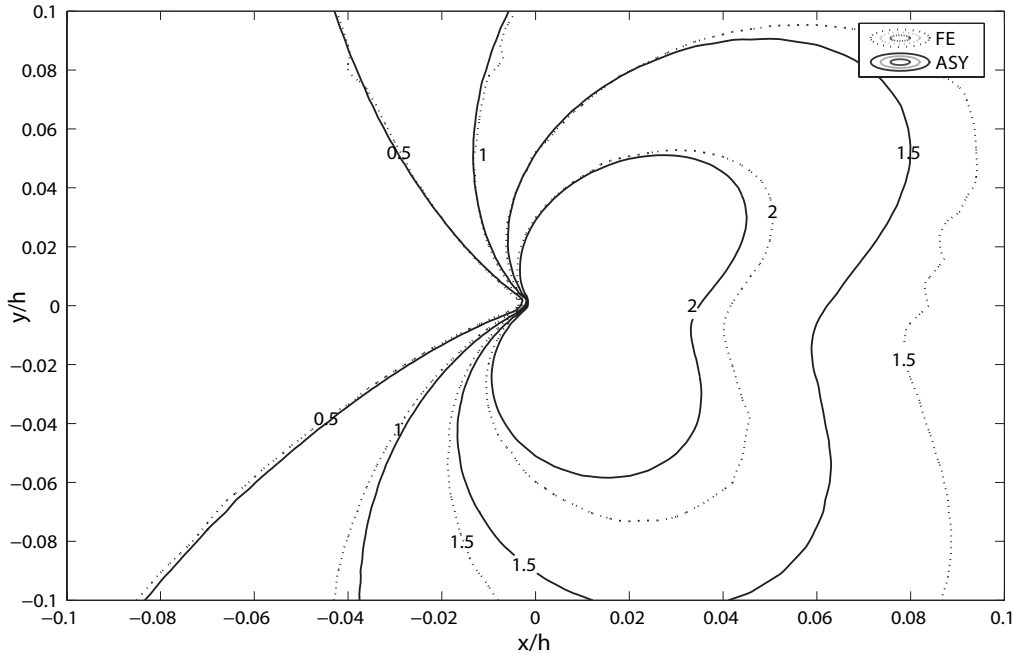

Figure 3.101. Contour plot of σ_{yy} for $E_2/E_1 = 10$, $a/h = 0.4$ and $\alpha = 30^o$ around right crack tip

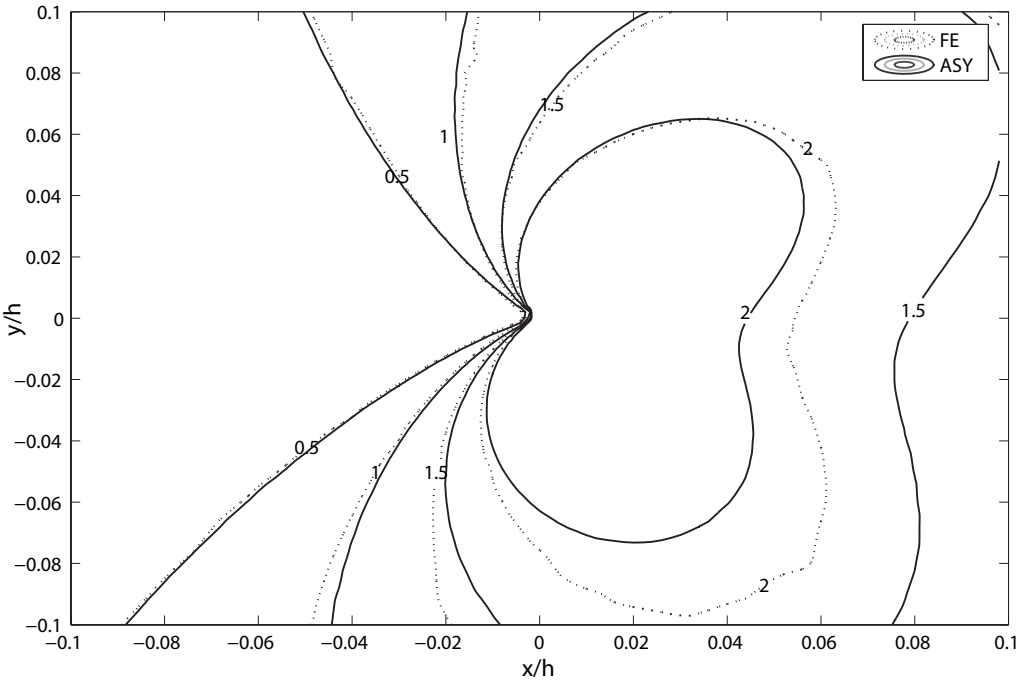

Figure 3.102. Contour plot of σ_{yy} for $E_2/E_1 = 20$, $a/h = 0.4$ and $\alpha = 30^o$ around right crack tip

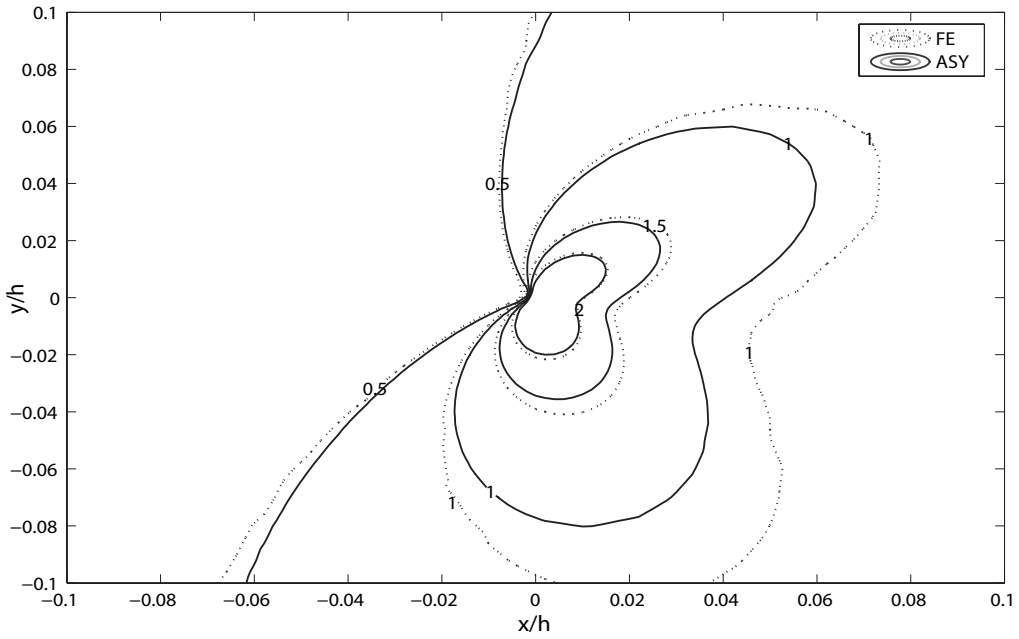

Figure 3.103. Contour plot of σ_{yy} for $E_2/E_1 = 2$, $a/h = 0.4$ and $\alpha = 45^o$ around right crack tip

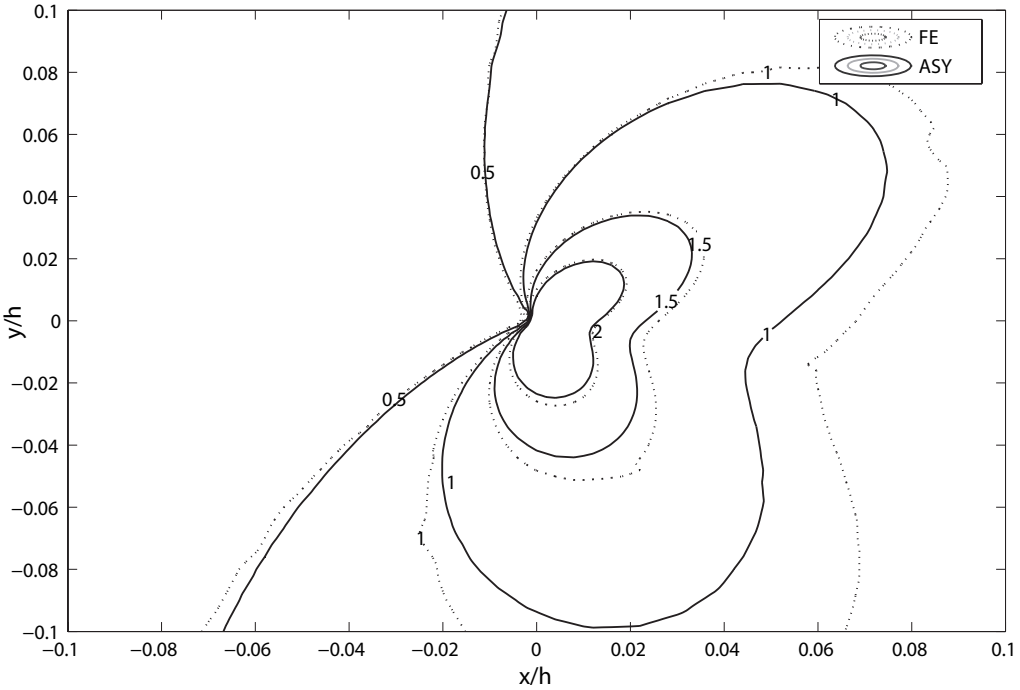

Figure 3.104. Contour plot of σ_{yy} for $E_2/E_1 = 5$, $a/h = 0.4$ and $\alpha = 45^o$ around right crack tip

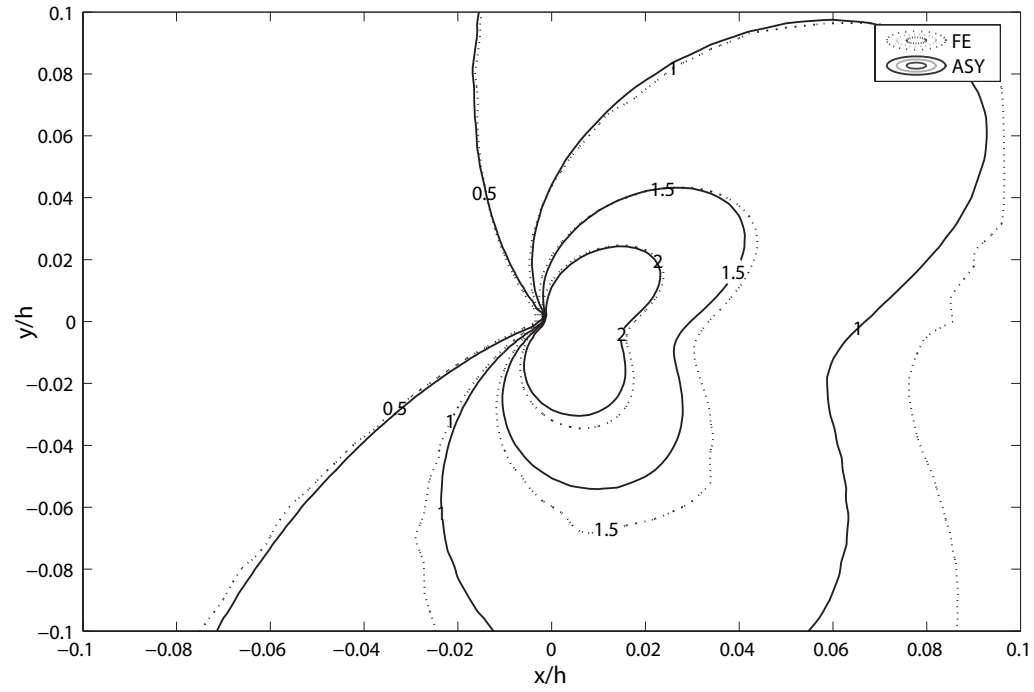

Figure 3.105. Contour plot of σ_{yy} for $E_2/E_1 = 10$, $a/h = 0.4$ and $\alpha = 45^o$ around right crack tip

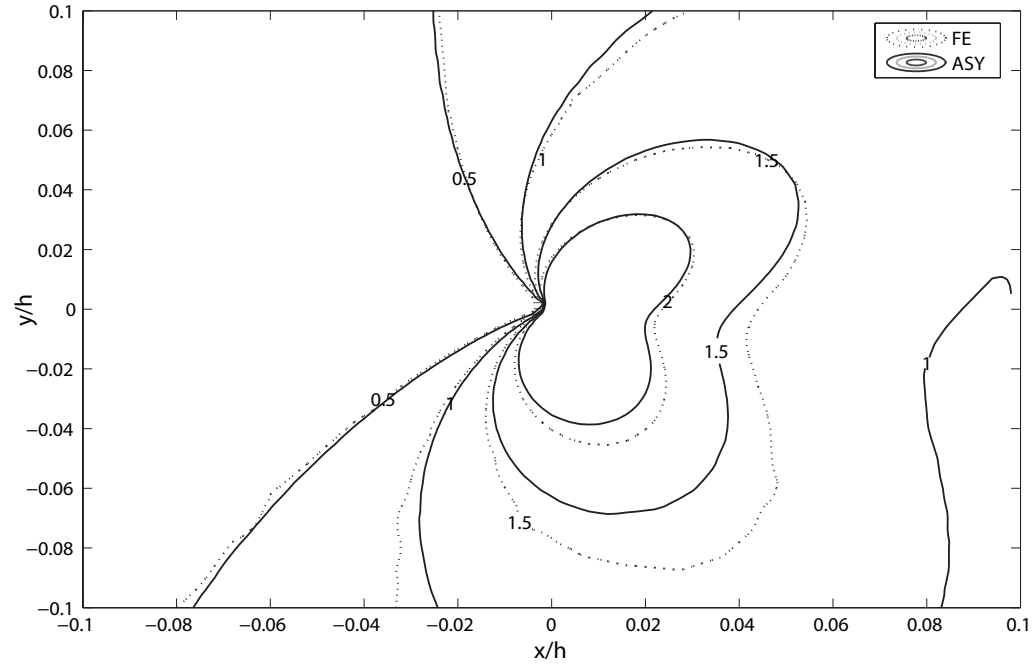

Figure 3.106. Contour plot of σ_{yy} for $E_2/E_1 = 20$, $a/h = 0.4$ and $\alpha = 45^o$ around right crack tip

The error contours are plotted to understand the difference between ASY and FE stress fields. The error contours for $E_2/E_1 = 5$ with $\alpha = 15^o$, 30^o are given for different crack lengths in Figure 3.107 - 3.108. Again, one of the smallest error value is selected to plot for different crack lengths in the same figure. In each crack angle value, it can be seen easily that K-dominant region increases with an increase in the crack length. This result is in accordance with the result concluded from the stress contours given previously.

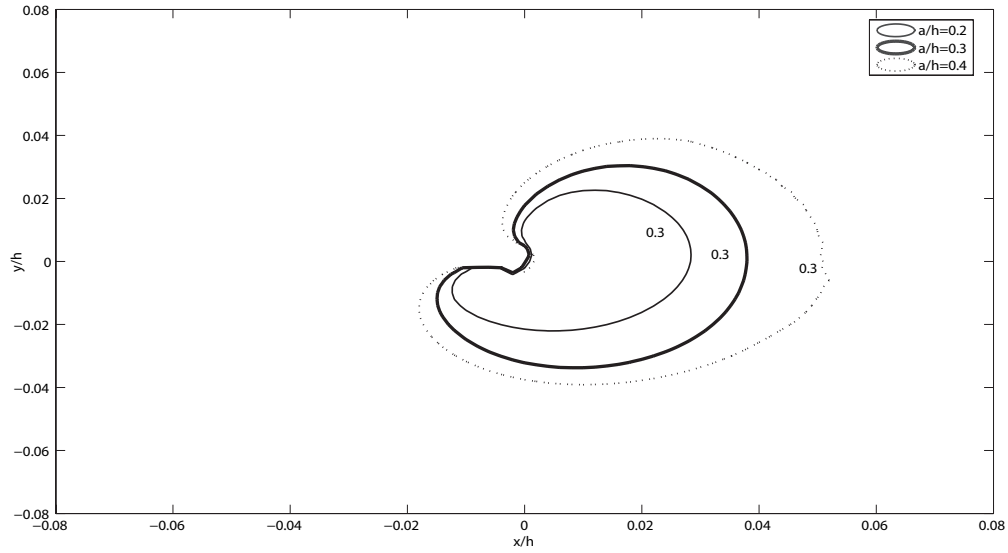

Figure 3.107. Error contours with $\alpha = 15^o$ and $E_2/E_1 = 5$ for different a/h ratios around right crack tip

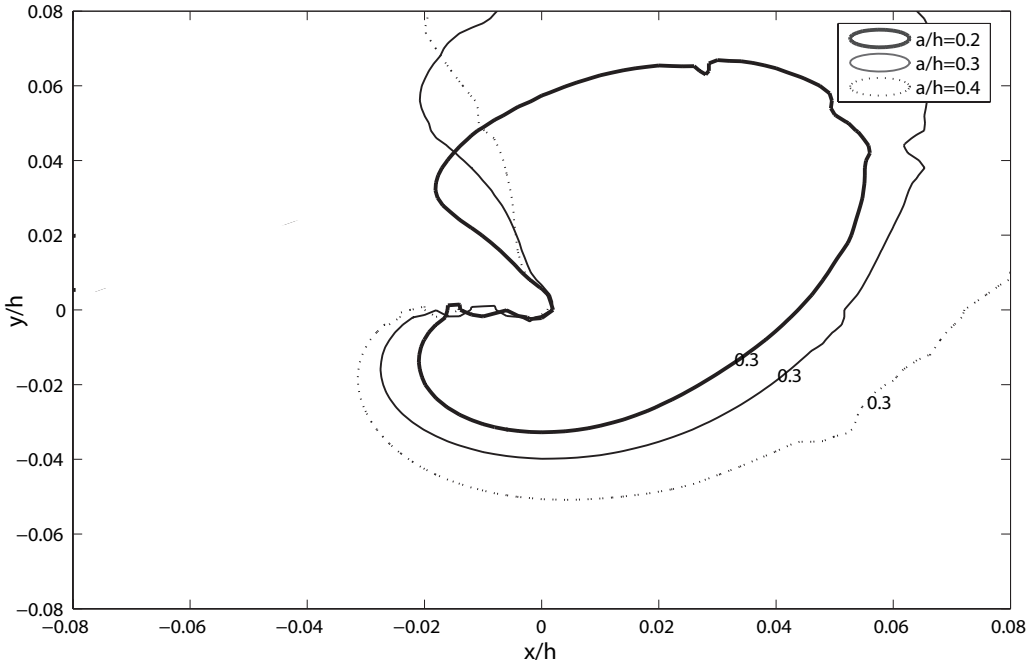

Figure 3.108. Error contours with $\alpha = 30^o$ and $E_2/E_1 = 5$ for different a/h ratios around right crack tip

3.3.4. Extent of K-dominant Region with Asymptotic Stress Equations Derived by Konda and Erdogan [12]

Up to now asymptotic stress fields are calculated using the asymptotic formulation given by Equations 2.1 - 2.3. These expressions are derived for homogeneous materials by Williams [23]. Konda and Erdogan [12] derived the asymptotic stress field near the crack tip for nonhomogeneous material. They assumed the change of shear modulus as $\mu(x, y) = \mu_0 e^{\beta x+\gamma y}$ and the poisson's ratio, ν, as constant. The explicit form of Equation 1.2 are rewritten below. The two set of equations for the asymptotic stress fields are compared, it can be seen that the only difference between them is the influence of the nonhomogeneity $e^{r(\beta cos\theta)}$.

$$\sigma_{xx} = e^{r(\beta cos\theta)}([\frac{K_I}{\sqrt{2\pi r}} cos\frac{\theta}{2}(1 - sin\frac{\theta}{2}sin\frac{3\theta}{2})] - [\frac{K_{II}}{\sqrt{2\pi r}} sin\frac{\theta}{2}(2 + cos\frac{\theta}{2}cos\frac{3\theta}{2})]), \quad (3.2)$$

$$\sigma_{yy} = e^{r(\beta cos\theta)}([\frac{K_I}{\sqrt{2\pi r}} cos\frac{\theta}{2}(1 + sin\frac{\theta}{2}sin\frac{3\theta}{2})] + [\frac{K_{II}}{\sqrt{2\pi r}}(sin\frac{\theta}{2}cos\frac{\theta}{2}cos\frac{3\theta}{2})]), \qquad (3.3)$$

$$\sigma_{xy} = e^{r(\beta cos\theta)}([\frac{K_I}{\sqrt{2\pi r}} cos\frac{\theta}{2}sin\frac{\theta}{2}cos\frac{3\theta}{2}] + [\frac{K_{II}}{\sqrt{2\pi r}}(cos\frac{\theta}{2}(1 - sin\frac{\theta}{2}sin\frac{3\theta}{2})]). \qquad (3.4)$$

To see the difference between the two asymptotic stress calculations (ASY and ASY NEW) and finite element solution (FE), σ_{yy}/σ_o curves are plotted on the symmetry axis in Figures 3.109 - 3.120. The plots are given for $a/h = 0.2$ and 0.3, crack angles $\alpha = 15^o$, 30^o, material nonhomogeneities $E_2/E_1 = 2$, 5, 10 for stress fields around the right crack tip. The effects of crack length, material nonhomogeneity and crack angle are studied.

In general it is seen that ASY NEW give better results than the ASY probably becuse it contains the effect of nonhomogeneity in the asymptotic expression. As E_2/E_1 increases from 2 to 10 the difference between ASY and ASY NEW stress values get higher and ASY NEW values are much closer to FE results when the effect of crack angle change is studied, the difference between ASY and ASY NEW reduces as the crack angle increases. Thus, ASY NEW is more accurate when compared to FE results for $\alpha = 15^o$ than for $\alpha = 30^o$. Last, if stress fields are compared for different crack lengths, ASY NEW values are closer to FE than ASY values for all crack lengths.

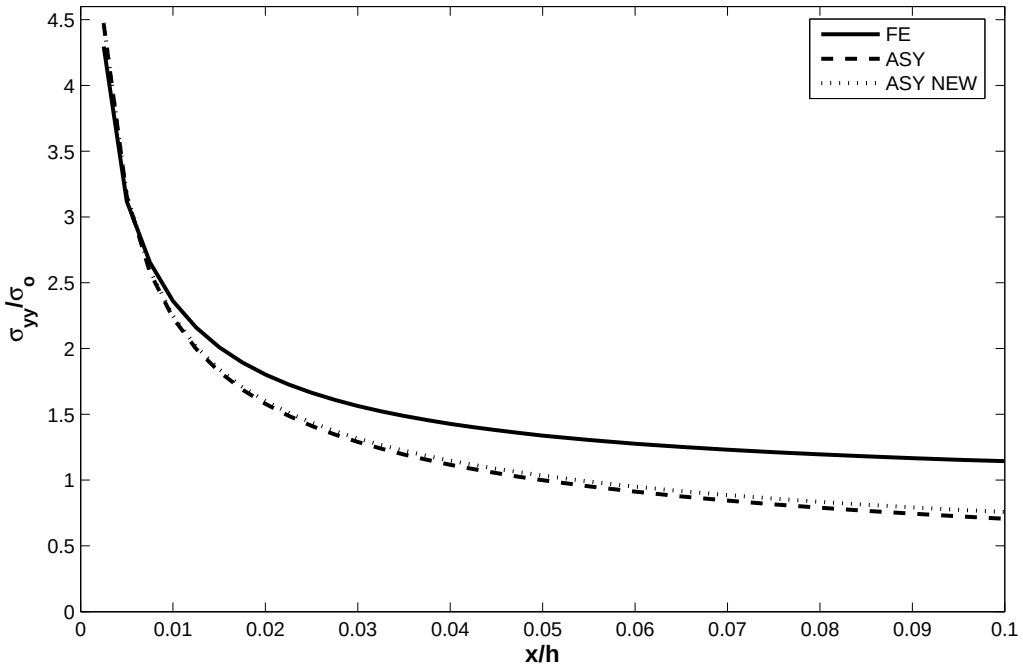

Figure 3.109. σ_{yy}/σ_o vs x/h for $\alpha = 15^o$, $E_2/E_1 = 2$ and $a/h = 0.2$

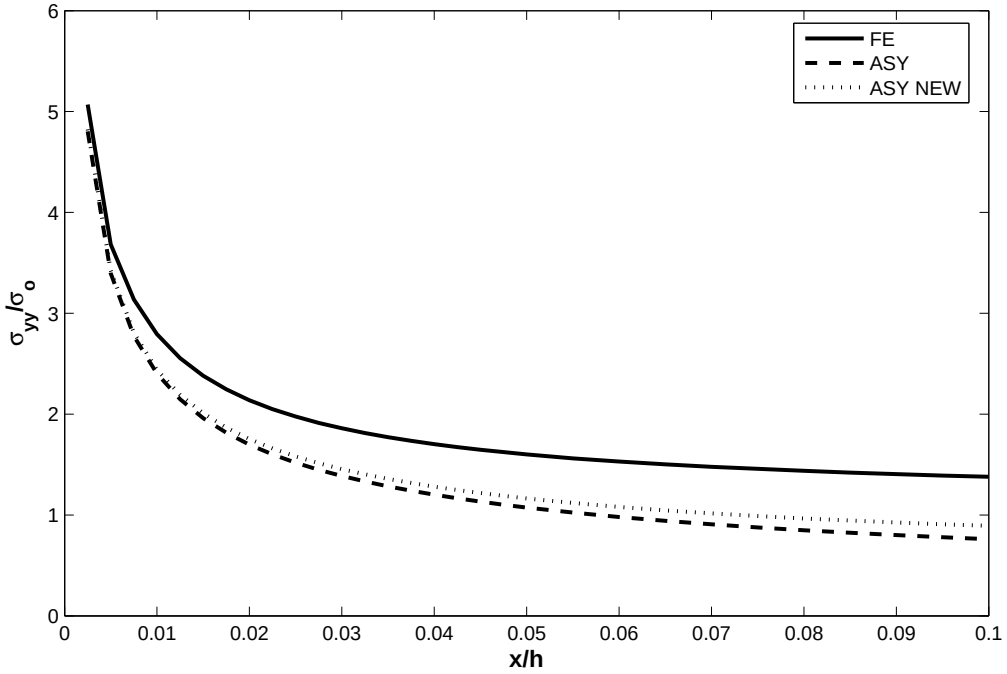

Figure 3.110. σ_{yy}/σ_o vs x/h for $\alpha = 15^o$, $E_2/E_1 = 5$ and $a/h = 0.2$

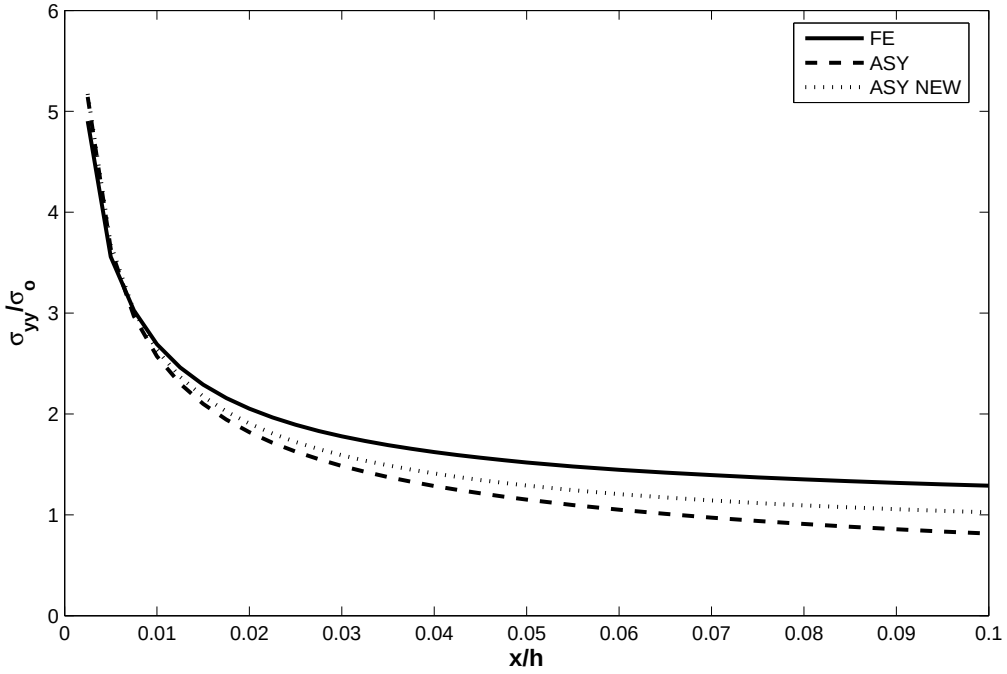

Figure 3.111. σ_{yy}/σ_o vs x/h for $\alpha = 15^o$, $E_2/E_1 = 10$ and $a/h = 0.2$

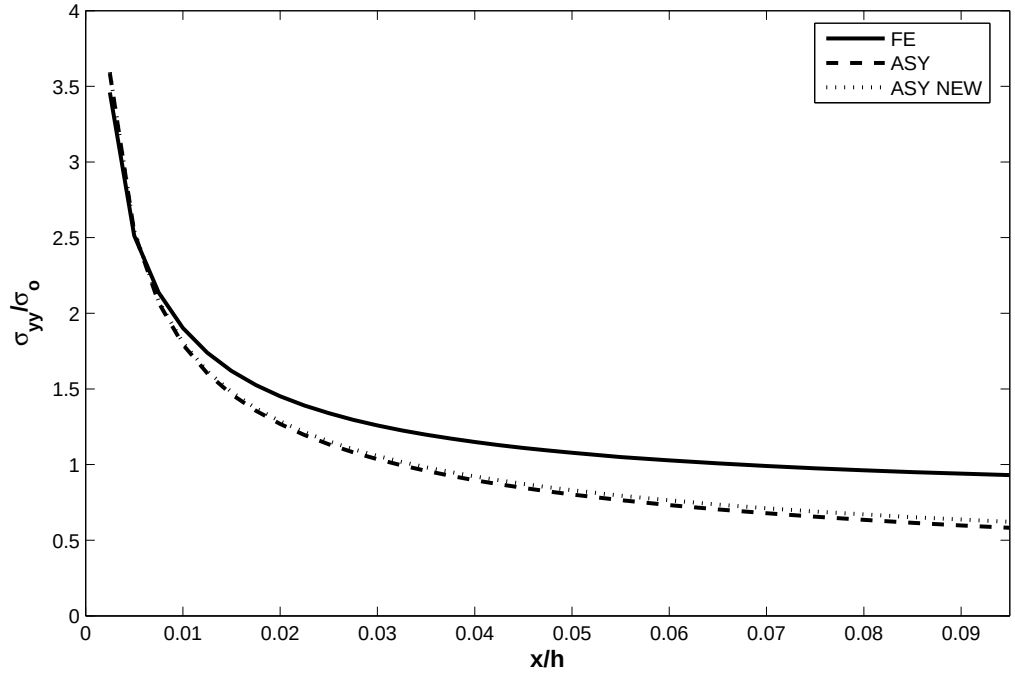

Figure 3.112. σ_{yy}/σ_o vs x/h for $\alpha = 30^o$, $E_2/E_1 = 2$ and $a/h = 0.2$

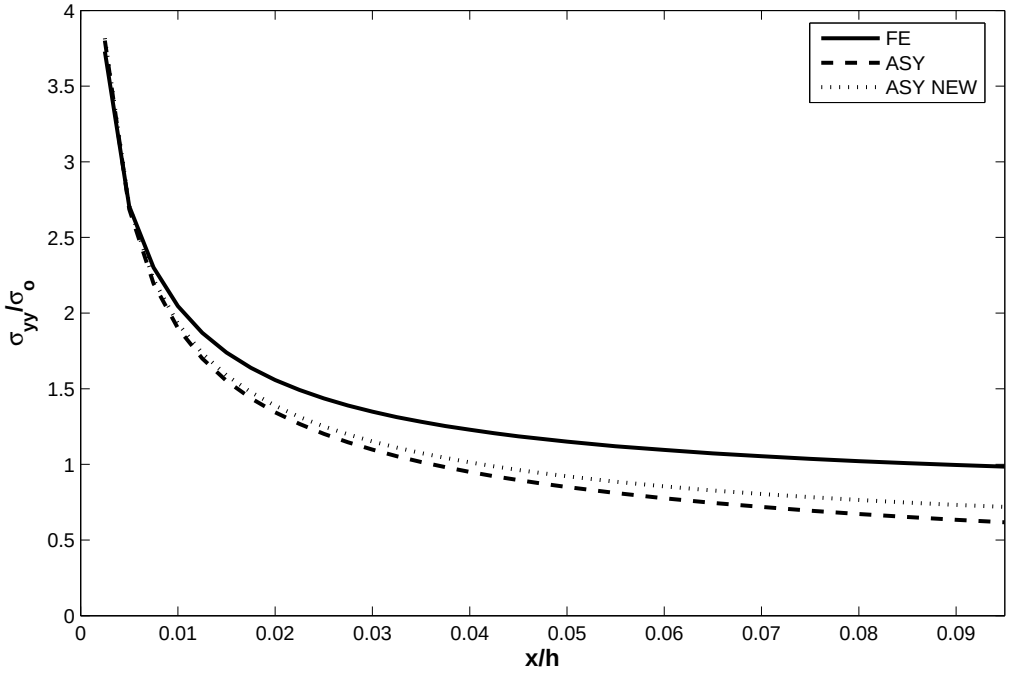

Figure 3.113. σ_{yy}/σ_o vs x/h for $\alpha = 30^o$, $E_2/E_1 = 5$ and $a/h = 0.2$

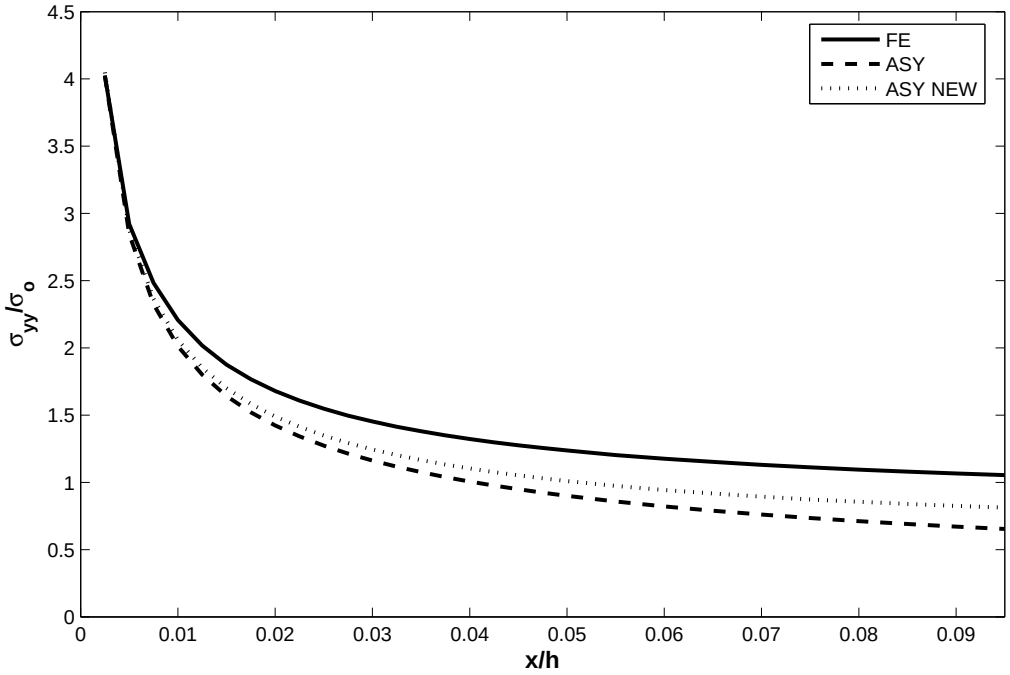

Figure 3.114. σ_{yy}/σ_o vs x/h for $\alpha = 30^o$, $E_2/E_1 = 10$ and $a/h = 0.2$

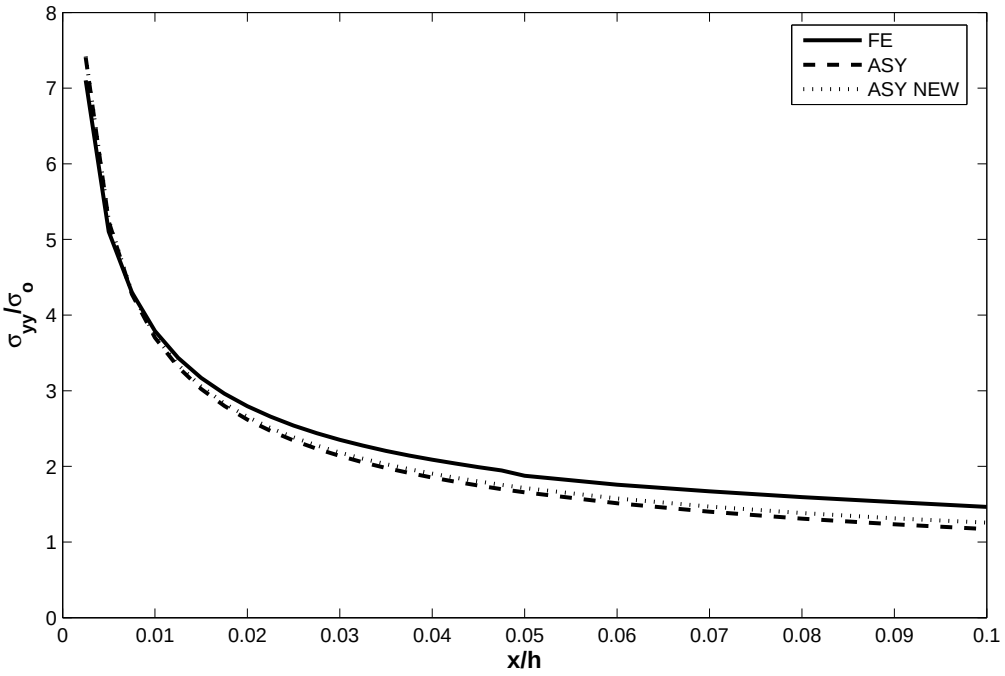

Figure 3.115. σ_{yy}/σ_o vs x/h for $\alpha = 15^o$, $E_2/E_1 = 2$ and $a/h = 0.4$

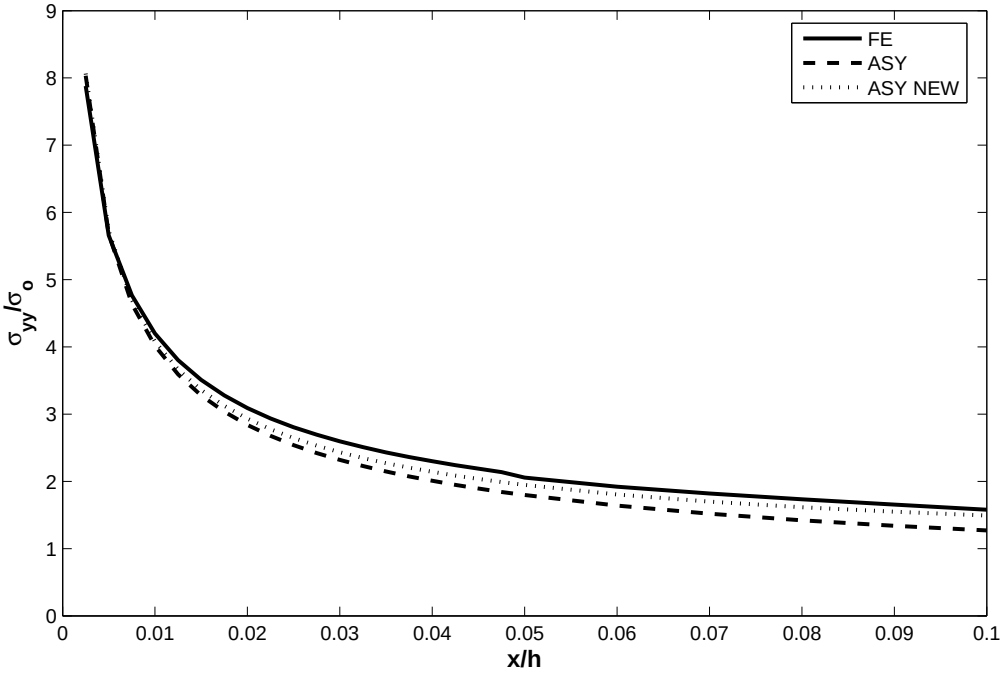

Figure 3.116. σ_{yy}/σ_o vs x/h for $\alpha = 15^o$, $E_2/E_1 = 5$ and $a/h = 0.4$

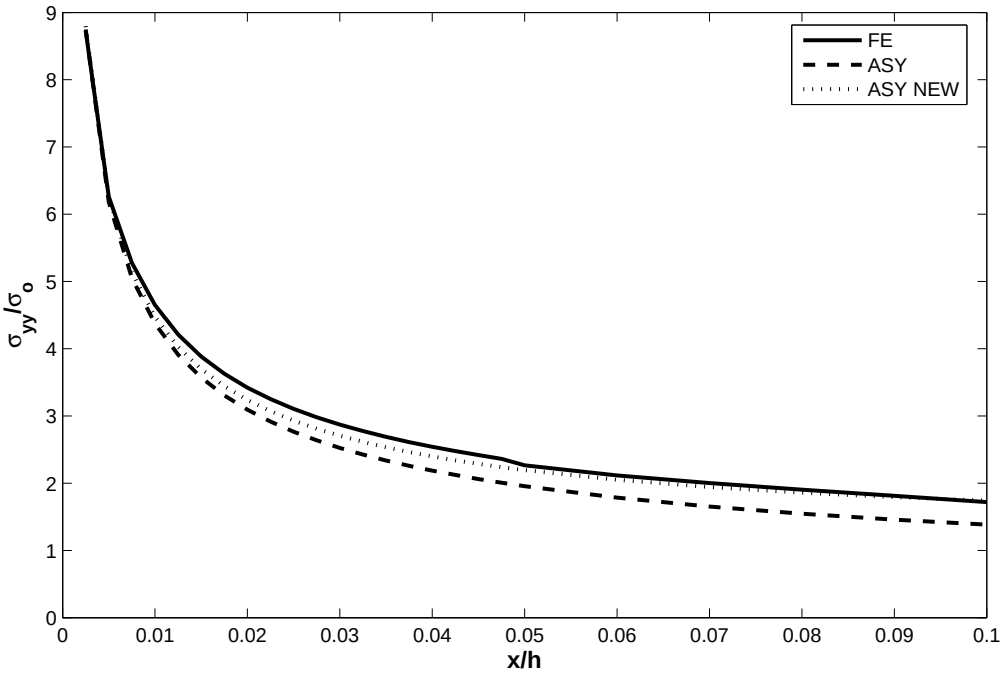

Figure 3.117. σ_{yy}/σ_o vs x/h for $\alpha = 15^o$, $E_2/E_1 = 10$ and $a/h = 0.4$

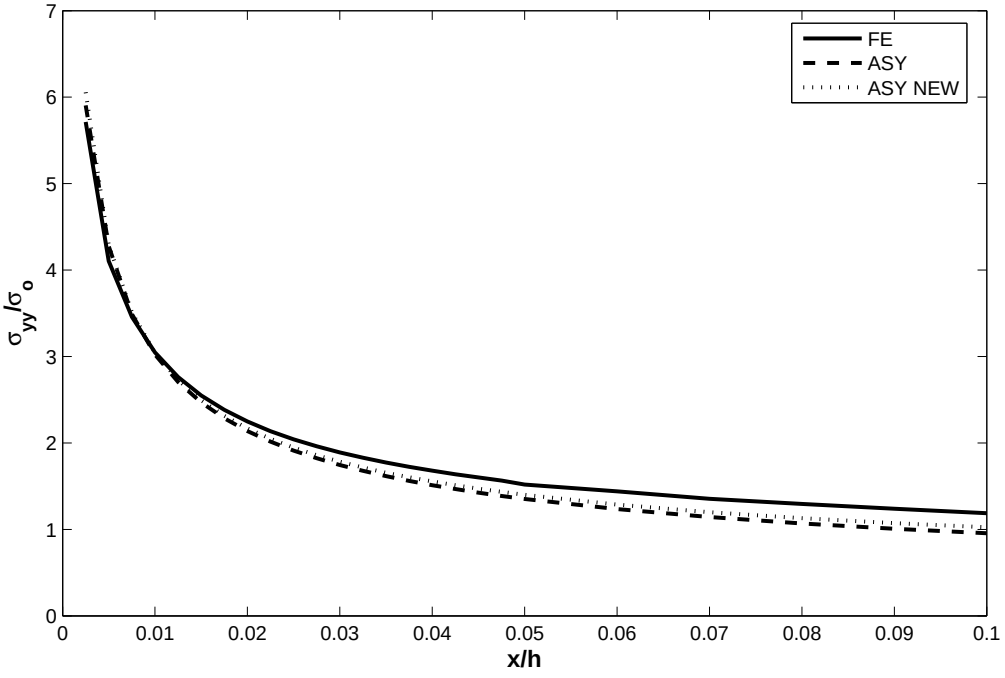

Figure 3.118. σ_{yy}/σ_o vs x/h for α= 30^o, E_2/E_1=2 and a/h=0.4

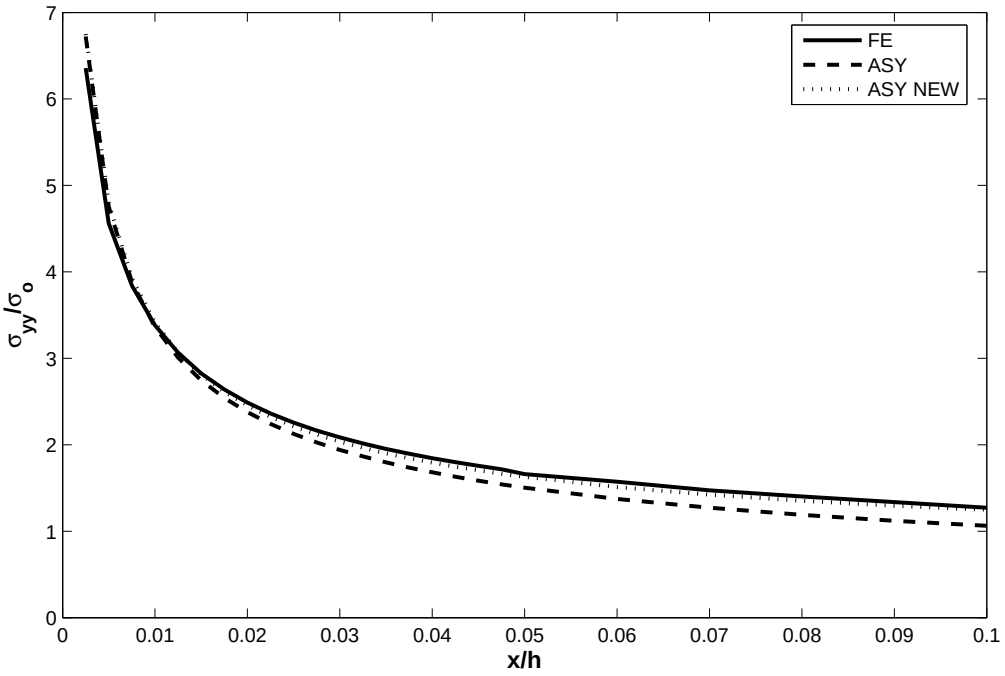

Figure 3.119. σ_{yy}/σ_o vs x/h for $\alpha = 30^o$, $E_2/E_1 = 5$ and $a/h = 0.4$

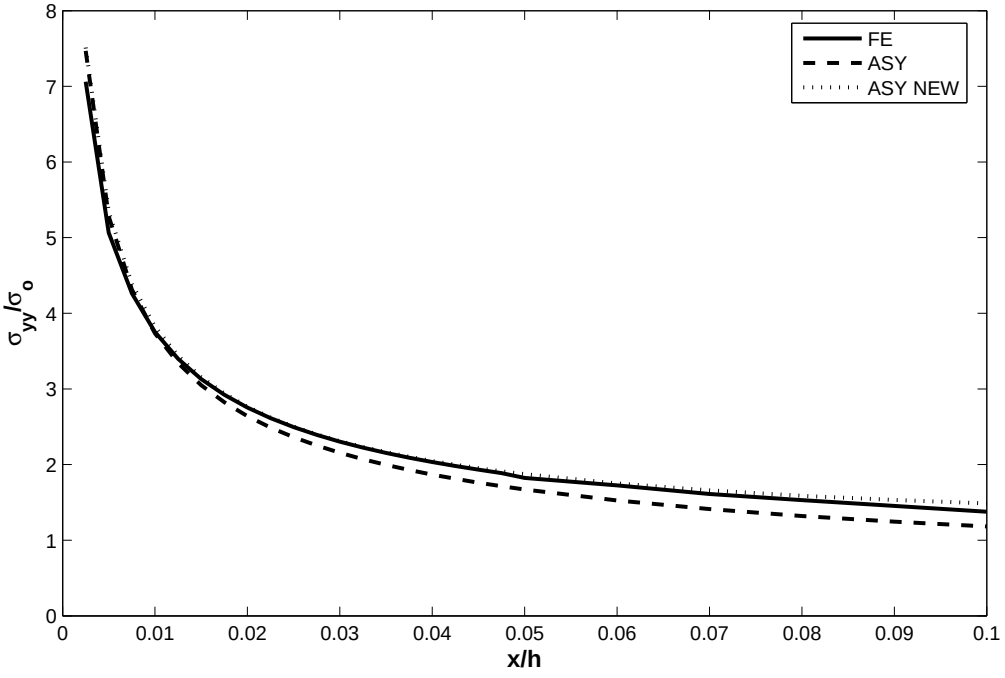

Figure 3.120. σ_{yy}/σ_o vs x/h for $\alpha = 30^o$, $E_2/E_1 = 10$ and $a/h = 0.4$

Opening stress plots are not sufficient for the comparison of the two asymptotic stress fields since σ_{yy}/σ_o are only given on symmetry axis. Error contours of the two fields are also plotted. To plot less crowded figures, only some error contours near the crack tip are used.

First, error contours for $\alpha = 15^o$, $a/h = 0.2$ and $E_2/E_1 = 5$ and 10 are given in Figures 3.121 - 3.122. It is seen that ASY NEW error contours cover larger area than contour plots obtained using ASY at this crack length and as material nonhomogeneity increases ASY NEW and ASY contours become closer to each other. Second, error contours for $a/h = 0.2$ and $E_2/E_1 = 2$ with $\alpha = 0^o$, 15^o and 30^o are plotted in Figures 3.123 - 3.125. ASY NEW and ASY are very close to each other in $\alpha = 0^o$. While the crack angle grows to $\alpha = 30^o$, the difference between two stress field increases. Last, the error contours for $a/h = 0.4$ and $E_2/E_1 = 2$ with $\alpha = 0^o$, 15^o and 30^o are plotted in Figures 3.126 - 3.128. These plots are given to investigate the extent of K-dominant region for different crack lengths. The plots show that ASY NEW results are better for short crack but the case is not true for longer cracks. For example, high nonhomogeneity value together with longer crack is given and ASY NEW solution is not better than ASY solution in Figure 3.128. Although there is no geometric unsymmetry in center-cracked plate compressive stresses can form in case of longer cracks with high material nonhomogeneity. Because of these compressive stresses K-dominant region for asymptotic field ASY NEW decreases.

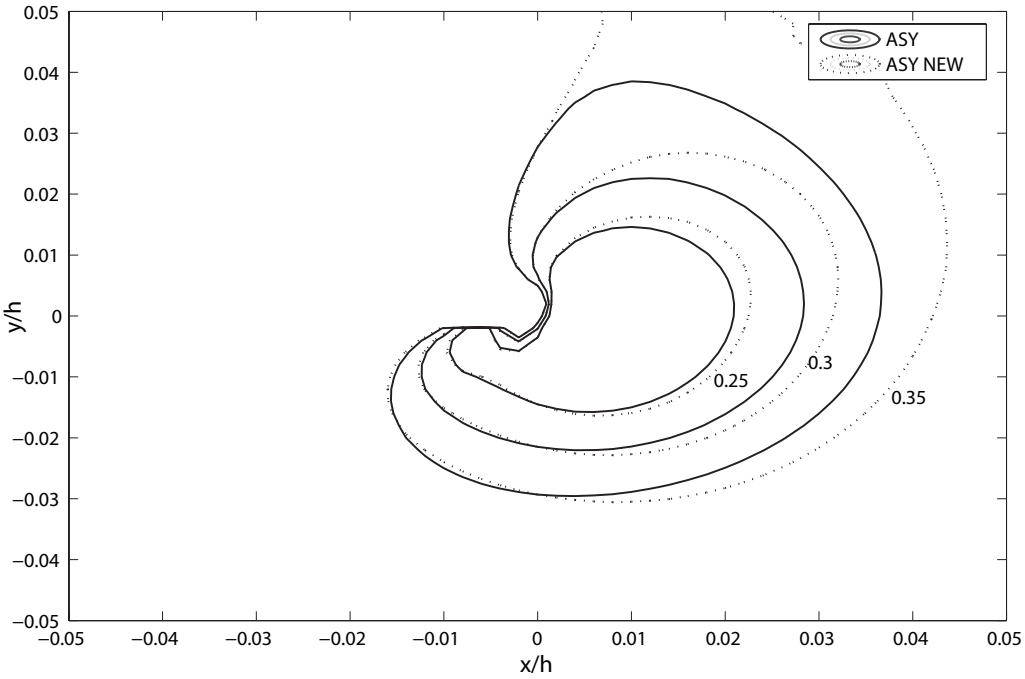

Figure 3.121. Error contours around crack tip for $\alpha = 15^o$, $E_2/E_1 = 5$ and $a/h = 0.2$

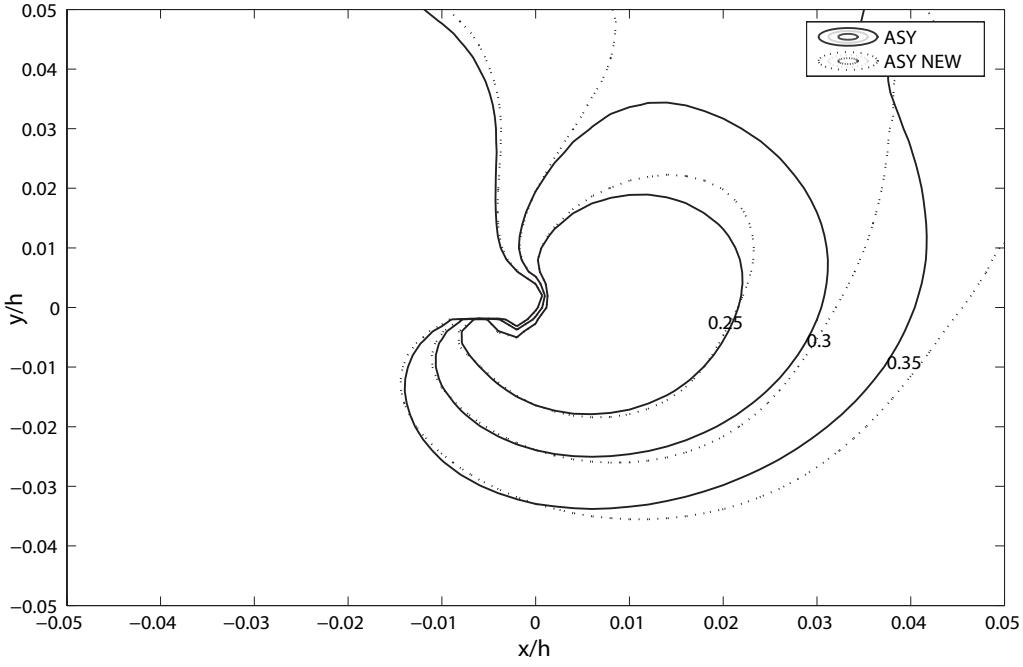

Figure 3.122. Error contours around crack tip for $\alpha = 15^o$, $E_2/E_1 = 10$ and $a/h = 0.2$

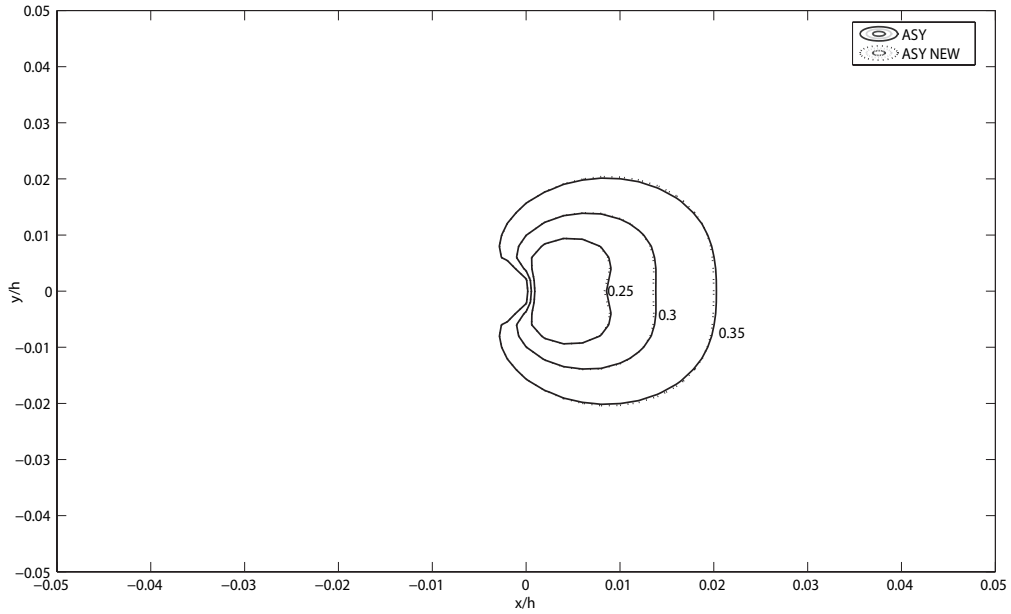

Figure 3.123. Error contours around crack tip for $\alpha = 0^o$, $E_2/E_1 = 2$ and $a/h = 0.2$

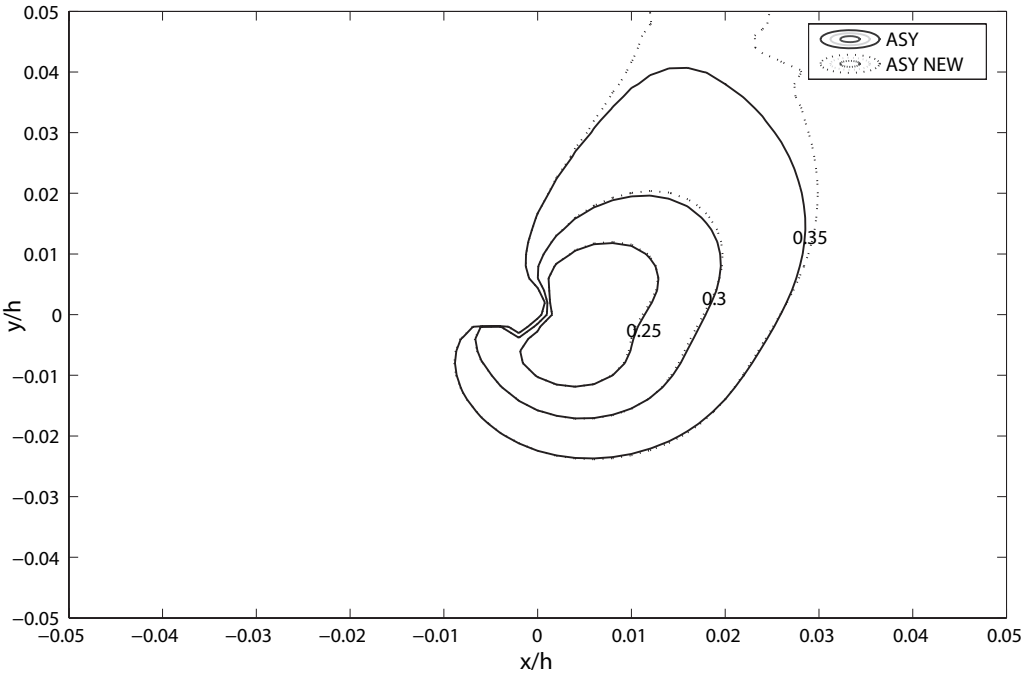

Figure 3.124. Error contours around crack tip for $\alpha = 15^o$, $E_2/E_1 = 2$ and $a/h = 0.2$

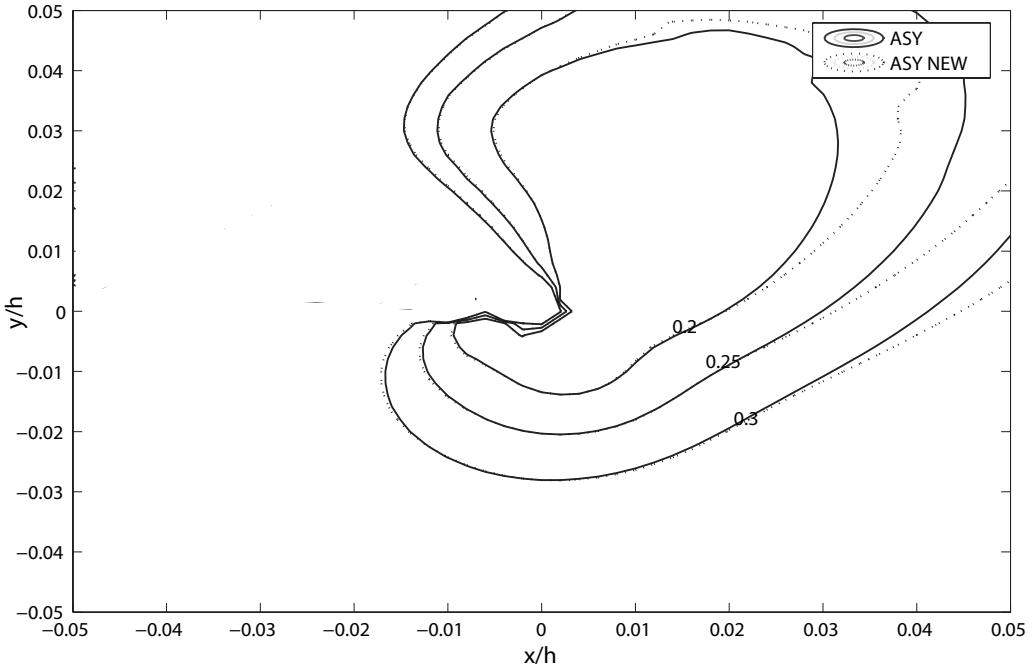

Figure 3.125. Error contours around crack tip for $\alpha = 30^o$, $E_2/E_1 = 2$ and $a/h = 0.2$

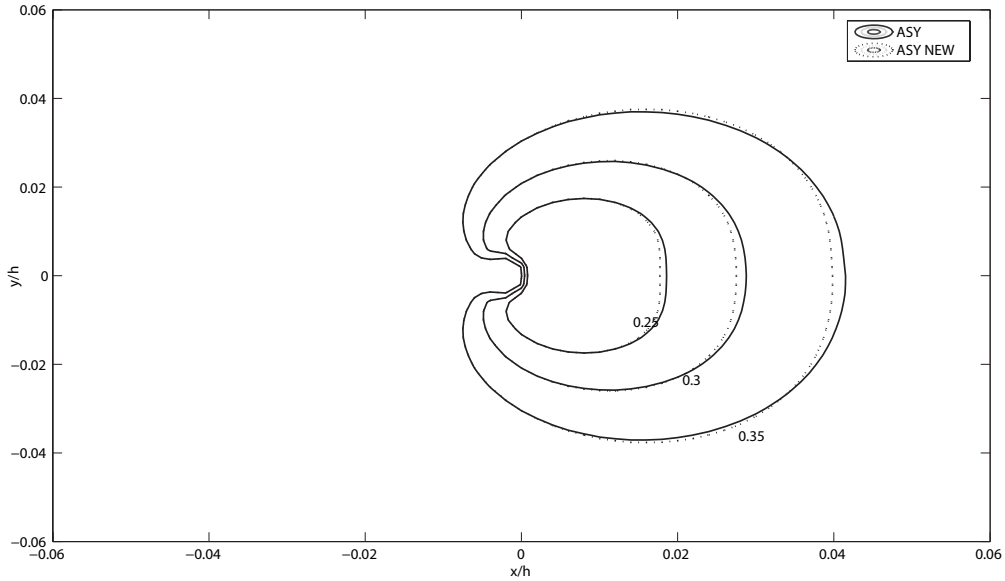

Figure 3.126. Error contours around crack tip for $\alpha = 0^o$, $E_2/E_1 = 2$ and $a/h = 0.4$

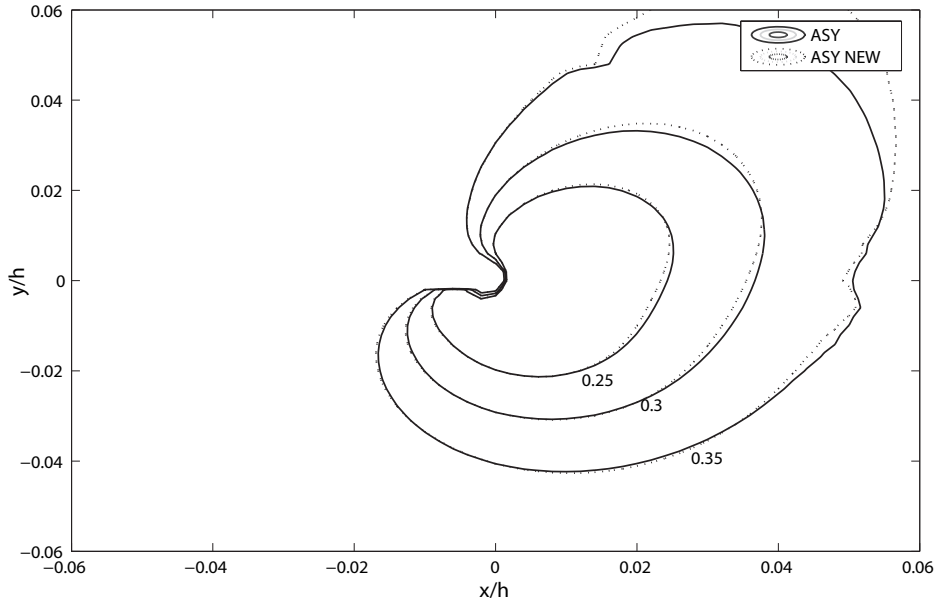

Figure 3.127. Error contours around crack tip for $\alpha = 15^o$, $E_2/E_1 = 2$ and $a/h = 0.4$

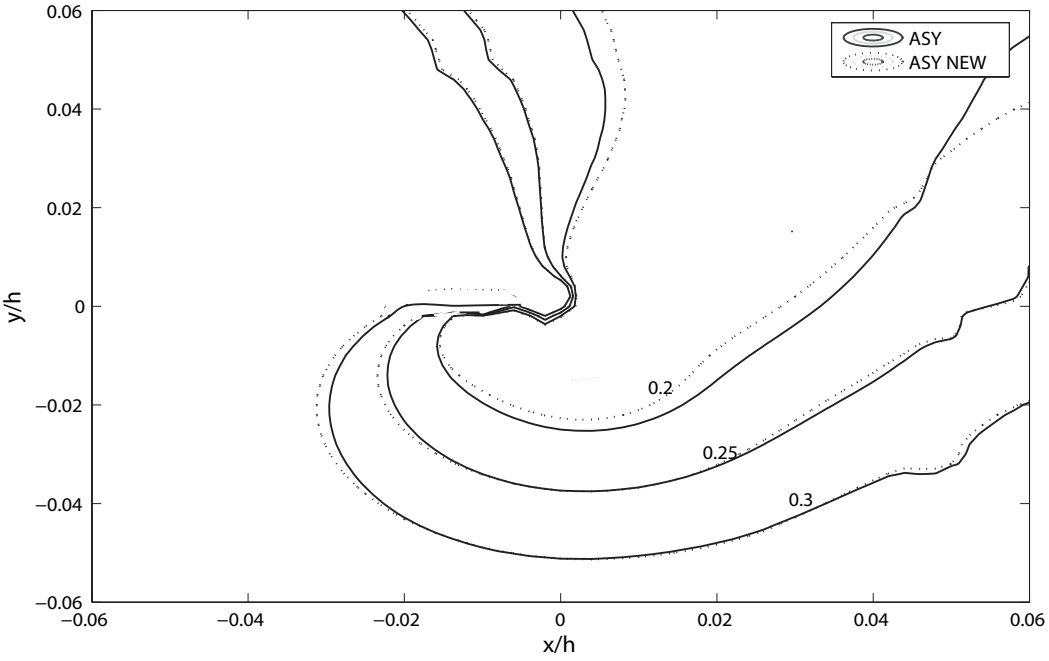

Figure 3.128. Error contours around crack tip for $\alpha = 30^o$, $E_2/E_1 = 2$ and $a/h = 0.4$

3.3.5. Effect of T-stress on K-dominant Region

Up to now, asymptotic stress equations are used including only r terms. However, T-stress which is the nonsingular stress has a significant influence on crack tip. T-stress is shown in Equations 2.1 - 2.3.

3.3.5.1. Calculation of T-stress. There are numbers of methods to calculate T-stress for a variety of loading conditions and geometries. For mixed mode loading, stress equations show that only σ_{xx} contains T. Using Equations 2.1 - 2.3 T can be determined by calculating σ_{xx} - σ_{yy} along the crack on $\theta = 0$. In this study, σ_{xx} and σ_{yy} values are calculated using FE on nodes along $\theta = 0$. Then, numerical T values are obtained for same nodes. T values are plotted versus the distance from the crack tip and a linear curve is fitted to T data. The intercept of the curve fit is approximated as the single T-stress value.

To check the accuracy of the model and the method used, T-stresses are calculated for the geometry given in Figure 2.12 with $\beta a = 0$, 0.25 and 0.5. For the homogeneous case ($\beta a = 0$), calculated T stresses are compared with the results of closed form solution given in Equation 2.17 for both $a/h = 0.05$ and 0.1. The results are tabulated in Table 3.5. It is seen that although the results for $a/h = 0.05$ are much closer to the closed form solution values, $a/h = 0.1$ results are also sufficiently good to use.

For the nonhomogeneous material, T stresses calculated using the method described above are compared with the results of Kim and Paulino [30] in Table 3.6. Kim and Paulino [30] evaluated T-stresses in FGMs using interaction integral in conjunction with FE. It is seen that there is a reasonably good agreement between the results of present study and their results.

After the method is verified, T-stress values are calculated using the model given in Figure 3.1 for different crack lengths of $a/h = 0.3$, 0.4 with $E_2/E_1 = 2$, 5, 10, 20 and $\alpha = 15^o$, 30^o, 45^o and 60^o. The results for both right and left crack tip are given

Table 3.5. T-stress values for $\beta a = 0$ (homogeneous) with $\sigma_{yy} = \overline{\varepsilon} E_0 e^{\beta x}$

	$a/h = 0.05$		$a/h = 0.1$
Method	α/pi	$T(a)$	$T(a)$
Closed form solution	0	-1.000	-1.000
	0.1	-0.809	-0.809
	0.2	-0.309	-0.309
	0.3	0.309	0.309
Present solution	0	-0.999	-1.001
	0.1	-0.812	-0.815
	0.2	-0.313	-0.319
	0.3	0.297	0.298

Table 3.6. T-stress values for $\beta a = 0.25$ and $\beta a = 0.5$ with $\sigma_{yy} = \overline{\varepsilon} E_0 e^{\beta x}$

		$\beta a = 0.25$		$\beta a = 0.5$	
Method	α	$T(a)$	$T(-a)$	$T(a)$	$T(-a)$
Present study	0	-1.0079	-0.8984	-0.9341	-0.8250
	15	-0.8658	-0.8323	-0.7847	-0.7691
	30	-0.4978	-0.5001	-0.4416	-0.4523
	45	-0.0067	-0.0084	0.0122	0.0094
Kim and Paulino [30]	0	-0.9589	-0.9430	-0.8878	-0.8606
	15	-0.8310	-0.8191	-0.7655	-0.7494
	30	-0.4790	-0.4763	-0.4288	-0.4371
	45	-0.0077	-0.0019	0.0391	0.0109

in Table 3.6. For both crack tips $(a, -a)$, these results show that T-stress changes sign when crack angle $\simeq 45^o$.

First, σ_{xx} contours are plotted for $E_2/E_1 = 2$ and $a/h = 0.3$ for different crack angles of $\alpha = 15^o$, 30^o and 45^o. The σ_{xx} contours of the value 1 are only plotted. In Figures 3.129 - 3.131, it is seen that stress contours cover larger area as the crack angle increases. In each plot stress contours including T-stress are closer to the FE stress values than the ones without T-stress. It can be concluded that T-stress effects the extent of K-dominant region. For crack angle of $\alpha = 15^o$ the difference between ASY stress values and ASY (T-stress) is high, and ASY (T-stress) is closer to FE. However, for $\alpha = 45^o$ ASY and ASY (T-stress) are very close to each other. Because as it is seen in Table 3.7, the value of T-stress is approximately 0 for $\alpha = 45^o$.

Table 3.7. T-stress values for a center cracked FGM plate

		$a/h = 0.3$		$a/h = 0.4$	
E_2/E_1	α	$T(a)$	$T(-a)$	$T(a)$	$T(-a)$
2	15	−0.9428	−1.0638	−1.0170	−1.1382
	30	−0.5727	−0.6416	−0.6529	−0.7218
	45	−0.0669	−0.072	0.1147	−0.1198
	60	0.4532	0.4855	0.4227	0.455
5	15	−0.8453	−1.1244	−0.8769	−1.1561
	30	−0.5110	−0.669	−0.5628	−0.7258
	45	−0.0522	−0.0655	−0.0827	−0.0960
	60	0.4368	0.4904	0.4041	0.4577
10	15	−0.7563	−1.1591	−0.7471	−1.1499
	30	−0.4513	−0.681	−0.4695	−0.6992
	45	−0.0333	−0.0547	−0.0433	−0.0647
	60	0.4248	0.5294	0.3951	0.4997
20	15	−0.6509	−1.1708	−0.5903	−1.1102
	30	−0.3776	−0.6842	−0.3575	−0.6614
	45	−0.0081	−0.0391	00016	0.0323
	60	0.414	0.5496	0.3927	0.5283

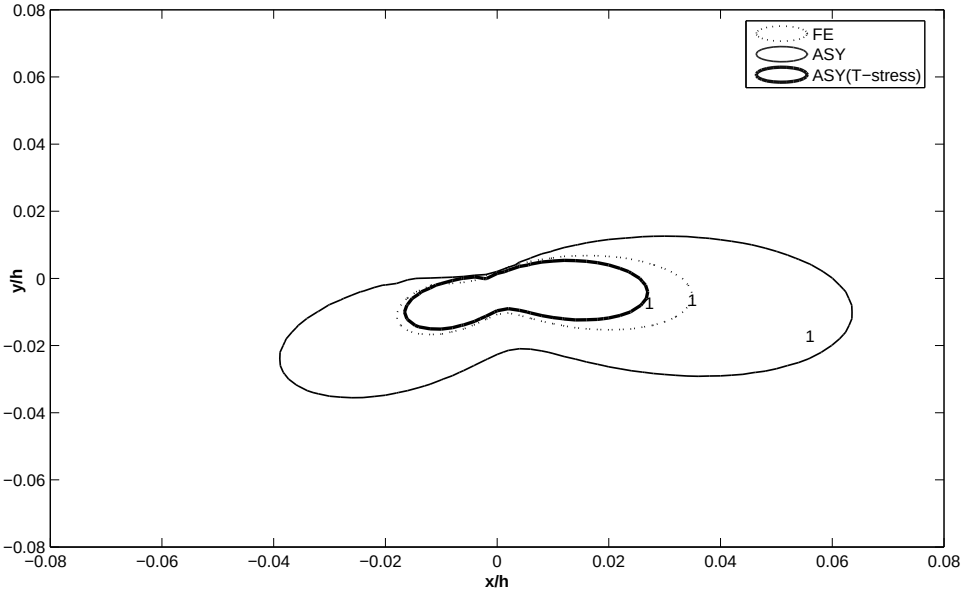

Figure 3.129. σ_{xx} for $\alpha = 15^o$, $E_2/E_1 = 2$ and $a/h = 0.3$ around right crack tip with and without T stress

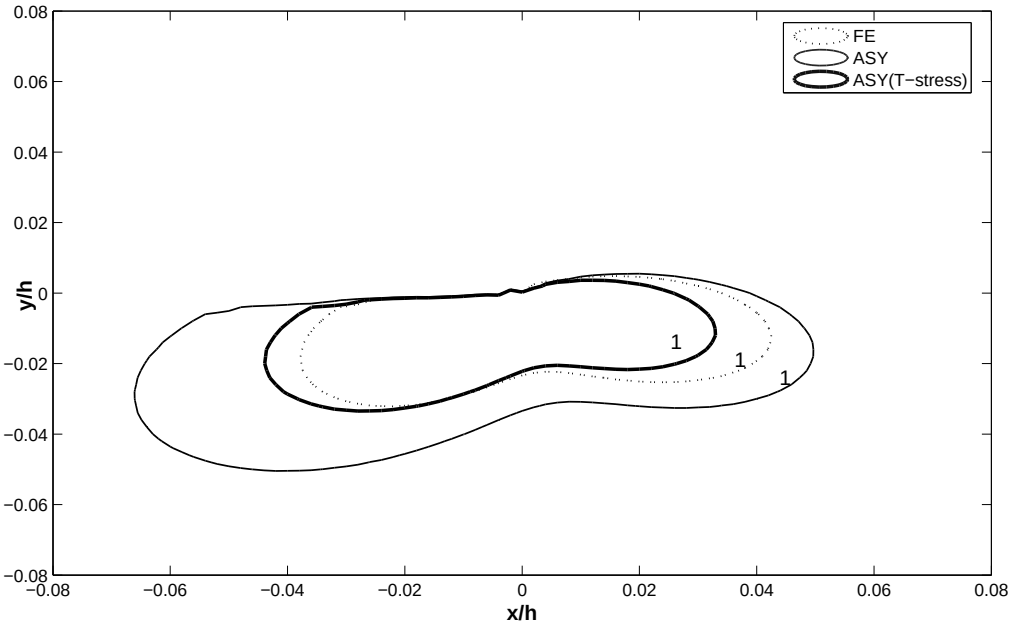

Figure 3.130. σ_{xx} for $\alpha = 30^o$, $E_2/E_1 = 2$ and $a/h = 0.3$ around right crack tip with and without T stress

σ_{xx} contours are also plotted for $\alpha = 30^o$ and $E_2/E_1 = 5$ with $a/h = 0.3$ and 0.4. As it is seen in Figures 3.132 - 3.133, an increase in the crack length causes all stress values to increase. K-dominant region is extended by increasing the crack angle since compressive stresses occurs at the larger crack lengths. Again, ASY (T-stress) solutions are closer to FE stress values than ASY solution in each plot.

Last, the effect of T-stress on σ_{xx} with changing material nonhomogeneity is investigated. Figures 3.134 - 3.136 show σ_{xx} contours for $\alpha = 15^o$ and $a/h = 0.3$ with $E_2/E_1 = 5$, 10 and 20 around right crack tip. It is seen that ASY (T-stress) stress values are again closer to FE stress values than ASY. However, as the material nonhomgeneity increases the deviation between FE and ASY (T-stress) for the same stress contour gets higher. The same graphs are plotted for left crack tip and given in Figures 3.137 - 3.139. The stress contours around left crack tip have similar trend like right crack tip.

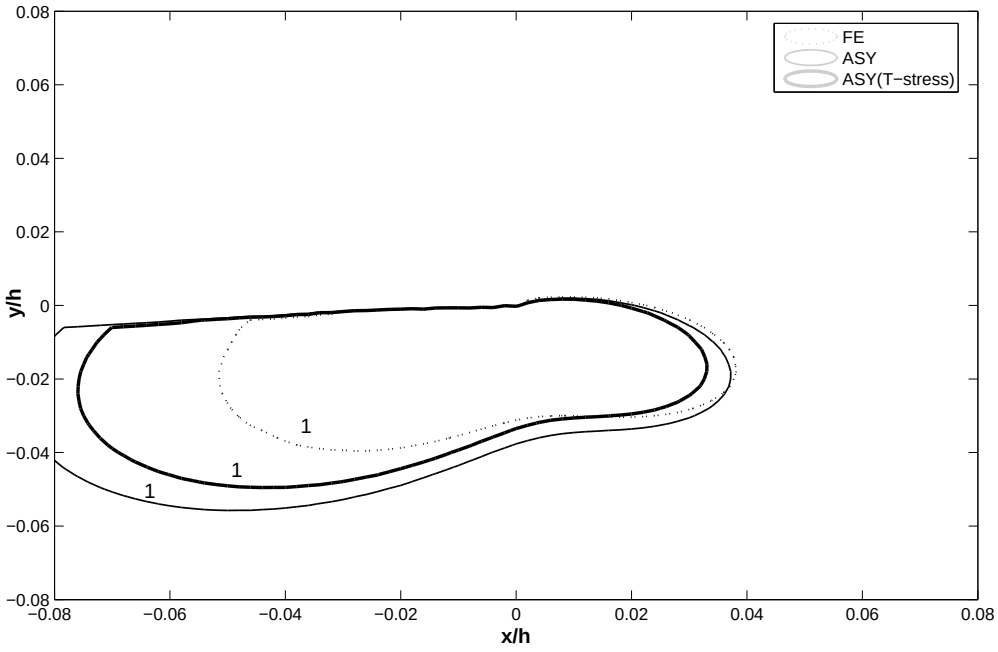

Figure 3.131. σ_{xx} for $\alpha = 45^o$, $E_2/E_1 = 2$ and $a/h = 0.3$ around right crack tip with and without T stress

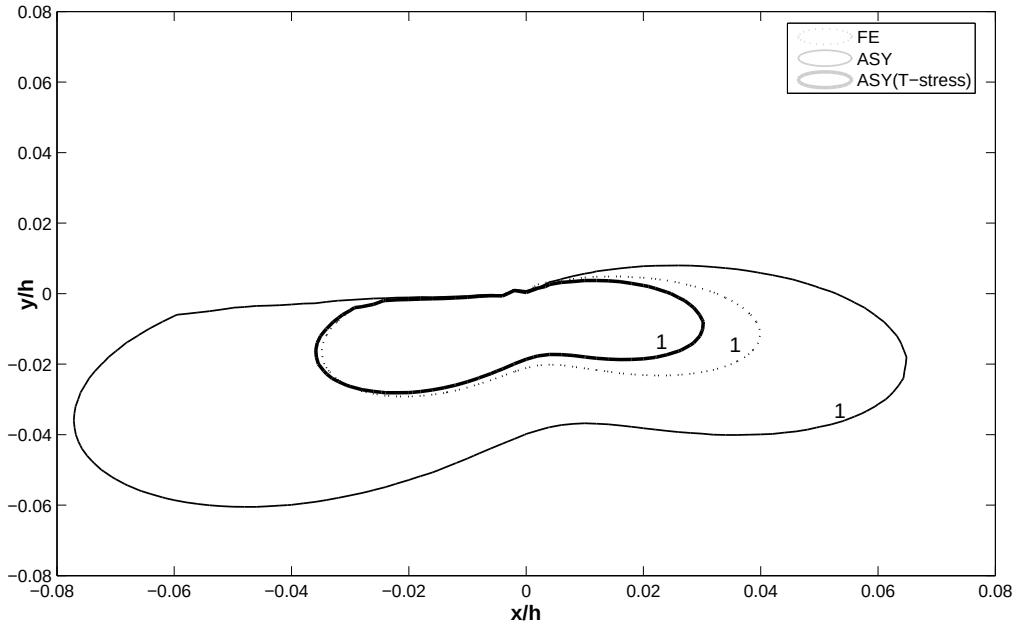

Figure 3.132. σ_{xx} for $\alpha = 30^o$, $E_2/E_1 = 5$ and $a/h = 0.3$ around right crack tip with and without T stress

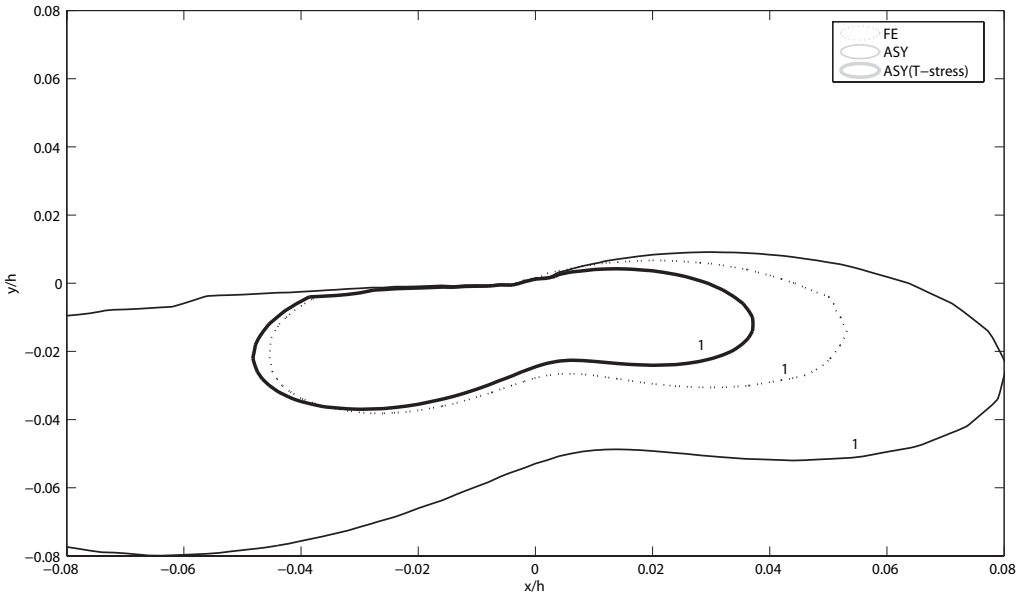

Figure 3.133. σ_{xx} for $\alpha = 30^o$, $E_2/E_1 = 5$ and $a/h = 0.4$ around right crack tip with and without T stress

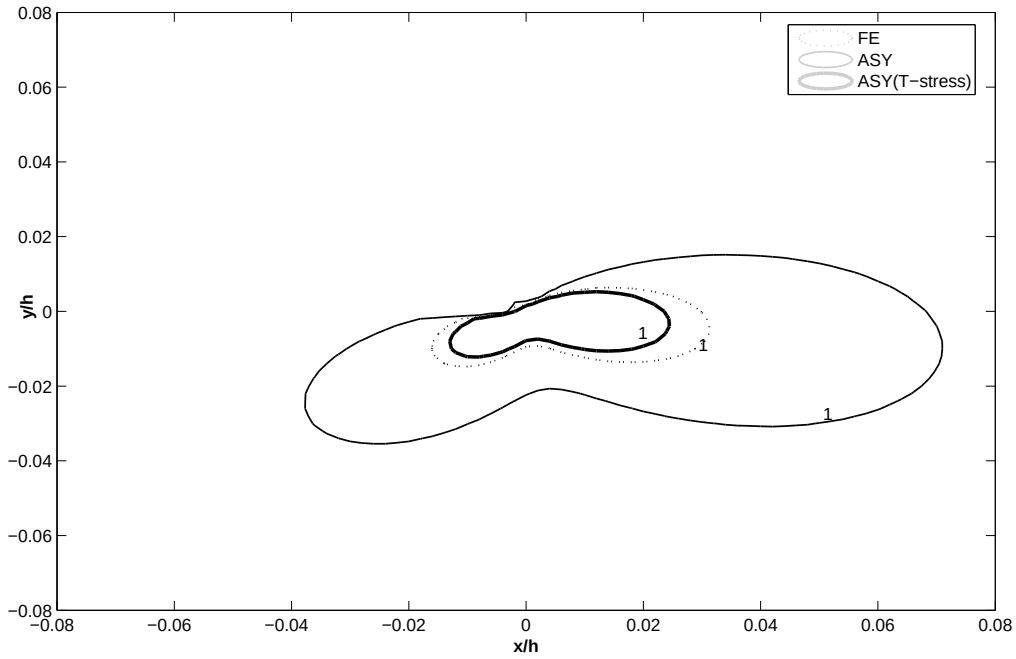

Figure 3.134. σ_{xx} for $\alpha = 15^o$, $E_2/E_1 = 5$ and $a/h = 0.3$ around right crack tip with and without T stress

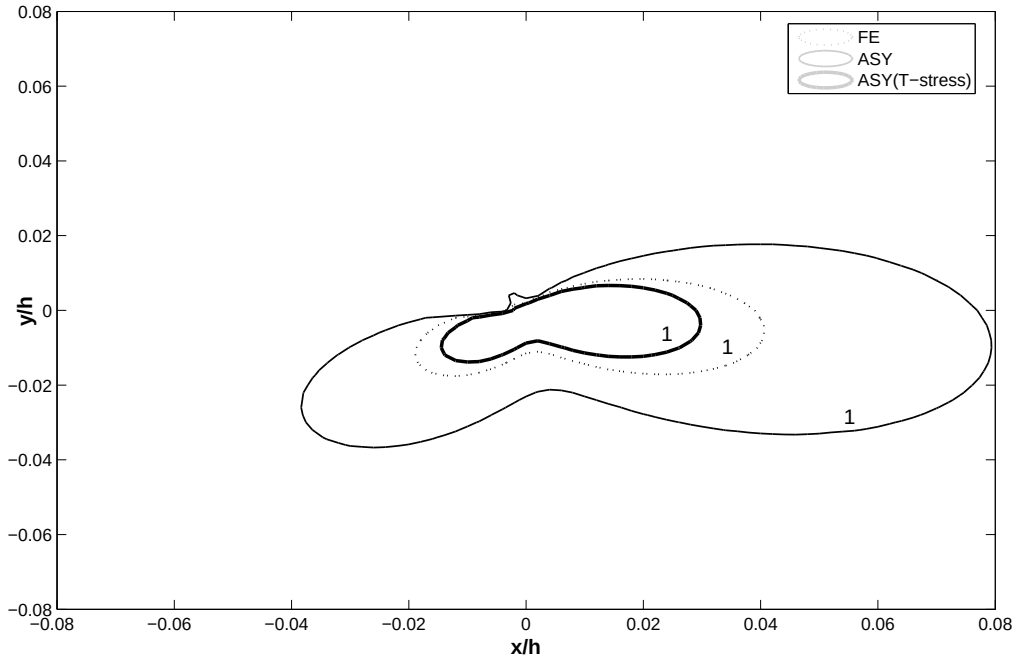

Figure 3.135. σ_{xx} for $\alpha = 15^o$, $E_2/E_1 = 10$ and $a/h = 0.3$ around right crack tip with and without T stress

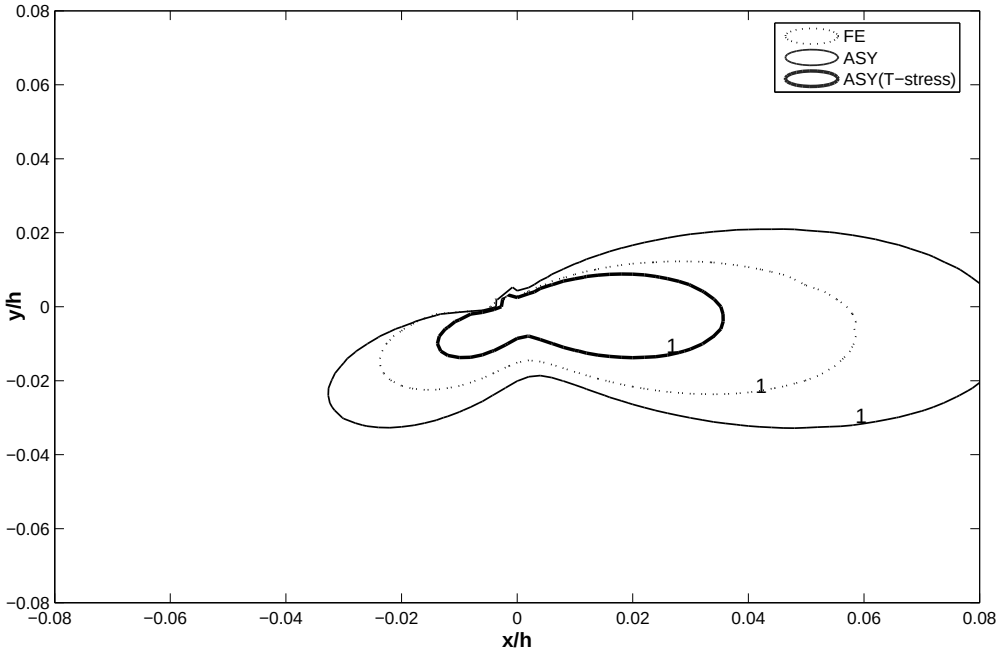

Figure 3.136. σ_{xx} for $\alpha = 15^o$, $E_2/E_1 = 20$ and $a/h = 0.3$ around right crack tip with and without T stress

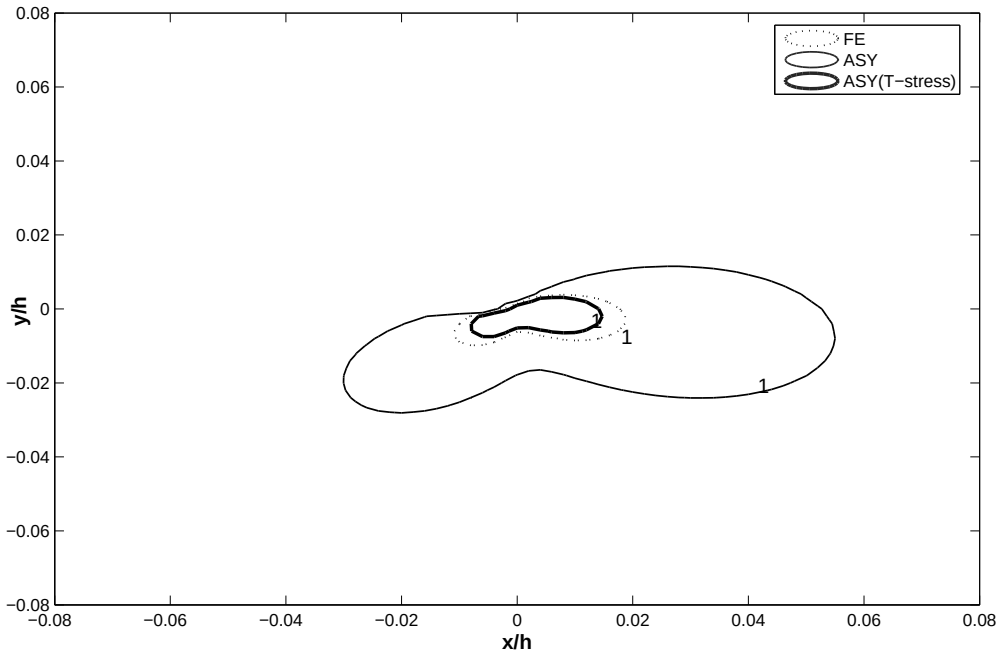

Figure 3.137. σ_{xx} for $\alpha = 15^o$, $E_2/E_1 = 5$ and $a/h = 0.3$ around left crack tip with and without T stress

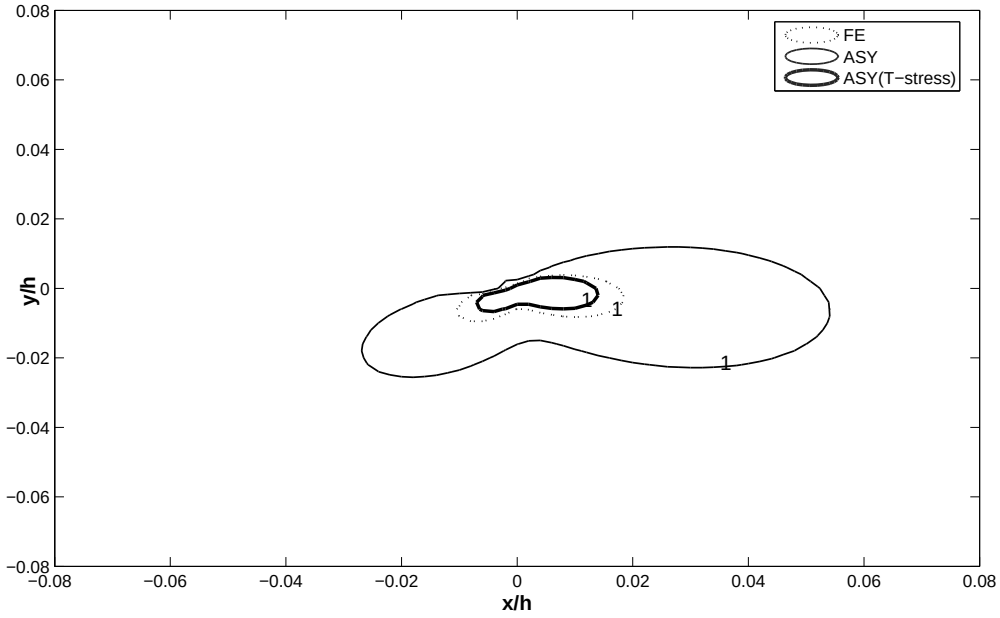

Figure 3.138. σ_{xx} for $\alpha = 15^o$, $E_2/E_1 = 10$ and $a/h = 0.3$ around left crack tip with and without T stress

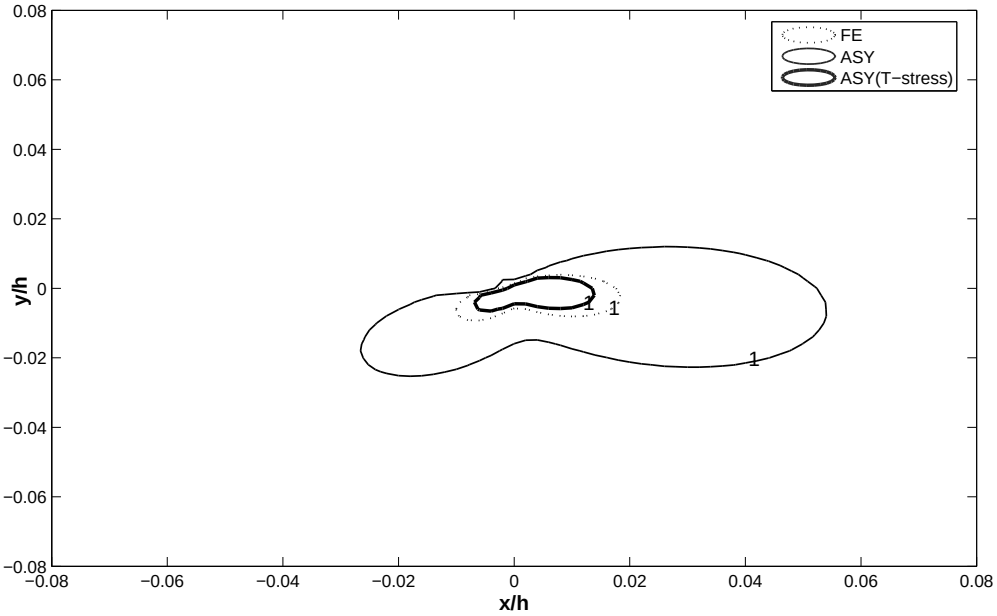

Figure 3.139. σ_{xx} for $\alpha = 15^o$, $E_2/E_1 = 20$ and $a/h = 0.3$ around left crack tip with and without T stress

4. SUMMARY AND CONCLUSION

The aim of this study is to analyze the extent of K-dominant region in a functionally graded plate under mixed mode loading. Poisson's ratio, ν, of the medium is assumed to be constant and the elastic modulus varies exponentially along x-axis, $E = E_0 e^{\beta x}$, with the x-coordinate parallel to the crack. The shape and the extent of K-dominant region is investigated by comparing asymptotic stress fields to stress field calculated using finite elements around right and left crack tips separately.

Before analyzing the K-dominant region, to verify the method, stress intensity factors and T-stresses for a center cracked plate are determined for both homogeneous and functionally graded materials. Results are compared to the results of Konda and Erdogan [12]. It is seen that a sufficient agreement exists when the present method is used in all cases.

Stress intensity factors and T-stresses are determined for a center cracked plate under uniform loading are shown in Figure 3.1. The effect of material nonhomogeneity, crack angle and crack length on the extent of K-dominant region is studied. Three different ratios of crack length to plate width namely 0.2, 0.3, and 0.4 are examined. For crack angle, α, five different values are used, namely 0^0, 15^0, 30^0, 45^0, 60^0. A wide range of material nonhomogeneity, E_2/E_1, varying from 1, 2, 5, 10 to 20 is used. The elastic modulus increases in the crack propagation direction when the right crack tip is studied and decreases in the crack propagation direction for the left crack tip (softening case).

In chapter 3, K-dominance analysis is done for different α, E_2/E_1 and a/h values. Results in forms of graphs are discussed in detail. A summary of the results may be given as follows: First, the behavior of K-dominant region for different E_2/E_1 ratios is studied for a center cracked plate. Change of nonhomogeneity in crack propagation directions of two crack tips is different. One tip goes into a hardening, the other tip goes into a softening region. As a result, the behavior of the K-dominant zone around

two crack tips is different. For the right crack tip, K-dominant region gets larger as the material nonhomogeneity increases. As it is expected, for the left crack tip, the extent of K-dominant region is larger for the homogeneous case, $E_2/E_1 = 1$, and diminishes as the material nonhomogeneity increases.

Then, the effect of mode mixity is investigated by changing crack angle,α. It is understood that as the crack angle increases σ_{yy} values decrease for both asymptotic (ASY) and finite element (FE) results and ASY stress values underestimate the FE stress field. An example graph is given for $\alpha = 15^o$ and 45^o in Figure 4.1. Besides, the opening stress values along right crack tip are higher than the values along the left crack tip. From the error contours, it is seen that K-dominant region increases dramatically as the crack angle increases.

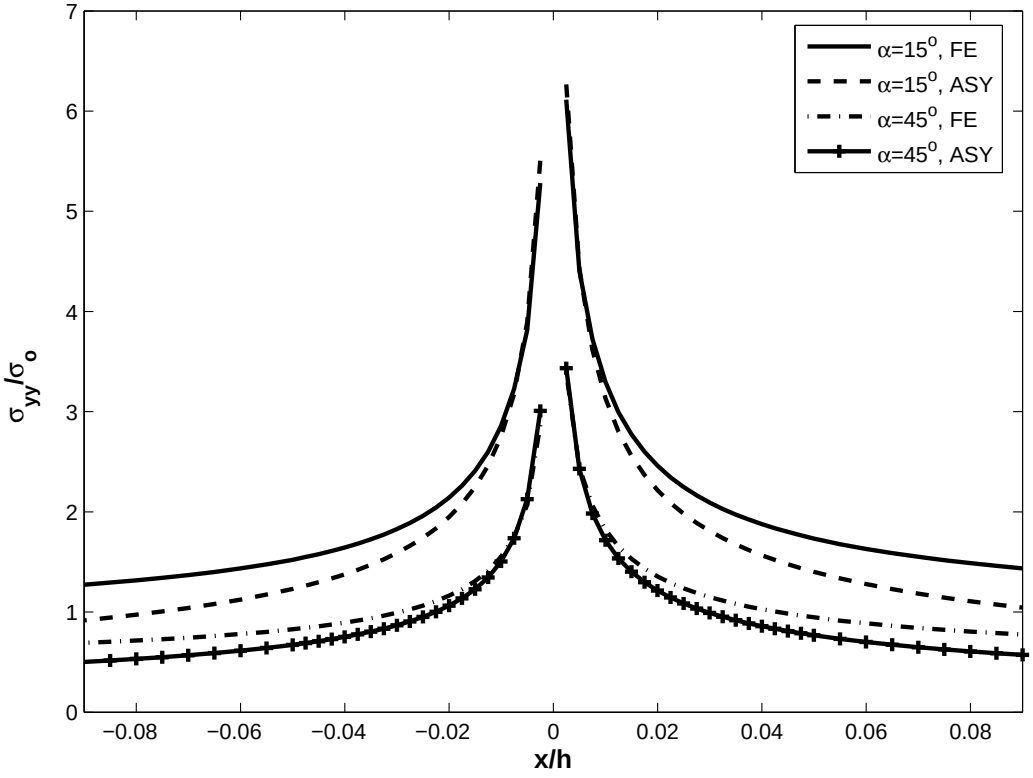

Figure 4.1. σ_{yy}/σ_o for $E_2/E_1 = 5$, $a/h = 0.2$ and α= 15^o, 45^o

Lastly, the effect of crack length on K-dominant region shows that an increase in the crack length causes FE and ASY stress values to increase. Because compressive

stresses become more effective for longer cracks, FE results of σ_{yy} do not increase as much as those of ASY solution. Stress contours get closer as the crack length increases which means that K-dominant region increases with an increase in the crack length.

The different asymptotic field derived by Konda and Erdogan[12] is used to study two asymptotic solutions (ASY and ASY NEW). Graphs are plotted for different mode mixities, E_2/E_1 and a/h ratios. ASY NEW results are better than ASY results since ASY NEW contains the effect of nonhomogeneity in the asymptotic expression. However, this is not valid for long cracks. For example, high nonhomogeneity values together with long crack are given in Figure 3.128 and ASY NEW solution does not yeild a better result than ASY solution. Although there is no geometric unsymmetry in center-cracked plate, compressive stresses form for long cracks in the case of high material nonhomogeneity. Because of these compressive stresses, K-dominant region when asymptotic field ASY NEW is used decreases.

T-stress is an important parameter and it effects the extent of K-dominant region. Asymptotic σ_{xx} fields including T-stress are compared to finite element results in Figures 3.132 - 3.139 . In each graphs, it is seen that stress contours including T-stress are closer to the FE stress values than the ones without T-stress. However, for $\alpha = 45^o$ the ASY and ASY (T-stress) become closer to each other since the value of T-stress is approximately 0 for $\alpha = 45^o$.

Overall, some difficuites are encontered while calculating the results. One of them is that since the mesh does not have a definite shape, the curves for finite element results are fluctuating at some points in the graphs. Last, only the stress fields around the crack tips are considered. A larger area may also be considered. Besides, the error parameter defined by Lee and Rosakis [24] is used. Another error parameter may be considered to investigate the extent of K-dominant region.

REFERENCES

1. Koizumi, M., "FGM Activities in Japan", *Composite Part B*, Vol. 28B, pp. 1-4, 1997.

2. Kim, J. H. and G. H. Paulino, "Simulation of Crack Propagation in Functionally Graded Materials Under Mixed-mode and Non-proportional Loading", *International Journal of Mechanics and Material in Design*, Vol. 1, pp. 63-94, 2004.

3. Abanto-Bueno J. and J. Lambros, "Parameters Controlling Fracture Resistance in Functionally Graded Materials Under Mode I Loading", *International Journal of Solids and Structures*, Article in Press, May 2005.

4. Keiback, B., A. Neubrand and H. Riedel, "Processing Techniques for Functionally Graded Materials", *Materials Science and Engineering*, Vol. A362, pp. 81-105, 2003.

5. Kubair, D., P. H. Geubelle and J. Lambros, "Asymptotic Analysis of a Mode III Stationary Crack in a Ductile Functionally Graded Material", *Journal of Applied Mechanics*, Vol. 72, pp. 461-467, 2005.

6. Zhang, C., J. Sladek and V. Sladek, "Antiplane Crack Analysis of a Functionally Graded Material by a BIEM", *Computational Materials Science*, Vol. 32, pp. 611-619, 2005.

7. Gibson, R. E., "Some Results Concerning Displacements and Stresses in a Nonhomogeneous Elastic Half-space", *Gotechnique*, Vol. 17, pp. 58-67, 1967.

8. Delale, F. and F. Erdogan, "The Crack Problem for a Nonhomogeneous Plane", *Journal of Applied Mechanics*, Vol. 50, pp. 609-614, 1983.

9. Erdogan, F., "The Crack Problem for Bonded Nonhomogeneous Materials Under

Antiplane Shear Loading",*Journal of Applied Mechanics*, Vol. 52, pp. 823-828, 1985.

10. Eischen, J. W., "Fracture of Nonhomogeneous Materials", *International Journal of Fracture*, Vol. 34, pp. 3-22, 1987.

11. Jin, Z. and N. Noda, "Crack-tip Sigular Fields in Nonhomogeneous Materials", *Journal of Applied Mechanics*, Vol. 61, pp. 738-740, 1994.

12. Konda, N. and F. Erdogan, "The Mixed Mode Crack Problem in a Nonhomogeneous Elastic Medium", *Enginering Fracture Mechanics*, Vol. 47, No. 4, pp. 533-545, 1994.

13. Tohgo, K., M. Sakaguchi and H. Ishii, "Applicability of Fracture Mechanics in Strength Evaluation of Functionally Graded Materials", *Transactions of the Japanese Society of Mechanical Engineering*, Vol. 61, No. 592, pp. 2453-2551, 1995.

14. Erdogan, F. and B. H. Wu, "The Surface Crack Problem for a Plate With Functionally Graded Properties", *Journal of Applied Mechanics*, Vol. 64, pp. 449-456, 1997.

15. Gu, P. and R. J. Asaro, "Cracks in Functionally Graded Materials", *International Journal of Solids and Structures*, Vol. 34, No. 1, pp. 1-17, 1997.

16. Jin, Z. H. and R. C. Batra, "Some Basic Fracture Mechanics Concepts in Functionally Graded Materials", *Journal of Mechanics and Physics of Solids*, Vol. 44, No. 8, pp. 1221-1235, 1996.

17. Marur, P. R. and H. V. Tippur, "Numerical Analysis of Crack-tip Fields in Functionally Graded Materials with Crack Normal to the Elastic Gradient", *International Journal of Solids and Structures*, Vol. 37, pp. 5353-5370, 2000.

18. Gu, P., M. Dao and R. J. Asaro, "A Simplified Method for Calculating the Crack-tip Field of Functionally Graded Materials Using the Domain Integral", *Journal*

of Applied Mechanics, Vol. 66, pp. 101-108, March 1999.

19. Anlas, G., J. Lambros and M. H. Santare, "Dominance of Asymptotic Crack Tip Fields in Elastic Functionally Graded Materials", *International Journal of Fracture*, Vol. 115, pp. 193-204, 2002.

20. Kim, J. H. and H. Paulino, "Finite Element Evaluation of Mixed Mode Stress Intensity Factors in Functionally Graded Materials", *International Journal for Numerical Methods in Engineering*, Vol. 53, pp. 1903-1935, 2002.

21. Dolbow, J. E. and M. Gosz, "On the Computation of Mixed-mode Stress Intensity Factors in Functionally Graded Materials", *International Journal of Solids and Structures*, Vol. 39, pp. 2557-2574, 2002.

22. Shim, D. J., G. H. Paulino and R. H. Dodds, "Effects of Material Gradation on K-dominance of Fracture Specimens", *Engineering Fracture Mechanics*, Vol. 73, pp. 643-648, 2006.

23. Williams, M. L., "On the Stress Distribution at the Base of Stationary Crack", *Journal of Applied Mechanics*, Vol. 24, pp. 109-114, 1957.

24. Lee, Y. J. and A. J. Rosakis, "Interfacial Cracks in Plates: A Three Dimensional Numerical Investigation", *International Journal of Solids and Structures*, Vol. 30, No. 22, pp. 3139-3158, 1993.

25. Mattheck, C. and H. Moldenhauer, "Mode-extraction Method From Mixed Mode Analysis of Cracks by Special Filter Technique", *International Journal of Fracture*, Vol. 34, pp. 209-218, 1987.

26. Li, F. Z., C. F. Shih and A. Needleman, "A Comparison of Methods for Calculating Energy Released Rates", *Engineering Fracture Mechanics*, Vol. 21(2), pp. 405-421, 1985.

27. Gu, P., M. Dao and R. J. Asaro, "A Simplified Method for Calculating the Crack-

Tip Field of Functionally Graded Materials Using the Domain Integral", *Journal of Applied Mechanics*, Vol. 66, pp. 101-108, 1999.

28. Anlas, G., M. H. Santare and J. Lambros, "Numerical Calculation of Stress Intensity Factors in Functionally Graded Materials", *International Journal of Fracture*, Vol. 104, pp. 131-143, 2000.

29. Yılmaz, S., 2001, *The Effect of Crack Size, Boundary and Nonhomogeneity in K-dominance Analysis of 2-D Problems of Functionally Graded Materials*, M.S. Thesis, Bogazici University.

30. Kim, J. H. and G. H. Paulino, "T-stress, Mixed-mode Stress Intensity Factors, and Crack Initiation Angles in Functionally Graded Materials: A Unified Approach Using the Interaction Integral Method", *Computer Methods in Applied Mechanics and Engineering*, Vol. 192, pp. 1463-1494, 2003.